A study of hot and dense strongly interacting systems with the quark-hadron chiral parity-doublet model

Dissertation
zur Erlangung des Doktorgrades
der Naturwissenschaften

vorgelegt beim Fachbereich Physik
der Johann Wolfgang Goethe-Universität
in Frankfurt am Main

von
Ayon Mukherjee
aus Kolkata, West Bengal, India

Frankfurt am Main 2018
D30

ii

vom Fachbereich Physik der
Johann Wolfgang Goethe-Universität als Dissertation angenommen.

Dekan: Prof. Dr. Michael Lang

Gutachter: Prof. Dr. Stefan Schramm
Prof. Dr. Horst Stöcker

Datum der Disputation: December 17, 2018

Diese Arbeit basiert auf folgenden Publikationen:

- Higher-order baryon number susceptibilities: interplay between the chiral and the nuclear liquid-gas transitions (Mukherjee, Steinheimer, and Schramm, 2017)

- The application of the Quark-Hadron Chiral Parity-Doublet Model to neutron star matter (Mukherjee et al., 2017)

- Nuclear interactions and net-proton number fluctuations in heavy ion collisions at the SIS18 accelerator (Steinheimer et al., 2018b)

- Effects of a non-zero strangeness-chemical potential in strong interaction models (Mukherjee, Bhattacharyya, and Schramm, 2018)

und Tagungsbänden:

- Concluding Remarks: Connecting Relativistic Heavy Ion Collisions and Neutron Star Mergers by the Equation of State of Dense Hadron- and Quark Matter as signalled by Gravitational Waves (Hanauske et al., 2017)

- Dense and hot matter in compact stars and heavy-ion collisions (Schramm et al., 2018b)

- Neutron stars and the equation of state (Schramm et al., 2018a)

- The Hot and Dense QCD Equation of State in Heavy Ion Collisions and Neutron Star Mergers (Steinheimer et al., 2018a)

Zusammenfassung

Theoretische und experimentelle Implikationen eines möglichen Quark-Gluon-Plasmas (QGP) werden seit den 1970er Jahren diskutiert. Der Versuch, dieses Plasma aus freien Quarks und Gluonen, den Grundbausteinen der Materie, und den Phasenübergang zu diesem Plasma zu lokalisieren, indem die Fluktuationen eines heißen, dichten Feuerballs, der durch eine Schwerionenkollision (HIC) erzeugt wird, zu untersuchen, ist ebenfalls keine neue Idee. Das Problem ist jedoch, dass die Kopplungskonstante der zugrunde liegende Theorie, der Quantenchromodynamik (QCD), für kleine Werte des Impulsübetrages Q^2 ins Unendliche geht. Die einzige Möglichkeit, die QCD zu lösen, bieten direkte numerische Simulationen wie die Gitter-QCD. Diese Gitterrechnungen benötigen riesige Rechenressourcen. Ein weiteres Problem ist das sogenannte "Fermion-Sign-Problem", welches die Analyse dynamischer Observablen einschränkt und Rechnungen auf verschwindende baryochemische Potentiale einschränkt. Unter diesen Umständen besteht eine praktikable Lösung darin, einen effektiven Lagrangian der QCD aufzustellen. Dieser beinhaltet einige grundlegende Eigenschaften der QCD. Die Modelle, die diese effektiven Lagrangian verwenden, werden treffend als "Effektive Modelle" bezeichnet.

Das 3-Flavor SU(3) chiral Parity Quark-Hadron-Modell (QχP) ist ein solches Modell (Steinheimer, Schramm, and Stocker, 2011b), dass erweitert wurde, um einen De-confinement-Übergang zu einem Gas von Quarks und Gluonen zu beschreiben. Die Berechnungen werden unter Verwendung eines skalaren Meson-Selbstwechselwirkungs-Potentials durchgeführt, das mehrere wichtige Eigenschaften der QCD enthält. Ein Nachteil dieses speziellen Modells ist, dass die Korrekturen der Eigenvolumen der Hadronen zu unrealistischen Werten der Inkompressibilität von Kernmaterie führten, die viel höher waren als die experimentell beobachtete obere Grenze.

In der vorliegenden Arbeit wurde das oben genannte Modell modifiziert, indem das mesonische Selbstwechselwirkungspotential nach Motohiro, Kim, and Harada, 2015 verändert wurde, was die Überarbeitung sowohl physikalischer als auch numerischer Parameter erforderlich machte. Der resultierende neue (Un)Kompressibilitätswert von 267 MeV liegt innerhalb der phänomenologischen Grenzen von $200 - 280$ MeV.

Hinsichtlich der experimentellen Nachweisbarkeit dieser Modifikationen ist es allgemein akzeptiert, dass die Materie, die in einer Schwerionen-Kollision (HIC) erzeugt wurde, sich lokal in einem thermodynamischen Gleichgewicht befindet. Daher können thermische sowie kritische Fluktuationen verwendet werden, um die Anwesenheit eines Phasenübergangs nachzuweisen und die Eigenschaften des QGP zu ermitteln. Bevor man große Geldsummen in solche Experimente investiert, ist eine theoretische/numerische Vorhersage nötig, um den Erfolg solcher Experimente zu ermöglichen. Einige der üblicherweise verwendeten
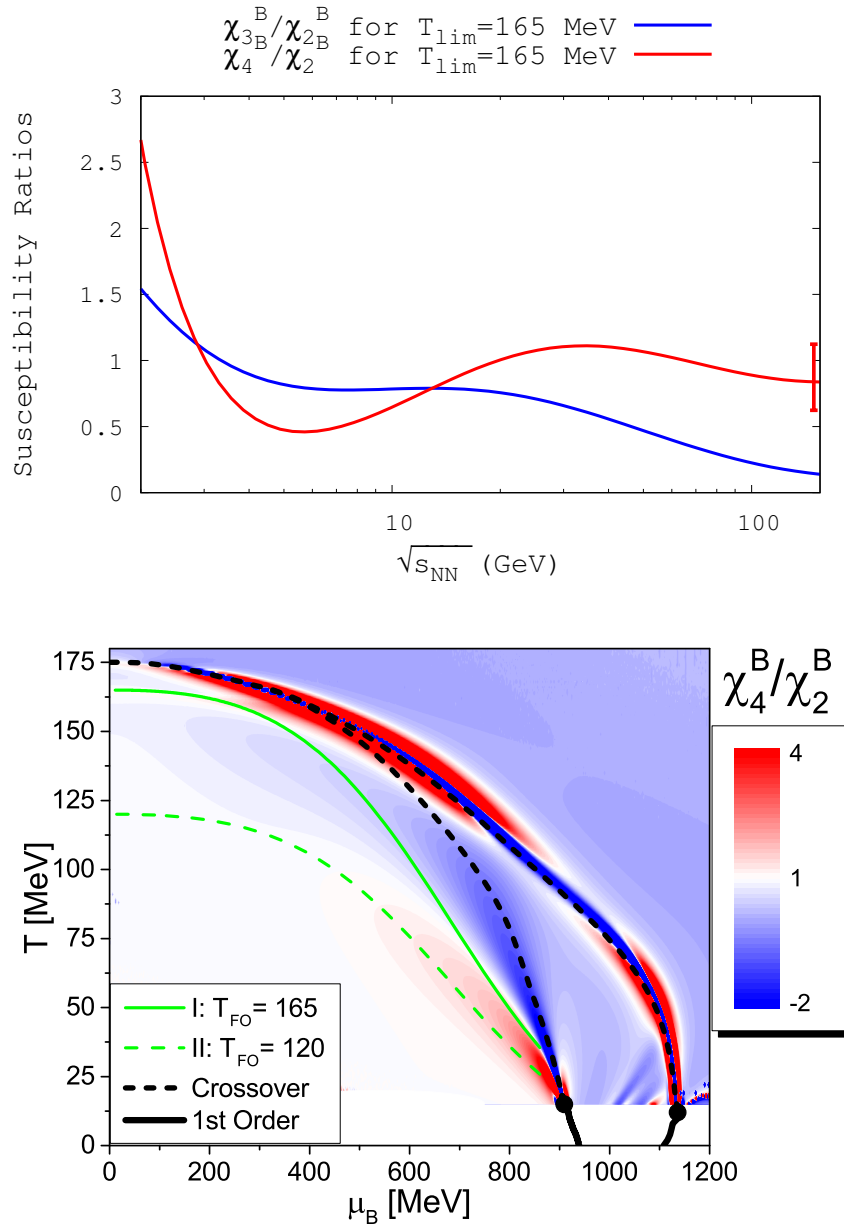
FIGURE 1: Abhängigkeit der Suszeptibilitätsverhältnisse von der Strahlenergie (oberere Abbildung) und von den thermodynamischen Größen Temperatur und chemisches Potential (untere Abbildung).

Observablen sind die lokalen Fluktuationen von global erhaltenen Quantenzahlen. Diese kann man mit den theoretisch berechneten Kumulanten, auch Suszeptibilitäten, der erhaltenen Ladungen des Systems, in Verbindung bringen. Die Fluktuationen, die während des Übergangs des Systems von einer gebrochenen chiralen Symmetrie zu einer wiederhergestellten entstehen, können möglicherweise durch alle Zwischenzustände des Systems überleben. Folglich werden die Suszeptibilitätsverhältnisse, welche in Fig. 5.1 (obere Figur)

gezeigt werden, von ihrem reinen Hadron-Gas-Wert (=1) abweichen. Sie können daher verwendet werden, um die Existenz dieses Übergangs experimentell zu verifizieren.

In der vorliegenden Arbeit wurde auch gezeigt, dass durch die relative Nähe der beiden Übergänge, Kern-Flüssig-Gas und Chiraler/Deconfinement Übergang, viele Komplikationen hervorgehen. Dabei kommt es zu einem Wechselspiel der Suszeptibilitäten in der Region zwischen den beiden Übergängen und damit zu starken Änderungen eben dieser. Darüber hinaus wurde ein starker Einfluss des Verlaufs der Ausfrierkurve im QCD-Phasenübergang auf die Energieabhängigkeit der Suszeptibiliätsverhältnisse gezeigt.

Die Abhängigkeit der Phasenstruktur vom seltsamen chemischen Potential wurde durch die Variation des Seltsamkeitgehalts des Mediums untersucht. Es wurde beobachtet, dass sich, bei großem seltsamen chemischen Potential, der Phasenübergang des Quark-Hadron-Deconfinements zu einem "reinen" Crossover abschwächte, und zwar in der gesamten T-μ-Ebene. Ein solches Szenario, mit nicht-verschwindener lokaler Seltsamkeitsdichte kann auch in HIC-Experimenten erwartet werden (Steinheimer et al., 2009). Aufgrund der kurzen Zeitskalen der Evolution einer Schwerionenkollision, können die erzeugten Hyperonen nicht über den schwachen Zerfall in nicht-seltsame Hadronen zerfallen (Schaffner et al., 1993; Schulze et al., 1998; Nakamura and Group, 2010; Yao and Group, 2006; Beringer and Group, 2012). Über die Messung der Teilchenmultiplizitäten und ihre Fluktuationen kann der vermutete Einfluss der Seltsamkeit auf die Evolution des Systems bestätigt werden. Der kritische Endpunkt im QχP-Modell tritt jedoch bei sehr niedrigen Temperaturen auf, was es schwierig macht, einen solchen Effekt direkt mit Ionenkollisionen zu beobachten. Wenn man bedenkt, dass die aus der experimentellen Datenanalyse gewonnenen Werte für das chemische Potential bei etwa $20 - 25\%$ des Wertes des baryochemischen Potentials liegen (cf. Braun-Munzinger, Redlich, and Stachel, 2011; Kovács and Szép, 2008; Becattini, Gazdzicki, and Sollfrank, 1998; Braun-Munzinger, Heppe, and Stachel, 1999), müssen diese Änderungen, die bei niedrigen Temperaturen im Phasendiagramm induziert werden, berücksichtigt werden.

Im Folgenden wurde die Zustandsgleichung von kalter und heißer, hoch dichter, Isospin-assymetrischer Materie, wie in Neutronensternen und deren Kollisionen erwartet wird, untersucht. Es wurde gezeigt, dass die Werte der Symmetrieenergie und deren Dichteabhängigkeit außergewöhnlich gut mit den von astrophysikalischen Messungen aufgestellten Einschränkungen übereinstimmen. Das resultierende Masse-Radius-Diagramm von Neutronensternen, das durch Lösen der Tolman-Oppenheimer-Volkoff-Gleichungen mit der zuvor erzeugten EoS berechnet wurde, zeigt eine maximale Mögliche Neutronensternmasse von 2 $M_\odot$ bei einem 10,25 km Radius, in Übereinstimmung mit den jüngsten Beobachtungen. Es wurde auch gezeigt, dass der von der QχP EoS erzeugte Maximalmassenstern sehr kompakt ist und dass daher der hadronischen direkten Urca-Prozess unterdrückt wird. Das verhalten der EoS bei sehr hohen chemischen Potentialen stimmt gut mit vorhandenen störungstheoretischen QCD-Rechnungen überein. Somit kann dieses effektive Modell nun Sterne mit einer hadronischen und einer Quarkphase effizient beschreiben; mit einer hybriden EoS, die zu kompakteren Sternen führt und immer noch einen großen Quarkanteil erlaubt, während das Auftreten von Hyperonen nicht explizit verhindert wird wird.

Eine einfache Art, die Eigenschaften einer EoS mit der maximal erreichbaren Kompression

einer relativistischen Kollision zu verbinden, ist die Verwendung der Rankine-Hugoniot-Taub-Adiabatengleichung. Da relativistische Kollisionen nicht nur in HIC-Experimenten, sondern auch in Neutronensternkollisionen stattfinden, wurde die Kollisions-Energie Abhängigkeit der Netto-Baryon-Dichte und der Temperaturen für diese zwei verschiedenen Szenarien untersucht. Es zeigte sich, dass die Dichtekompression nehezu unabhängig vom Isospin-Gehalt und der chemischen Zusammensetzung des Systems ist und dass die QχP EoS eine konsistente und realistische temperaturabhängige EoS zur Beschreibung der NS-Materie und Kollisionen ist.

Das QχP-Modell ermöglicht es thermodynamische Größen im großkanonischen Limes zu berechnen. Dies erschwert einen direkten Vergleich mit Daten aus Schwerionenkollisionen. Das System in relatistischen Kollisionen von schweren Ionen ist vergleichweise klein und expandiert sehr schnell, thermodynamischen Größen ändern sich daher sehr schnell. Es ist folglich nötig die dynamische Evolution eines solchen Systems mit zu berücksichtigen.

Um die Entwicklung eines von einer Schwerionenkollision erzeugten Systems zu beschreiben wurde die aktuelle effektive EoS in ein dynamisches Modell implementiert, dem relativistischen 3+1 dimensionalen Fluid-dynamik SHASTA code. Dieser ist geeignet, die Entwicklung eines von einem HIC erzeugten Feuerballs zu untersuchen. Alternativ wurde der relativistische Transportansatz des UrQMD Modells verwendet um nicht-Gleichgewichtsphänomene im zusammenhang mit Teilchenzahlfluktuationen zu Untersuchen. Die zwei Teilarbeiten sind folgendermaßen zu beschreiben:

Zum Ersten wurde die Behauptung, dass der nukleare Flüssig-Gas Übergang und das Wechselspiel mit dem Chiralen/Deconfinement-Übergang einen beträchtlichen Einfluss auf die Fluktuationen des Systems hat, durch die Einführung nuklearer Wechselwirkungspotentiale in UrQMD-Simulationen von Schwerionenkollisionen am GSI-Beschleuniger SIS18 überprüft. Es zeigte sich, dass nukleare Wechselwirkungen einen signifikanten Einfluss auf die Kumulantenverhältnisse der Multiplizitätsverteilung der Netto-Baryon-Zahl in Schwerionenkollisionen bei SIS18-Strahlenergien haben. Dies wurde für die Kumulantenverhältnisse sowohl im Orts- als auch im Impulsraum beobachtet. Darüber hinaus wurde gezeigt, dass in der frühen Phase der Kollision die repulsive Wechselwirkung dominiert und alle Kumulantenverhältnisse verringert werden. Eine signifikante Erhöhung der gemessenen Kumulantenverhältnisse ist nach dem Ausfrieren, und im Impulsraum, nur für ein kleines Akzeptanzfenster sichtbar. Die Kumulantenverhältnisse in größeren Akzeptanzintervallen werden vom Einfluss der Baryon-Zahl-Erhaltung dominiert. Zusätzlich wurde gezeigt, dass der Effekt der verstärkten Fluktuationen verringert wird, wenn nur die Nettoprotonen gemessen werden. Dies ist verständlich, da der Isospin durch inelastische Streuprozesse zufällig unter den Baryonen verteilt wird. Obwohl der qualitative Effekt der nuklearen Wechselwirkungen in Übereinstimmung mit Vorhersagen von großkanonischen Modellen (Vovchenko et al., 2015; Mukherjee, Steinheimer, and Schramm, 2017) war, ist das quantitative Signal aufgrund mehrerer Faktoren, signifikant kleiner. Daher ist es schwer zwischen Korrelationen aus nuklearen Wechselwirkungen oder kritischem Verhalten, durch die Messung der Kumulanten der Protonenzahl in Schwerionenkollisionen, zu unterscheiden.

Zum Zeiten wurden die Ergebnisse von Fluid-dynamik-Simulationen von HICs mit zwei verschiedenen QχP-EoS, in Zusammenarbeit mit der Gruppe von Prof. Tetyana Galatyuk, mit der Di-Lepton-Produktion des HADES-Experiments verglichen. Dies sollte zeigen, dass der QCD-Phasenübergang messbare Auswirkungen auf die frühe Raum-Zeit-Entwicklung eines HIC-Systems hat. Photonen und Di-Leptonen, die nur an elektromagnetische Wechselwirkungen koppeln, eignen sich als effektive Sonden für die frühe Entwicklung des stark wechselwirkenden Systems mit kurzer Lebensdauer, da sie nach der Produktion im Wesentlichen vom System abgekoppelt werden. Die erste der verwendeten Zustandsgleichungen hatte einen kritischen Endpunkt unter 50 MeV Temperatur und kann als ein "reiner" 'Crossover Übergang' angesehen werden. Die zweite der beiden hatte einen nicht-physikalischen erster-ordnung Phasenübergang für alle baryochemischen Potentiale. Dieser wurde als Referenz verwendet, um in Zukunft festzustellen, ob es merkliche Änderungen des invarianten Massenspektrums der Di-Leptonen gibt, wenn das System einen Übergang erster Ordnung von einem QGP zu Hadronen durchläuft. Die Emissivität des Systems; definiert durch die Strahlungsrate virtueller Photonen (Di-Leptonen) aus einer Zelle mit stark wechselwirkender Materie pro Zeiteinheit und Vierimpuls; ist erforderlich, um die Di-Lepton-Emission eines Mediums zu berechnen. Die Emissivität in einem thermisch equilibrierten System hängt von seinen intensiven Eigenschaften ab; wie der Temperatur, dem Druck und der chemische Zusammensetzung. Sie kann daher als ein Raum-Zeit-Integral dieser Größen über das gesamte Reaktionsvolumen und die Lebenszeit berechnet werden. Diese Größen wurden durch Ausführen der Fluid-Dynamischen Simulationen relativistischer HICs und der Strahlenergie des HADES-Experiments erzeugt. Die gewichteten Mittelwerte der Temperatur, Baryonenzahldichte und des relativen Quarkanteils wurden berechnet bevor die Simulationsergebnisse der HADES-Gruppe an GSI übergeben wurden. Dies können nun verwendet werden um die Emissivität und die Di-Lepton-Ausbeute zu berechnen. Die Simulationen zeigten eine erhebliche Abhängigkeit der Mittelwerte dieser Größen von der Zustandsgleichung. Die EoS erster Ordnung führte zu einer fast 150% igen Erhöhung der Baryonenzahldichte und einer fast 1000% igen (oder zehnfachen) Erhöhung des Quark Anteils im Vergleich zum Crossover durch die stärkere Kompression. Diese Abhängigkeiten beeinflussen das gemessene invariante Massenspektrum der Di-Leptonen und demonstrieren ihren Wert als Variablen, die verwendet werden, um die Zustandsgleichung in heißer, dichter, stark wechselwirkender Materie zu untersuchen.

Insgesamt zeigt diese Arbeit, wie wichtig es ist, die Auswirkungen nuklearer Wechselwirkungen und Veränderungen, die sich aus der sich schnell entwickelnden chemischen Zusammensetzung eines Systems ergeben, konsistent, im Rahmen eines einzigen effektiven Lagrange-Chiral-Mean-Field-Modells, zu berücksichtigen.

Solche Untersuchungen, sowohl isospinsymmetrischer als auch isospinasymmetrischer, heißer und dichter Kernmaterie in Schwerionenkollisionen sowie Neutronensternkollisionen sind essentiell für die Interpretation experimenteller Daten die aus eben diesen Kollisionen erzeugt werden.

Contents

List of Figures

List of Tables

Chapter 1

Introduction

The study of dense and hot hadronic matter is a central topic of nuclear physics. It is directly linked to the search for the phase transition to chirally restored and deconfined matter in ultra-relativistic heavy-ion collisions as well as to the study of extremely dense but rather cold matter inside compact stars.

In spite of several decades of experimental and theoretical research the phase structure of strongly interacting matter remains uncertain with the exception of the regime around cold saturated nuclear matter and, to some extent the transition behaviour at vanishing chemical potential, where lattice gauge calculations indicate a cross-over transition to chirally restored and deconfined matter, at a temperature currently determined to be around 150 to 160 MeV (Borsanyi et al., 2010b; Bazavov and Petreczky, 2010).

At finite chemical potential (μ_B), the phase structure of QCD is even less clear. While early extensions of lattice studies to finite μ_B proposed the existence of a critical endpoint at rather small chemical potential (Fodor and Katz, 2002; Fodor and Katz, 2004), other lattice investigations cannot confirm evidence of its existence (Forcrand and Philipsen, 2008; Endrodi et al., 2011).

A central point of these investigations is the understanding of the phase transition in the hadronic and quark-hadron matter. Recent lattice calculations and their analysis in terms of a hadron resonance gas hint to the importance of hadronic degrees of matter in driving the phase transition to a quark-gluon plasma (Bazavov and Petreczky, 2010; Huovinen and Petreczky, 2010; Huovinen and Petreczky, 2011). Furthermore, the low temperature of the chiral transition (Aoki et al., 2009; Bazavov and Petreczky, 2010), the good agreement (Borsanyi et al., 2010a) with chiral perturbation theory below T_c and the apparent sensitivity on the hadron properties (Bazavov and Petreczky, 2010) (caused by lattice discretisation effects) supports the idea that the chiral transition could be explained with hadronic interactions. Therefore, a study of purely hadronic models and their properties, especially the restoration of chiral symmetry is also important. One main benchmark for any useful comprehensive model of that kind is a reasonable description of saturated nuclear matter.

In order to have a realistic description of highly excited matter, strange hadrons have to be included in the model description. In a simple linear sigma-model, it is not possible to have stable bound nuclear matter. Therefore a number of extended approaches adding vector and dilaton fields were discussed (Boguta, 1983; Glendenning, 1986; Mishustin,

Bondorf, and Rho, 1993; Heide, Rudaz, and Ellis, 1994), including extensions to flavour SU(3) (Papazoglou et al., 1998; Papazoglou et al., 1999; Tsubakihara et al., 2010).

In order to better understand the circumstances regarding the aforementioned approaches, and introduce a new model in Chap. 2, a brief summary of QCD is in order.

1.1   A brief summary of QCD

In Quantum Chromodynamics, the Lagrangian is:

$$\mathcal{L} = -\frac{1}{4}\sum_{\alpha}F^{\alpha}_{\mu\nu}F^{\mu\nu\alpha} + i\sum_{q}\bar{\psi}^{i}_{q}\gamma^{\mu}(D_{\mu})_{ij}\psi^{j}_{q} - \sum_{q}m_{q}\bar{\psi}^{i}_{q}\psi_{qi} \tag{1.1}$$

where in the first (gluons-only) term, $\alpha = 1$ to 8 indicates the colour indices of gluons, and the field tensor,

$$F^{\alpha}_{\mu\nu} = \partial_{\mu}A^{\alpha}_{\nu} - \partial_{\nu}A^{\alpha}_{\mu} + g_{s}f^{\alpha\beta\gamma}A^{\beta}_{\mu}A^{\gamma}_{\nu} \tag{1.2}$$

contains the eight 4-vector potentials, A^{α}_{μ}, of the gluon field, with g_{s} being the colour charge and $f^{\alpha\beta\gamma}$ being the SU(3) structure constant. The last term in Eqn. (1.2) represents the self-interaction of gluons due to their non-zero colour charge (unlike photons in QED, since photons carry no electromagnetic charge). The second term in the Lagrangian describes the interaction of quarks with gluons, where each of the $\bar{\psi}^{i}_{q}$ are four-component Dirac spinors of the quark fields with colour i and flavour q, and the covariant derivative,

$$(D_{\mu})_{ij} = \delta_{ij}\partial_{\mu} + i\frac{g_{s}}{2}\sum_{\alpha}\lambda^{\alpha}_{ij}A^{\alpha}_{\mu} \tag{1.3}$$

where the λ_{ij}'s are 3x3 matrices and SU(3) group representations. The third and last term in the Lagrangian describes the self-interaction of quarks. Finally, the effective coupling strength of QCD can be written as:

$$\alpha_{s}(Q^{2}) = \frac{4\pi}{\beta_{0}\ln(Q^{2}/\Lambda^{2})}(1 + \text{higher logarithmic terms}) \tag{1.4}$$

In Eqn. (1.4), Λ is a scale constant, $\beta_{0} = 11 - \frac{2}{3}n_{f}$, where n_{f} denotes the number of light quarks. Typically, α_{s} is calculated at the mass of the Z^{0} boson and $\alpha_{s}(m_{Z^{0}}) = 0.118\pm0.002$, giving $\Lambda = 217^{+25}_{-23}$. For large values of Q^{2}, perturbative methods can be used in calculations. However; because the value of α_{s} is large at small Q^{2}, and goes to infinity if $Q^{2} = \Lambda^{2}$; in the perturbative approximation, the calculations do not always converge. Thus, more complex numerical methods are required. Lattice QCD methodology, introduced in 1974 (Wilson, 1974), is one such example. In lattice QCD, different actions; all identical to QCD in the limit of infinitely fine lattices; are evaluated with Monte Carlo sampling methods on a numerical grid. Though promising, lattice calculations are incredibly demanding on computer power and the results are very dependent on the computational power available. At the moment lattice calculations are still restricted on observables in non-dynamic systems of QCD.

Since it is much more complex to describe systems of hadrons from the quark level, one usually begins with models that already includes hadronic degrees of freedom. This is reasonable as we know that many hadronic states exist and that they are somehow created through the interactions of QCD. Using this method one formulates an effective Lagrangian that reproduces some fundamental features and symmetries of the QCD Lagrangian but is formulated in a hadronic language. One has to be careful, as such an approach is usually only valid in a certain applicability region of QCD, but often proves valuable in understanding some fundamental features of QCD. Such models are usually referred to as "Effective Models" of quantum chromodynamics (cf. Sec. 1.3).

1.2 Chiral symmetry

The QCD Lagrangian possesses the symmetries of the strong interaction. One of them is the invariance under a $U(1)$ transformation,

$$\Psi(x) \to \exp(i\theta)\Psi(x), \tag{1.5}$$

which results in the conservation of the baryon number current $\overline{\Psi}\gamma^{\mu}\Psi$ and the conservation of the baryon number:

$$B = \frac{1}{3}\int d^3x \Psi^{\dagger}\Psi \tag{1.6}$$

Chirality is the property of an object or system that says that it cannot be brought into congruence with its mirror image by a rotation around the mirror axis. The wave-function of a fermion for example can be divided into two pieces which can interchange through a parity transformation. The associate quantum mechanical quantity is called chirality. One can define a vectorial,

$$\psi \to \psi' = \exp(-i\Theta_V^a G_a)\psi \approx (1 - i\Theta_V^a G_a)\psi \tag{1.7}$$

and axial transformation.

$$\psi \to \psi' = \exp(-i\gamma_5\Theta_A^a G_a)\psi \approx (1 - i\gamma_5\Theta_A^a G_a)\psi. \tag{1.8}$$

where ψ is the wave-function of a defined quark flavour. Θ is the transformation parameter. $\gamma_5 = i\gamma_0\gamma_1\gamma_2\gamma_3$ (γ_μ are the Dirac matrices) and the G_a are the generators of the corresponding symmetry group. If the QCD Lagrangian is symmetric with respect to these transformations it has a chiral symmetry. The conserved currents associated with this symmetry are the vector currents:

$$V_a^{\mu} = \overline{\psi}\gamma^{\mu}\frac{\lambda_a}{2}\psi \tag{1.9}$$

and the axial-vector currents:

$$A_a^{\mu} = \overline{\psi}\gamma^{\mu}\gamma_5\frac{\lambda_a}{2}\psi \tag{1.10}$$

Chiral symmetry breaking

The above is only true in the case of zero quark masses. Introducing a quark mass in the Lagrangian adds terms of the form:

$$L_{m_i} = m_i \overline{\psi} \psi, \tag{1.11}$$

where m_i are the current quark masses. From experiment these are (Tanabashi et al., 2018):

$$m_u = 1.8 - 2.7 \text{ MeV}, \; m_d = 4.4 - 5.2 \text{ MeV}, \; m_s = 92 - 104 \text{ MeV}. \tag{1.12}$$

The mass term breaks the chiral symmetry of the QCD Lagrangian explicitly. But, since the masses of the light flavours are very small, this symmetry breaking is only very weak and one often speaks of an approximate chiral symmetry.

If chiral symmetry was an exact (or approximate) symmetry of QCD, this would lead to a degeneracy between states of different parity. In the vacuum, this is not the case. In fact, we observe a wide range of hadronic states with a mass hierarchy.

Thus, the chiral symmetry of QCD is most likely spontaneously broken in the vacuum. This means that while the Lagrangian of QCD is still symmetric with respect to the chiral transformation, the energetically most favourable state in the vacuum is not. The masses of the baryons are large due to the spontaneous breaking of chiral symmetry and the pions are massive Goldstone bosons because chiral symmetry is also broken explicitly.

This fundamental knowledge about the symmetries of QCD led to the development of numerous effective models. These models are based on an effective Lagrangian which has some or many of the symmetries of QCD and therefore should be able to capture certain physical aspects of the theory. An introduction to some basic models is presented in Sec. 1.3, adapted mainly from Steinheimer-Froschauer, 2011.

1.3 Effective chiral models

Here we introduce two very instructive examples of effective (phenomenological) models for QCD: the linear σ model and the non-linear σ model.

1.3.1 The linear sigma model

The linear $SU(2) \times SU(2)$ σ model (Schwinger, 1957; Gell-Mann and Levy, 1960); despite being a rather simple model; contains many properties of QCD. The linear sigma model is a hadronic model. In this sense it is a low energy model for QCD and in the following Ψ will denote the nucleon wave-function .

The model Lagrangian reads:

$$\mathscr{L}_{\text{LSM}} = \overline{\Psi} i \partial_\mu \gamma_\mu \Psi + \frac{1}{2} \partial_\mu \vec{\pi} \partial^\mu \vec{\pi} + \frac{1}{2} \partial_\mu \sigma \partial^\mu \sigma - g \overline{\Psi}(\sigma + i \vec{\tau} \vec{\pi} \gamma_5)\Psi - V_{\text{SSB}}$$

where V_{SSB} is a potential term which spontaneously breaks the chiral symmetry of the Lagrangian:

$$V_{\text{SSB}} = V(\sigma^2 + \pi^2) = -\frac{\mu^2}{2}(\sigma^2 + \pi^2) + \frac{\lambda}{4}(\sigma^2 + \pi^2)^2 \tag{1.13}$$

This potential is also called the Mexican-Hat potential. It is radially symmetric in the coordinates σ and $\pi = \vec{\pi}$ and the energetically favourable states are on the outside of the hat. The term of the form $(\sigma^2 + \pi^2)$ is called chiral invariant because a chiral transformation would not change the length of a vector in σ and π but rather rotate it which does not change the value of the potential. The parameter μ^2 has to be larger than 0 for spontaneous breaking of chiral symmetry to occur. The degenerate ground states then are defined by:

$$\sigma^2 + \pi^2 = v^2 \ \ \text{with} \ \ \text{v} = \sqrt{\frac{\mu^2}{\lambda}} \tag{1.14}$$

One can now choose the vacuum expectation values to take the following values:

$$\langle 0 \,|\pi|\, 0 \rangle = 0, \ \ \langle 0 \,|\sigma|\, 0 \rangle = \sqrt{\frac{\mu^2}{\lambda}} = v \tag{1.15}$$

In this case, fluctuations of the pionic fields do not require any energy, therefore the pions are the Goldstone modes of the model. On the other hand the sigma and nucleons are rather massive even though the Lagrangian is still fully symmetric under a chiral transformation. The nucleon mass in this model is then generated through coupling to the scalar field and its finite ground state expectation value. It is in agreement with QCD properties, as the explicit chiral symmetry breaking term in the QCD Lagrangian should be small. A corresponding term could also be included in the linear sigma model:

$$L_{\text{esb}} = m_\pi^2 f_\pi \sigma \tag{1.16}$$

It gives the correct pion mass, as the potential now has a distinct minimum and breaks the symmetry with respect to the axial current.

1.3.2 The non-linear sigma model

Despite being very successful in describing several aspects of QCD, the linear sigma model has some shortcomings. One main problem of the model is the direct coupling of the pion field to the nucleons which leads to problems with the description of direct pion nucleon scattering data. In addition heavy particles do not exist in chiral multiplets.

To cure these problems, a "non-linear representation" of the sigma model is used where one usually rewrites the chiral fields. As the chiral invariant corresponds to a radius in the chiral circle it is appropriate to use polar coordinates (Weinberg, 1967; Weinberg, 1968; for other advantages and a detailed introduction see Papazoglou et al., 1999):

$$\begin{aligned}
\mathscr{L}_{\text{NLSM}} &= \overline{N}(iD_\mu\gamma^\mu - \overline{A_\mu}\gamma^\mu\gamma_5 - g(v+S))N \\
&+ \frac{1}{2}\partial_\mu\vec{p}\partial^\mu\vec{p} + \frac{1}{2}\partial_\mu S\partial^\mu S - \frac{\mu^2}{2}(v+S)^2 - \frac{\lambda}{4}(v+S)^4
\end{aligned} \tag{1.17}$$

where $N = N_R + N_L = \xi^\dagger \Psi_R + \xi \Psi_L$ $(\xi = \exp{(i\vec{\tau}\gamma_5 \vec{p}/2v)})$ is the transformed nucleon wave-function and $D_\mu = \partial_\mu - \frac{1}{2}(\xi^\dagger \partial_\mu \xi + \xi \partial_\mu \xi^\dagger)$ is the modified derivative operator. The term $(v + S)$ is defined by the transformation:

$$\sigma + i\vec{\tau}\vec{\pi} \;\equiv\; (v + S)\,\exp{(i\vec{\tau}\gamma_5 \vec{p}/v)} \approx v + i\vec{\tau}\gamma_5 \vec{p} \tag{1.18}$$

$$(\sigma^2 + \vec{\pi}^2) \;=\; (v + S)^2 \tag{1.19}$$

$v = \sigma_0$ is the expectation value of the scalar field, S and $\vec{p}$ are the fluctuations of the σ- and $\vec{\pi}$-field.

In the NLSM the nucleons transform vectorially and thus, heavy particles can be included without spoiling the invariance under chiral transformation.

1.4 Experimental considerations

As seen above, some interesting new physics can be expected if one is able to produce a medium that is either very hot or very dense. In both cases, one can expect the chiral condensate $\left(\langle\overline{\psi}\psi\rangle\right)$, which is responsible for the spontaneous breaking of chiral symmetry, to melt; thereby leading to a restoration of chiral symmetry and a drastic change in the properties of the particles in the matter created. In addition one expects at some point to reach a temperature/density at which deconfinement can be realized and even a quasi-free gas of quarks and gluons can be formed, better known as the quark-gluon plasma (QGP). Experimentally such a system is not easy to produce. High energy heavy-ion collisions (HIC) aim at creating a system hot and dense enough simply by smashing gold or lead ions at very large energies against each other. In this process the kinetic energy is transformed into compressional energy and heat and, if the collision lasts long enough, a fireball of very hot QCD matter can be created. By changing the beam energy, and therefore the energy available for heating, and the system size one hopes to explore wide regions of the phase diagram of QCD especially the existence of a QGP (Harris and Müller, 1996; Bass et al., 1999).

1.4.1 Signatures of the quark-gluon plasma

Nucleus-nucleus collisions, $A + A$; as mentioned above; result in a hot and dense system of nuclear matter, with a time span of ~ 10 fm/c, thereby producing conditions conducive to the experimental investigation of QCD - especially, its phase diagram. The collisions have three main stages of evolution:

- Beginning at the point of collision, $t = 0$, a very hot, very energy-dense region is created.

- Next, the produced partons may interact to achieve local chemical and thermal equilibrium. This stage is characterised by a rapid expansion and cooling of the locally statistically-equilibrated system to the critical temperature, T_c. Direct photons are

produced and the development of collective flow begins at this stage. The QGP has an expected lifetime of between 1 to 10 fm/c and a size of at most a few femtometres in diameter. Local equilibration of the QGP allows for further evolution to be calculable, using relativistic fluid dynamics.

- Finally hadronisation occurs which is followed by chemical and kinetic freeze-out. In the subsequent hot hadronic gas phase following hadronisation, global observables must be interpreted to determine, a posteriori, the conditions of the fireball. Utilising observables, the signals of the QGP must be distinguished from the hadron background. Even these signals are modified by final-state interactions in the hadron background. Some signatures are briefly described below.

A basic feature of the QGP is an enhancement of strangeness content compared to $p + p$ collisions. Typically, in hadronic interactions, the production of strangeness is suppressed due to higher mass of the strange quark as compared to the up and down quarks. However, in the QGP environment, not only are quarks and gluons produced in abundance, but also the energy density and temperature are high (of the order of the strange-quark mass $m_s = 101^{+29}_{-21}$ MeV).

Another feature is that, in presence of a QGP, the bound state of $c\bar{c}$, the J/ψ, may be suppressed with increasing temperature due to a weakening of the heavy-quark effective potential (Matsui and Satz, 1986).

The bulk behaviour of the produced particles in a nucleus-nucleus collision can also relay information regarding the early stages of evolution and the production of a QGP. Particularly, when there is a non-central collision, the partons in the overlap region are subject to spatial anisotropy due to the random population of nucleons in the nucleus and the random orientation and magnitude of the impact parameter. The resulting anisotropic flow pattern may be used to determine the microscopic transport properties of the produced QGP.

1.4.2 Cumulants

In HIC's, we encounter fluctuations and correlations related to the initial state of the system, fluctuations reflecting the subsequent evolution of the system and trivial fluctuations, induced by the experimental measurement process. Initial state fluctuations are inhomogeneities in the initial energy and baryon number deposition. These fluctuations are quite substantial, and are reflected in higher harmonics of the radial flow field (Braun-Munzinger et al., 2016). If the system thermalises, and is described by fluid dynamics, then we expect that fluctuations in the subsequent evolution are mostly thermal. Thermal fluctuations are typically small, suppressed by $1/\sqrt{N}$; where N is the average number of particles in the volume considered. However, thermal fluctuations can become large in the vicinity of a second-order phase transition. This is the phenomenon of critical opalescence. Finally, fluctuations related to detectors need to be understood, controlled, and subtracted, in order to access the dynamical fluctuations; which tell us about properties of the system. Experimentally, fluctuations are most effectively studied by measuring so-called event-by-event fluctuations; where a given observable is measured on an event-by-event basis, and

its fluctuations studied for the ensemble of events. Alternatively, one may analyse the appropriate multi-particle correlations measured over the same region.

Thermal fluctuations

There is good evidence that the system created in an ultra-relativistic HIC is, to a very good approximation, in or close to local thermal equilibrium. Therefore, we focus on the thermal fluctuations. These are characterised by the appropriate cumulants of the partition function or, equivalently, by equal-time correlation functions, which in turn correspond to the space-like (static) responses of the system.

In the current work, we concentrate on fluctuations or cumulants of conserved charges, such as baryon number and electric charge. Therefore, we will work within the grand-canonical ensemble, where the system is in contact with an energy and "charge" reservoir. Consequently, the energy and the various charges are only conserved on the average, with their mean values being controlled by the temperature and the various chemical potentials. As far as heavy ion reactions are concerned, the grand-canonical ensemble appears to be a good choice, as long as one only considers a sufficiently small subsystem of the entire final state, and the final state hadron yields are properly described by a grand-canonical thermal system of hadrons.

Fluctuations of conserved charges are characterised by the cumulants, or susceptibilities, of that charge. For a given partition function of the system with conserved charges Q_i

$$Z = \mathrm{Tr}\left[\exp\left(-\frac{H - \sum_i \mu_i Q_i}{T}\right)\right] \tag{1.20}$$

the susceptibilities are defined as the derivatives with respect to the appropriate chemical potentials. In case of three flavour QCD, the conserved charges are the baryon number, strangeness and electric charge, (B, S, & Q respectively), and we have:

$$\chi^{B,S,Q}_{n_B,n_S,n_Q} \equiv \frac{1}{VT^3} \frac{\partial^{n_B}}{\partial(\mu_B/T)^{n_B}} \frac{\partial^{n_S}}{\partial(\mu_j/T)^{n_S}} \frac{\partial^{n_Q}}{\partial(\mu_Q/T)^{n_Q}} \ln Z \tag{1.21}$$

The above susceptibilities may also be expressed in terms of derivatives of pressure $P = \frac{T \ln Z}{V}$ as:

$$\chi^{B,S,Q}_{n_B,n_S,n_Q} = \frac{\partial^{n_B}}{\partial(\mu_B/T)^{n_B}} \frac{\partial^{n_S}}{\partial(\mu_j/T)^{n_S}} \frac{\partial^{n_Q}}{\partial(\mu_Q/T)^{n_Q}} \left(\frac{P}{T^4}\right) \tag{1.22}$$

Consequently, these susceptibilities also control the pressure at small values of the various chemical potentials. E.g., at small baryo-chemical potential, $\mu_B/T < 1$, the pressure can be Taylor expanded as:

$$\frac{P(T,\mu_B)}{T^4} = \frac{P(T,\mu_B = 0)}{T^4} + \sum_n c_n^B (\mu_B/T)^n \tag{1.23}$$

where the expansion coefficients are given by the baryon-number susceptibilities as:

$$c_n^B = \frac{\chi_n^B}{n!} \tag{1.24}$$

Due to the fermion sign problem, at present, lattice calculations can only be reliably carried out at vanishing chemical potentials. Therefore, the above Taylor expansion for the pressure is also employed in order to determine the QCD equation of state for small chemical potentials.

Chapter 2

The QχP Model

An elegant description of a transition to chirally restored matter can be obtained from the "quark-hadron chiral parity-doublet (QχP)" model. In this approach an explicit mass term for baryons is possible, where the signature for chiral symmetry restoration is the degeneracy of the baryons and their respective parity partners. There were several SU(2) studies of nuclear matter adopting this approach showing that it is possible to generate saturated matter in the parity doublet approach (DeTar and Kunihiro, 1989; Zschiesche et al., 2007; Dexheimer, Schramm, and Zschiesche, 2008; Dexheimer et al., 2008; Gallas, Giacosa, and Rischke, 2010; Sasaki and Mishustin, 2010). An SU(3) parity-doublet description of hadronic matter was still missing. In Nemoto et al., 1998, hyperonic decays in vacuum have been studied in such an approach.

2.1 A basic introduction

In the following, we outline the basic SU(3) parity model and with this ansatz, we study nuclear matter saturation; in order to fulfil one of the benchmarks for a useful model as mentioned above. Subsequently we calculate the phase diagram of isospin-symmetric matter, by varying the baryonic chemical potential and temperature of the system.

In a parity doublet model, positive and negative parity states of the baryons are grouped in doublets. The two components of the fields defining the parity partners, φ_+ and φ_-, have an opposite way of transforming under chiral transformations:

$$\begin{aligned}
\varphi'_{+R} &= R\varphi_{+R} & \varphi'_{+L} &= L\varphi_{+L} \\
\varphi'_{-R} &= L\varphi_{-R} & \varphi_{-L} &= R\varphi_{-L} \ ,
\end{aligned} \tag{2.1}$$

where L and R are rotations in the left- and right-handed sub-spaces. This allows for a chirally invariant mass term in the Lagrangian of the general form:

$$\begin{aligned}
m_0(\bar\varphi_- &\gamma_5\varphi_+ - \bar\varphi_+\gamma_5\varphi_-) = \\
m_0(\bar\varphi_{-L}\varphi_{+R} &- \bar\varphi_{-R}\varphi_{+L} - \bar\varphi_{+L}\varphi_{-R} + \bar\varphi_{+R}\varphi_{-L}),
\end{aligned} \tag{2.2}$$

where m_0 represents a mass parameter.

k_0	k_1	k_2
$(242.61 \text{ MeV})^2$	4.818	-23.357
k_6	ϵ	$g_\sigma^{1,1}$
$(0.276)^6 \text{ MeV}^{-2}$	$(75.98 \text{ MeV})^4$	-8.239296
$g_\sigma^{1,8}$	α_σ^1	$g_{N\omega}$
-0.936200	2.435059	5.45

TABLE 2.1: Model parameters: the F, D, and S-type couplings α_σ^1, $g_\sigma^{1,1}$ and $g_\sigma^{1,8}$ determine the couplings of the various baryons.

The general SU(3) extension of the approach using the non-linear representation of the fields is quite straightforward as shown in Nemoto et al., 1998.

As outlined in Papazoglou et al., 1998, one constructs SU(3)-invariant terms in the Lagrangian including the meson-baryon and meson-meson self-interaction terms; assuming a non-linear realization of chiral symmetry. The part of the Lagrangian coupling the baryon and the mesonic fields relevant in a mean-field approximation reads as:

$$
\begin{aligned}
\mathcal{L}_B \;=\;& \text{Tr}(\bar{\Xi}i\slashed{\partial}\Xi) + m_0\text{Tr}((\bar{\Xi}\gamma_5\tau_2\Xi) + D_s^{(1)}\text{Tr}(\bar{\Xi}\,\{\Sigma,\Xi\}) \\
&+\; F_s^{(1)}\text{Tr}(\bar{\Xi}\,[\Sigma,\Xi]) + S_s^{(1)}\text{Tr}(\Sigma)\text{Tr}(\bar{\Xi}\Xi) \\
&+\; D_s^{(2)}\text{Tr}(\bar{\Xi}\tau_3\,\{\Sigma,\Xi\}) + F_s^{(2)}\text{Tr}(\bar{\Xi}\tau_3\,[\Sigma,\Xi]) \\
&+\; S_s^{(2)}\text{Tr}(\Sigma)\text{Tr}(\bar{\Xi}\tau_3\Xi) + D_v\text{Tr}(\bar{\Xi}\gamma_\mu\,\{V^\mu,\Xi\}) \\
&+\; F_v\text{Tr}(\bar{\Xi}\gamma_\mu\,[V^\mu,\Xi]) + S_v\text{Tr}(V^\mu)\text{Tr}(\bar{\Xi}\gamma_\mu\Xi) \;.
\end{aligned}
\tag{2.3}
$$

Here Ξ is the baryon octet whereby each field is a doublet consisting of the baryon and its negative parity partner. Σ and V^μ are the multiplets of the scalar and vector mesons. The Pauli matrices τ_i act on the doublets. In general the various sets $D^{(i)}, F^{(i)}, S^{(i)}$ correspond to the D-type, F-type and singlet SU(3) invariant baryon-meson couplings. Note that the parity doublet models allow for two different scalar coupling terms $i = 1, 2$. In order not to be overwhelmed by coupling constants we will restrict the set of non-zero couplings in the actual calculations. As the term proportional to m_0 mixes the upper and lower components of the parity doublets, one diagonalizes the matrix by introducing new fields B with a diagonal mass matrix.

Taking along only the diagonal meson contributions, the scalar and vector condensates in the mean field approximation, the resulting Lagrangian $\mathcal{L}_B$ then reads

$$
\begin{aligned}
\mathcal{L}_B \;=\;& \sum_i (\bar{B}_i i\slashed{\partial}B_i) + \sum_i \left(\bar{B}_i m_i^* B_i\right) \\
&+\; \sum_i \left(\bar{B}_i\gamma_\mu(g_{\omega i}\omega^\mu + g_{\rho i}\rho^\mu + g_{\phi i}\phi^\mu)B_i\right) \;.
\end{aligned}
\tag{2.4}
$$

The effective masses of the baryons (assuming isospin symmetric matter) read

$$m_{i\pm}^* = \sqrt{\left[(g_{\sigma i}^{(1)}\sigma + g_{\zeta i}^{(1)}\zeta)^2 + (m_0 + n_s m_s)^2\right]} \pm g_{\sigma i}^{(2)}\sigma \pm g_{\zeta i}^{(1)}\zeta. \qquad (2.5)$$

where the various coupling constants $g_i^{(j)}$ are given as combinations of the original parameters $D^{(j)}, F^{(j)}, S^{(j)}$ in Eqn. (2.3) and further adding an SU(3) breaking mass term that generates an explicit mass corresponding to the strangeness n_s of the baryon.

The scalar meson interaction driving the spontaneous breaking of chiral symmetry can be written in terms of SU(3) invariants $I_2 = Tr(\Sigma^2) = (\sigma^2 + \zeta^2)$, $I_4 = Tr(\Sigma^4) = -(\sigma^4/2 + \zeta^4)$ and $I_6 = Tr(\Sigma^6) = (\sigma^6 + 4\zeta^6)$ as:

$$V = V_0 + \frac{1}{2}k_0 I_2 - k_1 I_2^2 - k_2 I_4 + k_6 I_6 \qquad (2.6)$$

where V_0 is fixed by demanding a vanishing potential in the vacuum.

In this work the last term, $k_6 I_6$, has been introduced, following Motohiro, Kim, and Harada, 2015, resulting in an improvement of the nuclear matter compressibility value well within the observed range (cf. Sec. 2.2.2).

The explicit symmetry breaking term that generates the correct pion and kaon masses with their corresponding decay constants can be written as

$$\mathcal{L}_{\mathrm{SB}} = m_\pi^2 f_\pi \sigma + \left(\sqrt{2}m_k^2 f_k - \tfrac{1}{\sqrt{2}}m_\pi^2 f_\pi\right)\zeta,$$

$$(2.7)$$

The set of scalar coupling constants are fitted in order to reproduce the vacuum masses of the nucleon, and the Λ, Σ, and Ξ hyperons, whereas the vector couplings are chosen to reproduce reasonable values for nuclear ground state properties. The resulting ε/ρ as function of density (ρ) is shown in Fig. 2.3.

One candidate for the parity partner of the nucleon is the N(1535) resonance. However, this assignment is unclear, the state might also be a broad structure, so essentially the mass of the particle (assuming its existence) is not determined. The parameters used in this study, which lead to an N* mass of 1535.00 MeV, are shown in Table 2.1.

An SU(3) description, in addition to enhancing the number of degrees of freedom, also necessarily increases the number of parameters. In order not to be overwhelmed by too many new parameters, for simplicity we assume that the splitting of the various baryon species and their respective parity partners is of the same value for all baryons, which is achieved by setting $g_{\sigma i}^{(2)} \equiv g^{(2)}$ and $g_{\zeta i}^{(2)} = 0$. This should be sufficient for a first investigation of the model approach. This assumption agrees quite well with the even less certain assignments of the parity partners of the hyperons.

Obvious candidates are the $\Lambda(1670)$ and $\Sigma(1750)$, whose masses roughly follow the equal splitting approximation, assuming the nucleonic parity partner to be the N(1535). In the case of the Ξ^*, the data are unclear.

The hyperonic vector interactions were tuned to generated reasonable optical potentials of the hyperons in ground state nuclear matter, with $U_\Lambda(\rho_o) = -28\,\text{MeV}$ and $U_\Xi(\rho_o) = -18\,\text{MeV}$. The mass difference due to the strange quark was fixed at $m_s = 150\,\text{MeV}$. The numbers used are summarized in Table 2.1.

Mesons and quarks

It is well known that at some temperature QCD exhibits a transition to a deconfined phase at which the quarks become the dominant degrees of freedom. When this deconfinement will appear and what the order parameter for this transition might be is still under heavy debate (Aoki et al., 2006; Bazavov and Petreczky, 2011). Assuredly one can only say that it occurs in a temperature region of $T_{\text{dec}} \approx 160 - 400$ MeV. Nevertheless at some point the hadronic parity doublet model will not be the appropriate effective description of QCD and one needs to introduce a deconfinement mechanism in the model. In this work we will apply a mechanism that has been introduced in Steinheimer, Schramm, and Stocker, 2011a to add a deconfinement transition in a chiral hadronic model. This is done by adding an effective quark and gluon contribution as done in the PNJL approach (Fukushima, 2004; Ratti, Thaler, and Weise, 2006). This model uses the Polyakov loop Φ as the order parameter for deconfinement. Φ is defined via $\Phi = \frac{1}{3}\text{Tr}[\exp{(i \int d\tau A_4)}]$, where $A_4 = iA_0$ is the temporal component of the SU(3) gauge field, distinguishing Φ, and its conjugate Φ^* at finite baryon densities (Fukushima and Hidaka, 2007; Allton et al., 2002; Dumitru, Pisarski, and Zschiesche, 2005). A more detailed description of the model is provided in Appendix A. In recent years, the PNJL model has been widely used and extended to include non-local interactions as well as an imaginary chemical potential (see also Ratti and Weise, 2004; Rößner, Ratti, and Weise, 2007; Sasaki, Friman, and Redlich, 2007b; Ratti, Roessner, and Weise, 2007; Roessner et al., 2008; Ciminale et al., 2008; Schaefer, Pawlowski, and Wambach, 2007; Fu, Zhang, and Liu, 2008; Hell et al., 2009; Abuki et al., 2008a; Fukushima, 2008b; Fukushima, 2008a; Costa et al., 2009b; Costa et al., 2009a; Hansen et al., 2007; Mukherjee, Mustafa, and Ray, 2007; Abuki et al., 2008b; Abuki et al., 2008c; Fukushima, 2009; Mao, Jin, and Huang, 2010; Schaefer, Wagner, and Wambach, 2010; Hell et al., 2010; Contrera, Dumm, and Scoccola, 2010; Radzhabov et al., 2011; Contrera, Orsaria, and Scoccola, 2010; Herbst, Pawlowski, and Schaefer, 2011; Pagura, Gomez Dumm, and Scoccola, 2012; Kashiwa, Hell, and Weise, 2011; Weise, 2010; Blaschke et al., 2010).

The effective masses of the quarks are generated by the scalar mesons except for a small explicit mass term ($\delta m_q = 5$ MeV and $\delta m_s = 150$ MeV for the strange quark) and m_0:

$$
\begin{aligned}
m_q^* &= g_{q\sigma}\sigma + \delta m_q + m_{0q}, \\
m_s^* &= g_{s\zeta}\zeta + \delta m_s + m_{0q},
\end{aligned}
\tag{2.8}
$$

with values of $g_{q\sigma} = g_{s\zeta} = 4.0$. As in the case of the baryons we also introduced a mass parameter $m_{0q} = 165$ MeV for the quarks. Again this additional mass term can be due to a coupling of the quarks to the dilaton field (gluon condensate). For this mass term

the quarks do not appear in the nuclear ground state which would be a physically invalid result. This allows to set the vector type repulsive interaction strength of the quarks to zero. A non-zero vector interaction strength would lead to a massive deviation of the quark number susceptibilities to lattice data as has been indicated in different mean field studies (Kunihiro, 1991; Ferroni and Koch, 2011; Steinheimer and Schramm, 2011).

A coupling of the quarks to the Polyakov loop is introduced in the thermal energy of the quarks. Their thermal contribution to the grand-canonical potential Ω, can be written as:

$$\Omega_q = -T \sum_{i \in Q} \frac{\gamma_i}{(2\pi)^3} \int d^3k \ln \left(1 + \Phi \exp \frac{E_i^* - \mu_i}{T} \right) \tag{2.9}$$

and

$$\Omega_{\bar{q}} = -T \sum_{i \in Q} \frac{\gamma_i}{(2\pi)^3} \int d^3k \ln \left(1 + \Phi^* \exp \frac{E_i^* + \mu_i}{T} \right) \tag{2.10}$$

The sums run over all quark flavours, where γ_i is the corresponding degeneracy factor, $E_i^* = \sqrt{m_i^{*2} + p^2}$ the energy and μ_i^* the chemical potential of the quark.

All thermodynamic quantities, energy density e, entropy density s as well as the densities of the different particle species ρ_i, are derived from the grand-canonical potential. It includes the effective potential $U(\Phi, \Phi^*, T)$, which controls the dynamics of the Polyakov-loop. In our approach we adopt the ansatz proposed in Ratti, Thaler, and Weise, 2006:

$$\begin{aligned} U & = & -\frac{1}{2}a(T)\Phi\Phi^* \\ & + & b(T)\ln \left[1 - 6\Phi\Phi^* + 4(\Phi^3\Phi^{*3}) - 3(\Phi\Phi^*)^2 \right] \end{aligned} \tag{2.11}$$

with $a(T) = a_0 T^4 + a_1 T_0 T^3 + a_2 T_0^2 T^2$, $b(T) = b_3 T_0^3 T$.

The parameters a_0, a_1, a_2 and b_3 are initially fixed, as in Ratti, Thaler, and Weise, 2006, by demanding a first order phase transition in the pure gauge sector at $T_0 = 270$ MeV, and that the Stefan-Boltzmann limit of a gas of gluons is reached for $T \to \infty$. In general of course the presence of quarks may have a significant influence on the Polyakov potential (Schaefer, Pawlowski, and Wambach, 2007) and in order to obtain a crossover transition at $\mu_B = 0$ we change T_0 to 200 MeV.

In the following we introduce excluded volumes for the hadrons in the system. As a consequence the hadronic contributions from the equation of state at high temperatures and densities will be suppressed. Including effects of finite-volume particles in a thermodynamic model for hadronic matter, was proposed long ago (Hagedorn and Rafelski, 1980; Baacke, 1977; Gorenstein, Petrov, and Zinovev, 1981; Hagedorn, 1983; Rischke et al., 1991; Cleymans et al., 1993; Kapusta and Olive, 1983; Bugaev et al., 2000; Bugaev, 2008; Satarov, Dmitriev, and Mishustin, 2009). In recent publications (Steinheimer, Schramm, and Stocker, 2011a; Steinheimer and Schramm, 2011) we adopted this ansatz to successfully describe a smooth transition from a hadronic to a quark dominated system (see also Sakai et al., 2012).

In particular we introduce the quantity v_i which is the volume excluded of a particle of species i where we only distinguish between hadronic baryons, mesons and quarks. Consequently v_i can assume three values:

$$
\begin{aligned}
v_{\text{Quark}} &= 0 \\
v_{\text{Baryon}} &= v \\
v_{\text{Meson}} &= v/a
\end{aligned}
$$

Where a is a number larger than one. In our calculations we choose a value of $a = 8$, which assumes that the radius r of a meson is half of the radius of a baryon. Note that at this point we neglect any possible density-dependent and Lorentz contraction effects on the excluded volumes as introduced in refs. Bugaev et al., 2000; Bugaev, 2008.

The modified chemical potential $\widetilde{\mu}_i$, which is connected to the real chemical potential μ_i of the i-th particle species, is obtained by the following relation:

$$\widetilde{\mu}_i = \mu_i - v_i \ P \tag{2.12}$$

where P is the sum over all partial pressures. To be thermodynamically consistent, all densities ($\widetilde{e}_i$, $\widetilde{\rho}_i$ and $\widetilde{s}_i$) have to be multiplied by a volume correction factor f, which is the ratio of the total volume V and the reduced volume V', not being occupied:

$$f = \frac{V'}{V} = (1 + \sum_i v_i \rho_i)^{-1} \tag{2.13}$$

$$e = \sum_i f \ \widetilde{e}_i \quad \rho_i = f \ \widetilde{\rho}_i \quad s = \sum_i f \ \widetilde{s}_i \tag{2.14}$$

As a consequence, the chemical potentials of the hadrons are decreased by the quarks, but not vice versa. In other words as the quarks start appearing they effectively suppress the hadrons by changing their chemical potential, while the quarks are only affected through the volume correction factor f.

2.2   Results for isospin-symmetric, non-strange nuclear matter

A new parametrisation of the model was used with the objective of improving the description of nuclear matter ground state properties; in particular - the (in)compressibility, as measured by experiment. However, a comparison with data obtained from lattice QCD (LQCD) calculations is necessary in order to first benchmark the model results and their modifications.
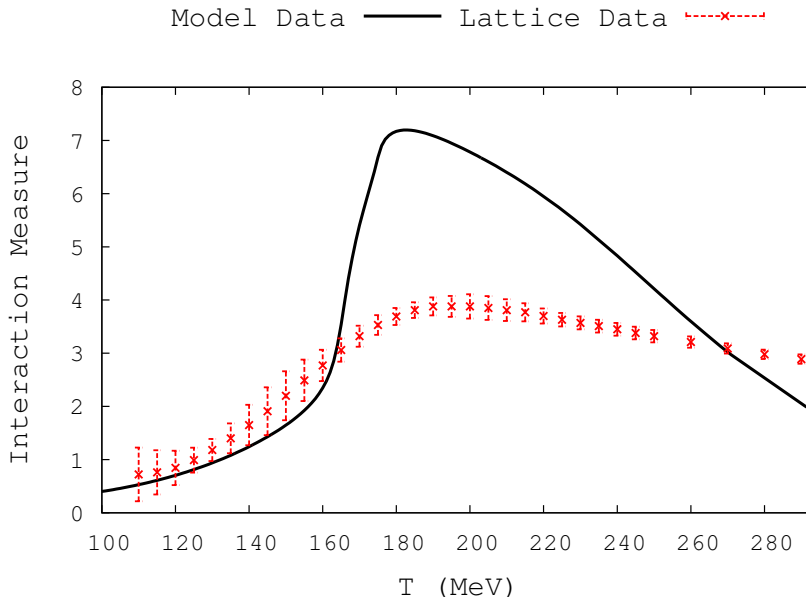
FIGURE 2.1: Interaction measure, as obtained from QχP (at $\mu_B = 0$) and from lattice data, as a function of temperature.

2.2.1 Comparison with lattice QCD

In order to perform the aforementioned comparison, we first determine the interaction measure, I, defined as:

$$I = \frac{\varepsilon - 3P}{T^4} \ , \tag{2.15}$$

with ε, P and T as the energy density, pressure and temperature, respectively. The model results for I at $\mu_B = 0$ as function of temperature, in comparison to available lattice data (Borsanyi et al., 2014), is shown in Fig. 2.1.

We observe that, indeed, the model gives a good description of LQCD thermodynamics below the pseudo-critical temperature T_c. But, although the shapes obtained from both sets of data are similar, the peak value of the interaction measure is much higher in case of the QχP model than that obtained from LQCD. This is likely a result of our use of the standard Polyakov loop potential for the description of the quark and gluon deconfinement. For future investigations, it is therefore interesting to implement an improved version of the Polyakov potential which better describes the thermodynamics at $\mu_B = 0$. In this study, however, instead of constraining our model parameters by a fit to LQCD results at $\mu_B = 0$, we constrain them by actual observables at large baryon-number densities and low temperatures, e.g., nuclear ground-state properties and neutron star observations. Starting from these parameters, we then extend the model to low densities where the remaining free parameters (mainly those of the Polyakov loop) are subsequently used, to get at least a reasonable description of low$-\mu_B$ lattice results. It should be noted, however, that an excellent agreement between the QχP and LQCD interaction measures
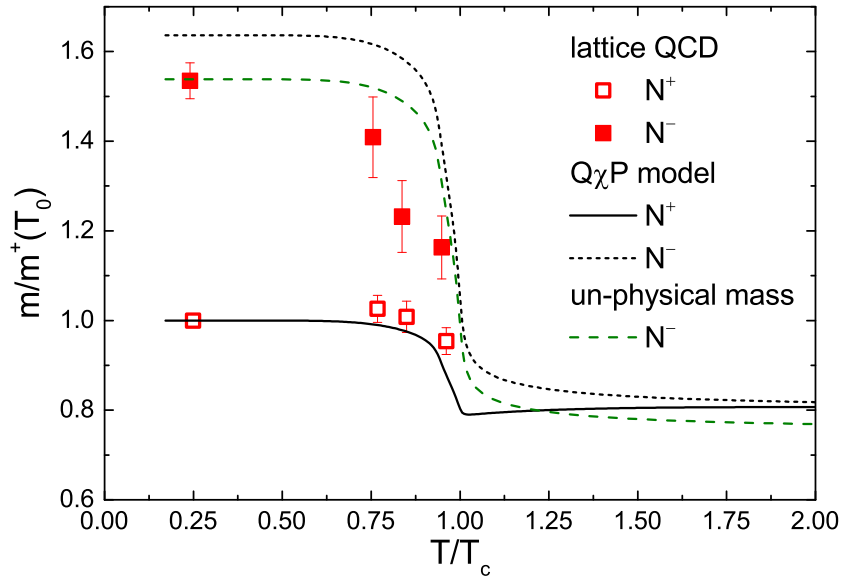
FIGURE 2.2: Mass of the (ground state) nucleon N^+ and its parity partner N^-, normalised to the N^+ mass, as functions of normalised temperature for $\mu_B = 0$, and isospin symmetric, matter. For comparison, we also include QχP results (green, dashed line), where N^- is normalised by the LQCD nucleon mass, which in the cited study is still non-physically large.

is possible, via modifications to the Polyakov potential and quarks-to-chiral fields coupling parameters; without affecting the concurrences with nuclear ground-state properties, as shown by Motornenko et al., 2018.

To further put the QχP model in the context of recent LQCD calculations, we show, in Fig. 2.2, a comparison of the mass of the nucleon and its parity partner with LQCD data (Aarts et al., 2017); as a function of temperature, at $\mu_B = 0$. Even though the vacuum mass of the nucleons in the LQCD calculations is still off its physical value, the temperature dependence shows a remarkable similarity with our results. This result indeed supports a basic assumption of the QχP model, where chiral symmetry restoration is observed in a mass degeneracy for hadrons and their parity partner but, not in a complete absence of mass.

2.2.2   Compressibility

The (in)compressibility of nuclear matter $K(\rho)$ as a function of density ρ is defined as:

$$K(\rho) = 9\rho^2 \frac{\partial^2(\varepsilon/\rho)}{\partial\rho^2}\bigg|_{\rho=\rho_0} , \qquad (2.16)$$

where ε is the energy density and ρ_0 is the density value at which ε/ρ is minimum. This formula effectively translates to:
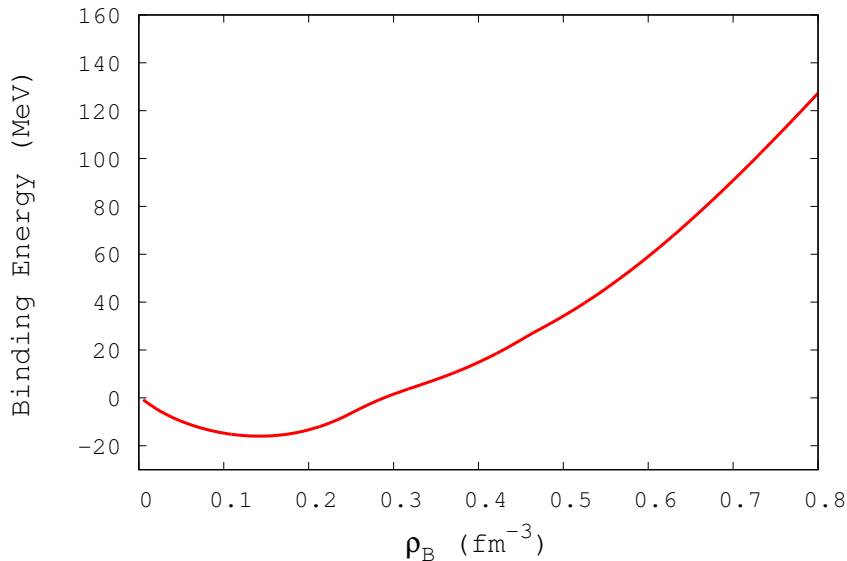
FIGURE 2.3: Binding energy variation with nuclear matter density for isospin symmetric matter.

$$K(\rho) = 9\rho^2 \frac{\partial^2(E/A)}{\partial \rho^2}\bigg|_{\rho=\rho_0} , \tag{2.17}$$

where E is the energy and A is the mass number. The variation of ε/ρ with density is shown in Fig. 2.3. As seen from the figure, the binding energy, E/A, reaches a minimum value of approximately **−16 MeV**, at a saturation density of $\rho_0 \sim$ **0.142 fm^{-3}**.

Using a five-point formula, the second derivative in Eqn. (2.16) is numerically calculated to obtain a compressibility value of **267.12 MeV**, which falls nicely within the phenomenological range of $200 - 280$ MeV.

In contrast to previous attempts, this calculation - for the first time - achieves a reasonably low value for the compressibility; within the bounds of a parity doublet approach. It is noteworthy, that this value has been obtained even after the incorporation of the excluded-volume correction, which tends to stiffen the Equation of State (cf. Motohiro, Kim, and Harada, 2015).

2.2.3 Susceptibilities

Before generating the phase structure of QCD, a brief description of said structure is in order. The QCD phase diagram, drawn on a temperature (T) and baryochemical potential (μ_B) plane, consists primarily of three parts:

1. the high μ_B region (extending over the whole range of temperatures), containing the quark-gluon plasma (QGP),

2. the low μ_B region (predominantly, at lower temperatures), containing stable nuclei; and

3. a region in between, made up of hadronic gas.

The transition from hadronic to quark matter is, for lower temperatures, a first-order, chiral, deconfinement phase transition; which switches to a continuous transition at a point known as the Critical End Point (T_c), characterised by a fixed value of T and μ_B. At values of μ_B lower than that at the critical point, the transition is called a 'Crossover'. The transition from a resonating gas of hadrons to bound hadrons inside a nucleus is also a first-order phase transition, generally called a liquid-gas phase transition due to its similarity to a first-order phase transition of a gaseous phase to a liquid phase.

As discussed in Sec. 1.4.2, the thermodynamics of QCD at small values of μ_B/T can be obtained by a Taylor expansion of lattice results at $\mu_B = 0$, in terms of baryochemical potential. The pressure $P = -\Omega = \frac{T \ln Z}{V}$ is expressed with the coefficients c_n^B, which can be related to the baryon number susceptibilities as:

$$\frac{\chi_n^B}{T^2} = n!c_n^B(T) = \frac{\partial^n(p(T,\mu_B)/T^4)}{\partial(\mu_B/T)^n} \tag{2.18}$$

The behaviour of these coefficients, and hence the susceptibilities, in and around the phase transitions can be revealing. But before calculating the susceptibilities, it is prudent to clearly identify the 'Crossover' and 'First Order Phase Transition' lines of the QCD phase diagram, subject to the specific parametrisation of the model.

For the nuclear liquid-gas transition we define the first-order transition line as the maximum of the derivative of the net-baryon density with respect to the baryochemical potential. Similarly, for the chiral transition, we define it as the maximum of the derivative of the σ field (chiral condensate) with respect to the baryochemical potential (or the temperature, for baryochemical potential values of $\mu_B < 400$ MeV, i.e. beyond the merger of the two transition lines, cf. Fig. 2.4). Note that both criteria can be used equivalently for either transition, as the net-baryon density and value of the sigma field are intimately related (cf. Walecka, 1974; Bender, Heenen, and Reinhard, 2003; Cohen, Furnstahl, and Griegel, 1992 and references therein). This means that when we observe a rapid change in the net baryon number density, we will also observe a rapid change in the chiral condensate and vice-versa. Thus, both criteria can be used to identify the crossover lines of the chiral and LG transition. Note that, if there was an additional separation of the chiral and deconfinement line (e.g., as discussed in Ferreira et al., 2014), the situation we try to describe would be even more complicated.

In the region where both first-order transitions switch to crossovers, we fit a double-Gaussian function to the derivative of the net-baryon density with respect to the baryochemical potential, assigning each peak to one transition line. One should, of course, note that the two transitions show clear differences. Even though the value of the chiral condensate changes slightly at the liquid gas transition, chiral symmetry is restored much later; after the chiral transition; where the chiral condensate, essentially, drops to zero.
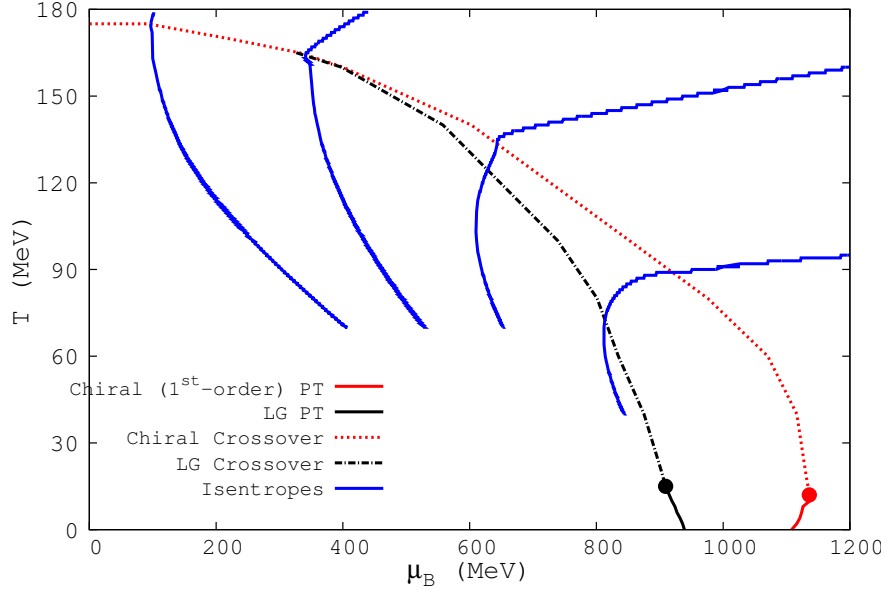
FIGURE 2.4: The liquid-gas and chiral phase transitions, along with their respective crossover regions & critical end-points (T_c), on a temperature & baryochemical potential plane. The blue lines represent the isentropes for S/A values 4, 10, 28 and 121, from left to right, respectively.

Fig. 2.4 shows the phase diagram with the 'Liquid-Gas Phase Transition' and the 'QGP-Hadron Phase Transition' lines for the parameter values mentioned in Table 2.1. We observe that both critical end-points occur at a very low temperatures. We also observe that the associated crossover lines, while first separated, merge at an intermediate chemical potential $\mu_B \approx 400$ MeV. The figure also shows lines of constant entropy-per-baryon (isentropes) for various values of entropy-per-baryon. The isentropes show a distinct structure, a bending over at the crossover, as the dominant degrees of freedom change from hadrons to quarks. At the junction of the liquid-gas and chiral crossover transitions, the isentropes signal a sharpening of the transition generated by the interplay of the two crossovers.

To calculate the experimentally relevant susceptibility ratios, χ_3^B/χ_2^B and χ_4^B/χ_2^B the equations of motion, following from Eqns. (2.4, 2.6 & 2.7), are solved self-consistently in mean field approximation by minimising the grand-canonical potential as a function of the baryochemical potential and temperature. Then, the second-, third- and fourth-order derivatives of Eqn. (2.18) are numerically calculated using the five-point formula for the numerical calculation of derivatives. For all temperatures ranging from 15 MeV to 180 MeV, and all baryochemical potential values ranging from 0 MeV to 1200 MeV, the aforementioned ratios result in the phase diagrams shown in Fig. 5.1.

The figure illustrates the effect of the two kinds of phase transitions on the susceptibility values. Before the first-order QGP-Hadron phase transition, the susceptibilities take values smaller than 1, while in the region after the LG phase transition (at values of μ_B lower than 600 MeV), they consistently stick to 1, since the system is composed of bound hadrons and
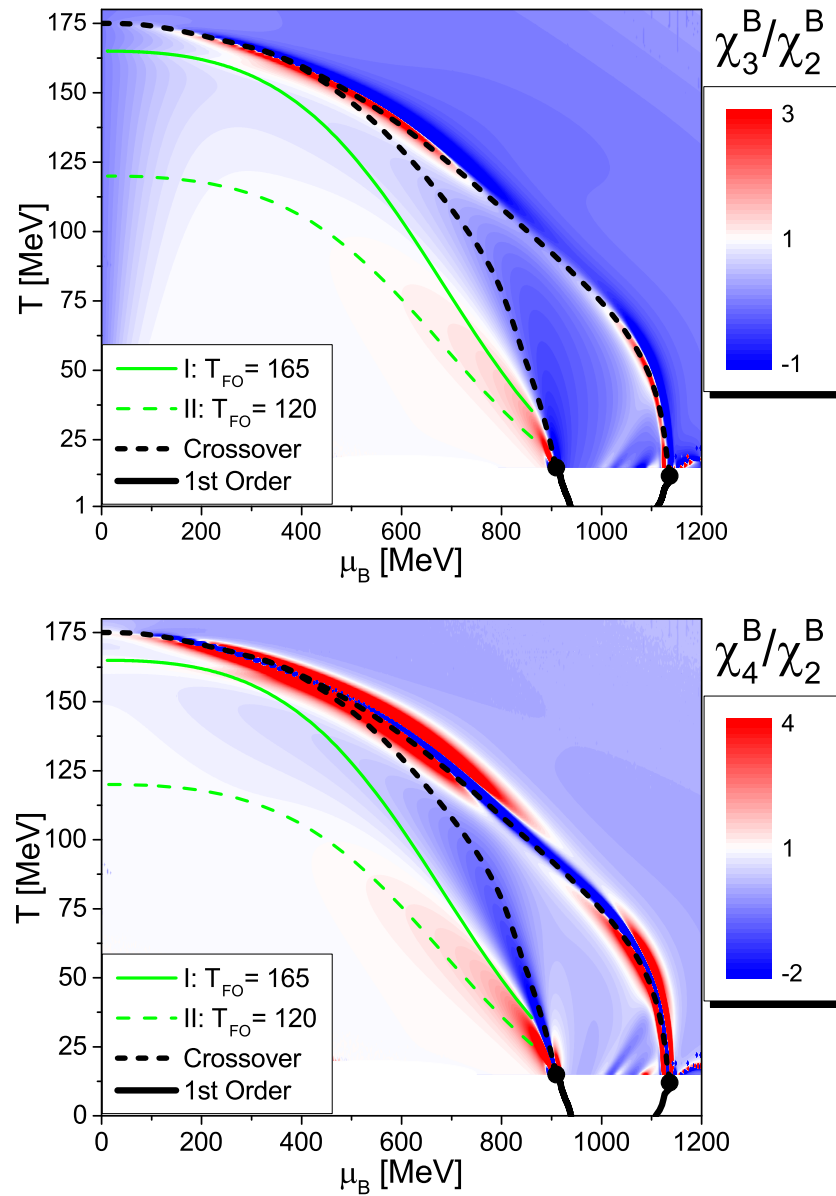
FIGURE 2.5: QCD Phase Diagrams with Susceptibility Ratios on a temperature & baryochemical potential plane.

a value of 1 for the cumulants of conserved charges is logically expected. For the region in between the Crossover transitions from liquid (bound hadrons) to gas (resonating hadrons) and from a hadronic gas to the QGP, an interplay between the two phase transitions can be observed. This results in the cumulants sometimes taking values below 1 - even negative values, and sometimes taking values greater than 1; in the interplay region. Further investigation into these interesting characteristics of the phase diagram have been done with the use of 'Freeze-out Curves' explained below.

Freeze-out curves

In order to give a rough estimate of the susceptibility ratios that could be expected from experiment, one has to define the point in the phase diagram at which the fluctuations are, essentially, frozen out. This point will be different for each beam energy and system size, and in general, is not trivially defined.

However, it has been found that the measured mean multiplicities of stable hadrons can be nicely described by a thermal fit, with a single value of T and μ_B, for a specific beam energy. For different beam energies, different T & μ_B values are obtained, thus producing the so-called 'Freeze-out Curve' (Andronic, Braun-Munzinger, and Stachel, 2009). By fitting experimental data, the equation of a freeze-out line can be obtained as:

$$T = T_{\lim} \frac{1}{1 + \exp\left(2.60 - \ln\left(\sqrt{s_{\mathrm{NN}}(\mathrm{GeV})}\right)/0.45\right)} \ , \tag{2.19}$$

where μ_B and s_{NN} are related as:

$$\mu_B \ (\mathrm{MeV}) = \frac{1303}{1 + 0.286\sqrt{s_{\mathrm{NN}}(\mathrm{GeV})}} \ , \tag{2.20}$$

with $\sqrt{s_{\mathrm{NN}}}$ being the beam energy in GeV.
One must keep in mind that Eqns. (2.19) and (2.20) represent a mere approximation, and the true freeze-out process is much more complicated than is assumed in this study (Steinheimer et al., 2016). Nevertheless, it is worthwhile to study the behaviour of the normalised cumulants along different possible freeze-out lines.
In this study, two freeze-out lines are obtained for two different values of the parameter $T_{\lim}$ (165 MeV and 120 MeV); shown as the green lines in Fig. 5.1. Here, the higher value corresponds to the expected latest point of chemical equilibrium while the lower value is closer to the kinetic freeze-out point. For an ideal, Boltzmann gas, the susceptibility ratio χ_4^B/χ_2^B along these freeze-out lines has been shown to be equal to 1.
The extracted values of the normalised cumulants are displayed in Figs. 2.6 and 2.7, as functions of the beam energy $\sqrt{s_{\mathrm{NN}}}$. In the case of the low freeze-out temperature, the measured cumulants essentially resemble those of an ideal HRG, down to beam energies $\sqrt{s_{\mathrm{NN}}} \leq 10$ GeV. Below that energy, the measured susceptibilities actually probe the critical behaviour of the nuclear liquid-gas transition and not that of the QCD chiral transition, as already found in Fukushima, 2015; Vovchenko et al., 2015; Vovchenko, Gorenstein,
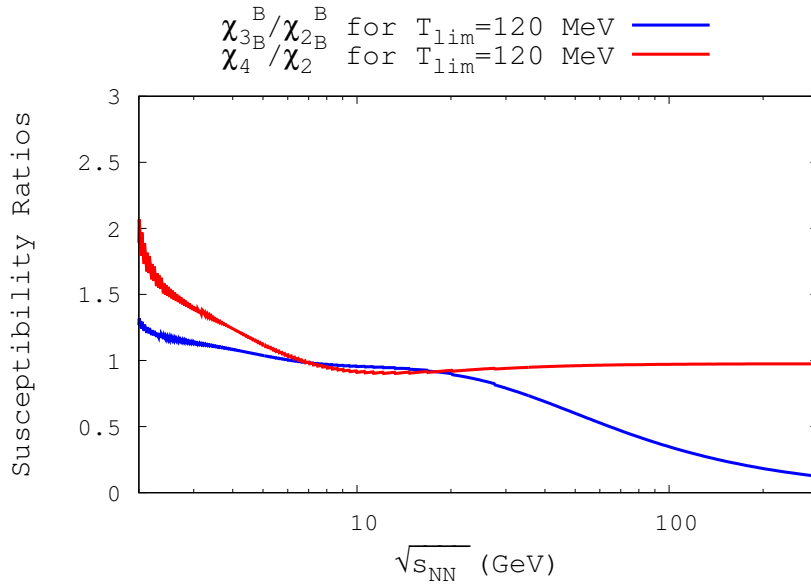
FIGURE 2.6: Susceptibility ratios as functions of beam energy along the
freeze-out line with $T_{\lim} = 120$ MeV.

and Stoecker, 2017. If, however, the higher freeze-out temperature is realised, one can observe a different dependence of the measured cumulants on the beam energy. A peak in the susceptibility ratio is then observed, at a beam energy of $\sqrt{s_{\mathrm{NN}}} \approx 20$ GeV, due to the steepening of the chiral crossover with respect to chemical potential, at finite μ_B (Note: not due to the appearance of a critical point). At lower beam energies, the critical behaviour of the nuclear liquid-gas transition can be observed again.

In Fig. 2.7 we also compare our results with the value of χ_4^B/χ_2^B which has been extracted from LQCD calculations at $\mu_B = 0$ and $T \approx 150$ MeV (Borsanyi et al., 2013). One can already see, that the lattice data slightly below T_{PC} still has a significant uncertainty, and a quantitative comparison with our results is difficult for low temperatures.

At this point, one could be tempted to directly compare our susceptibility ratios with experimental data. As has been shown in, e.g., Luo and Xu, 2017; the values of the cumulant ratios extracted from experiment depend strongly on the selected acceptance, as well as the centrality. Furthermore, experiments only measure net-protons; not net-baryons. It is, therefore, not clear what we should compare our grand canonical values to. One should also keep in mind, that a direct comparison of our grand canonical results with experimental data is not possible due to the many effects discussed in Bzdak and Koch, 2012; Bzdak, Holzmann, and Koch, 2016; Kitazawa, 2016; Feckova et al., 2015; Begun et al., 2004; Bzdak, Koch, and Skokov, 2013; Gorenstein et al., 2009; Gorenstein and Gazdzicki, 2011; Sangaline, 2015; Spieles et al., 1996; Kitazawa and Asakawa, 2012; Asakawa, Heinz, and Muller, 2000; Jeon and Koch, 2000; Steinheimer et al., 2016. The point of this thesis is, rather, to discuss the effects of including realistic nuclear matter; in a model with hadron-quark phase transition; on the baryon-number susceptibilities. The
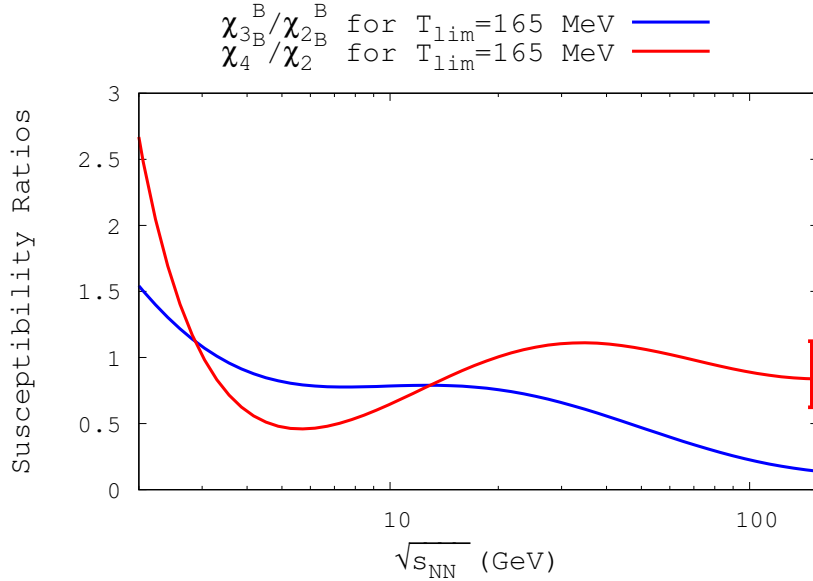
FIGURE 2.7: Same as Fig. 2.6 for $T_{\text{lim}} = 165$ MeV; with the value of χ_4^B/χ_2^B at $\mu_B \approx 0$, obtained from lattice data at $T = 150$ MeV (Borsanyi et al., 2013), represented by the thick, red bar.

eventual comparison of the cumulants to experimental observables has to be determined in a dynamical approach to heavy-ion collisions, which may use our model EoS as an input.

The critical end-point and the universality argument

It was pointed out in Chen et al., 2017 that, given a critical point of a particular universality class (and only one critical point!), the dependence of the normalised cumulants, as functions of one another, should show a particular universal banana-type shape.
Figs. 2.8 and 2.9 show the shapes obtained from the QχP model calculations. Due to the fact that this model actually has two separate transitions, which are difficult to disentangle, the resulting shapes do not resemble a banana, but are more complicated. In general, when there is an interplay between two phase transitions, the relationship between the skewness and the kurtosis is affected by the remnants of the crossover regions related to both the LG and the chiral transitions, as shown in Fig. 2.9. Even for the $T_{\text{lim}} = 120$ MeV freeze-out line (cf. Fig. 5.1), the aforementioned interactions, for $\sqrt{s_{\text{NN}}} \geq 2$ GeV, give results considerably different from those which are obtained using universality arguments (cf. Fig. 2.8), as only the liquid-gas transition is observed.

2.2.4   Pressure and quark fraction

Further investigation of the system may be conducted by observing the pressure of the system, along the transition lines, as a function of temperature.
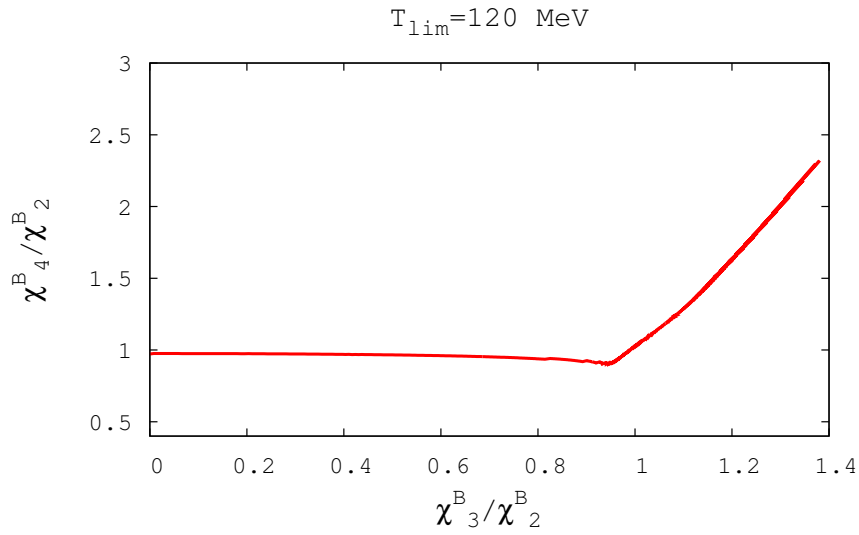
FIGURE 2.8: Susceptibility ratio χ_4^B/χ_2^B versus χ_3^B/χ_2^B, along the freeze-out line with $T_{\text{lim}} = 120$ MeV, for beam energies greater than 2 GeV.
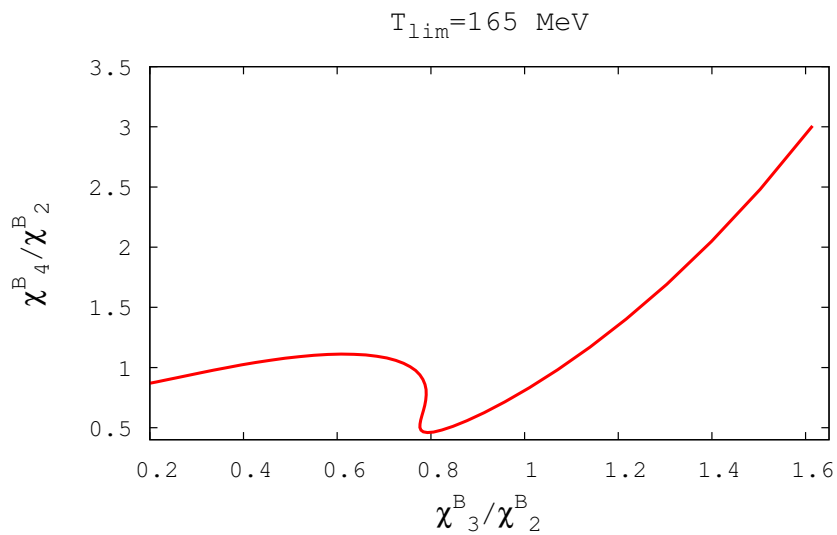
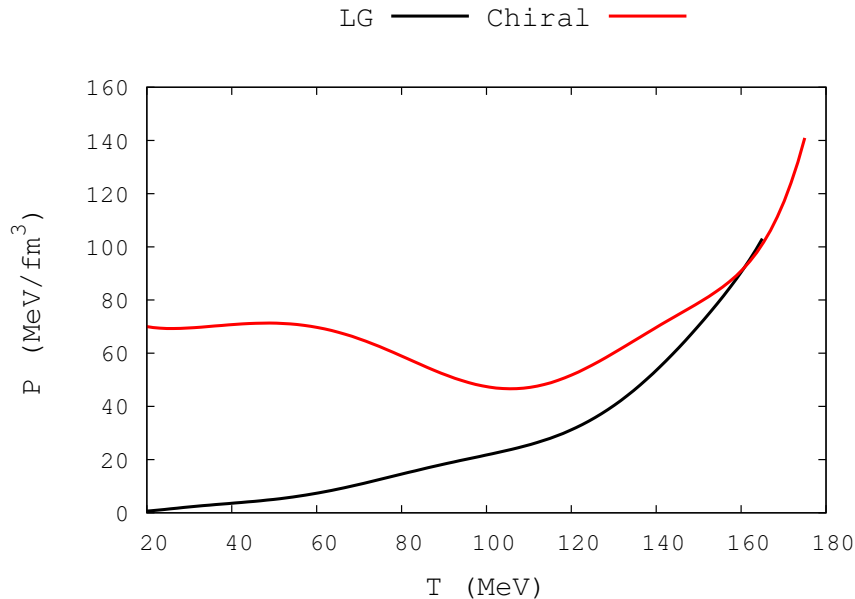FIGURE 2.9: Same as Fig. 2.8 for $T_{\text{lim}} = 165$ MeV.

FIGURE 2.10: Pressure, as a function of temperature, along the transition
lines.

Pressure

The model results for the pressure along the transition and crossover lines, are shown in
Fig. 2.10, where the baryochemical potential increases with decreasing temperature along
both lines (cf. Fig. 2.4).

The behaviour of the pressure along the transition line for the liquid-gas transition is
as expected. Since the baryon density along the liquid-gas transition does not change
considerably with increasing temperature, the change in the pressure is driven, primarily,
by the increase in the entropy caused by the increasing temperature. Such a behaviour
can be observed when the specific entropy in the gas phase is larger than that in the liquid
phase, as derived from the Clapeyron equation (Hempel et al., 2013).

For the chiral transition, the change of the pressure along the transition line is more compli-
cated. At large temperatures and small chemical potentials, the pressure essentially follows
the trend of the nuclear liquid-gas transition, as the meson-dominated system transitions
smoothly into a system dominated by quark and gluons. As the chemical potential in-
creases, however, the change in degrees of freedom is manifested more strongly in a change
of net baryon number, as the system transitions from heavy baryons to light baryons. Con-
sequently, the change in net baryon number dominates the change of pressure and thus, the
pressure along the transition line shows a behaviour opposite to that observed during the
liquid-gas transition. As the transition line goes to even lower temperatures, the behaviour
of the pressure changes direction again. This time, however, it is a result of the change in
curvature of the transition line in the $T - \mu_B$ diagram (cf. Fig. 2.4). This is, most likely,
an artefact of the Polyakov model, which is not very reliable at low values of temperature
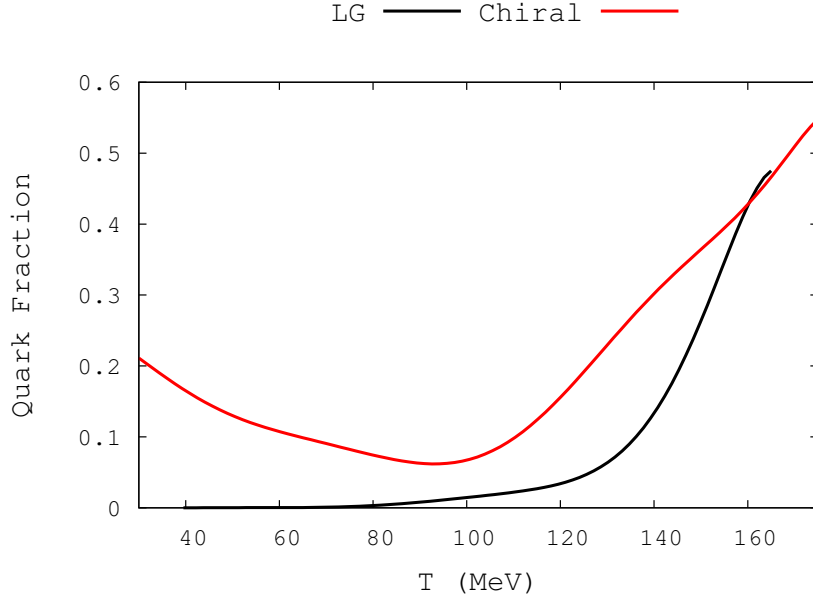
FIGURE 2.11: Quark fraction q_f, as a function of temperature, along the transition lines.

and large values of baryochemical potential.

In any case, it is important to note that the pressure at zero temperature for the deconfinement transition takes a finite value, which is an important property of a "realistic" model for the QCD EoS.

Quark fraction

In order to illustrate the change in degrees of freedom at the transition lines, one can determine the so-called quark fraction q_f, defined as:

$$q_f = \frac{\varepsilon_{\text{Quark}} + \varepsilon_{\text{Polyakov}}}{\varepsilon_{\text{Baryon}} + \varepsilon_{\text{Meson}} + \varepsilon_{\text{Polyakov}}} \ ; \tag{2.21}$$

with $\varepsilon_{\text{Quark}}$, $\varepsilon_{\text{Baryon}}$, $\varepsilon_{\text{Meson}}$ and $\varepsilon_{\text{Polyakov}}$ denoting the energy density contributions from the quarks, baryons (including quarks), mesons and the Polyakov loop contribution from the gluons, respectively. The variation in this quantity, as a function of temperature, is shown in Fig. 2.11 along both transition lines.

Along the LG transition line, the quark fraction is essentially zero for temperatures below 100 MeV (where the interplay between the two crossover transitions is negligible). Above this value it gradually rises (cf. Fig. 2.11) as the LG crossover line approaches the deconfinement crossover (cf. Fig. 2.4), thereby introducing an increasing number of quarks in the system.

For the chiral transition, the quark fraction starts to increase, quite sharply, at around 100 MeV (cf. Fig. 2.11). Below that temperature, the transition is, apparently, a dominantly

chiral one, with only a slow change in degrees of freedom. At very low temperatures, however, a slow change in the quark fraction is observed once again. This is because, at these temperatures, quarks can be introduced into the system due to the large chemical potential, coupled with the fact that the quark-suppressing effect of the Polyakov potential disappears at low temperatures.

This chapter has showcased the strong dependence of the range of values for the cumulant ratios, at large beam energies, on the choice of the freeze-out point. Since both transitions can have an impact on the observed cumulant ratios, it is therefore important to understand the point of origin, during the system's evolution, of the measured fluctuations, a problem which cannot be solved within the bounds of the present model, as it requires a dynamical description of the nuclear collisions, including the propagation of critical fluctuations.

2.3 Strangeness effects

In Sec. 2.2, model results were obtained for thermal fluctuations, using cumulants of conserved charges, for a range of temperatures and baryochemical potentials, at zero strangeness- (μ_S) and isospin-chemical potential (μ_I).

However, recent LQCD calculations and Hadron Resonance Gas (HRG) model (comparative) studies (cf. Bazavov, 2012a; Toublan and Kogut, 2005; Bhattacharyya et al., 2014; Borsanyi et al., 2012; Bellwied et al., 2015; and references therein) have established that for heavy-ion collisions, the effects of a non-zero μ_S on the QCD phase-diagram, and the fluctuations, are non-trivial and often yield interesting results. On the other hand, the influence of μ_I on the chiral phase transition can, in principle, be experimentally tested; and has been studied using both effective model and LQCD approaches (cf. Klein, Toublan, and Verbaarschot, 2003; Toublan and Kogut, 2003; Nishida, 2004; Barducci et al., 2003; Toublan, Klein, and Verbaarschot, 2005; Alford, Kapustin, and Wilczek, 1999).

In experiments, μ_S has been observed to have a value of $\sim 25\% - 30\%$ of μ_B, while μ_I hovers around $2\% - 5\%$ of μ_B (cf. Braun-Munzinger, Redlich, and Stachel, 2011; Kovács and Szép, 2008; Becattini, Gazdzicki, and Sollfrank, 1998; Braun-Munzinger, Heppe, and Stachel, 1999). Thus, the strangeness- and isospin-chemical potentials, though small, are not entirely negligible and it's worthwhile, even from an empirical standpoint, to study the QCD phase diagram with non-zero isospin-, strangeness- and baryochemical potentials. This includes potential fluctuations in the fireball produced by the collision, creating areas with positive and negative net-strangeness and net-isospin, respectively.

Motivated by the aforementioned factors, in this chapter, we focus on the strangeness aspect of a system at high-to-moderate temperatures and high densities.

2.3.1 The strangeness-chemical potential

In many-body systems, like those resulting from HICs, a chemical potential can be associated with each of the conserved charges of the system. In an HIC's case, the corresponding charges are the baryon-number, isospin and strangeness (Bass, Danielewicz, and Pratt,

2000; Karsch and Redlich, 2011b; Bazavov et al., 2012b), because of the short time elapsed between the formation of the fireball and the chemical, and kinetic, freeze-outs, assuming strangeness equilibration. During this time, only strong interactions play an important role, while electroweak interactions are practically negligible. As first argued in Ref. Rafelski and Muller, 1982, strangeness might be abundantly produced in the deconfined phase through gluon-gluon fusion, during the early stages of the system's evolution. The strange quarks are later rapidly redistributed in the hadronic phase, via multi-mesonic interactions, when the system is close to the transition (Greiner and Leupold, 2001).

Although the total strangeness of the entire system (fireball) remains zero throughout its formation and evolution, local distributions of non-zero strangeness (and anti-strangeness) regions could be formed as a result of fluctuations, resulting in a non-uniform distribution of strangeness within the system (Torrieri, 2006; Greiner et al., 1988; Schaffner-Bielich et al., 1997b; Schaffner-Bielich et al., 1997a). These local sub-systems can be considered as being in thermal equilibrium with the rest of the system; since they are considerably smaller in size compared to the entire system. Thus, they can be adequately described by a grand-canonical ensemble.

The pressure (P) for such a thermalised system can be written as:

$$P = -E + TH + \sum_j \left(B_j \mu_{B_j} + S_j \mu_{S_j} + I_j \mu_{I_j} \right) \ , \tag{2.22}$$

with E, T, H, μ, B_j, S_j and I_j representing the energy, temperature, entropy, chemical potential, baryon-number, strangeness and isospin, respectively, of the different particle species; and the relative sign between B and S being always negative. In the quark phase, strange-quarks (or anti-quarks) carry a baryon number of $1/3$ (or $-1/3$).

For the purpose of this chapter isospin effects are not considered and Eqn. (2.22) reduces to:

$$P = -E + TH + \sum_j \left(B_j \mu_{B_j} + S_j \mu_{S_j} \right) \ . \tag{2.23}$$

With this basic understanding of the grand-canonical ensemble; with a non-zero μ_S; in mind, we can move on to the slight changes that were made to the parametrisation of the model, to make it appropriately applicable to the system.

2.3.2   Tweaking the parameters of QχP

For the calculations done in this, and the following, section; the parametrisation is kept similar to that used earlier, the only difference being the omission of the baryon decuplet and other higher resonances from the particle mixture. This is a logical approximation because, with an increase in the magnitude of the strangeness-chemical potential, the system becomes increasingly stacked with hyperons and strange-quarks. Under this model approximation, the higher resonances do not couple directly to the fields, and hence, they do not have any direct contribution to driving the transitions. They do have an indirect effect
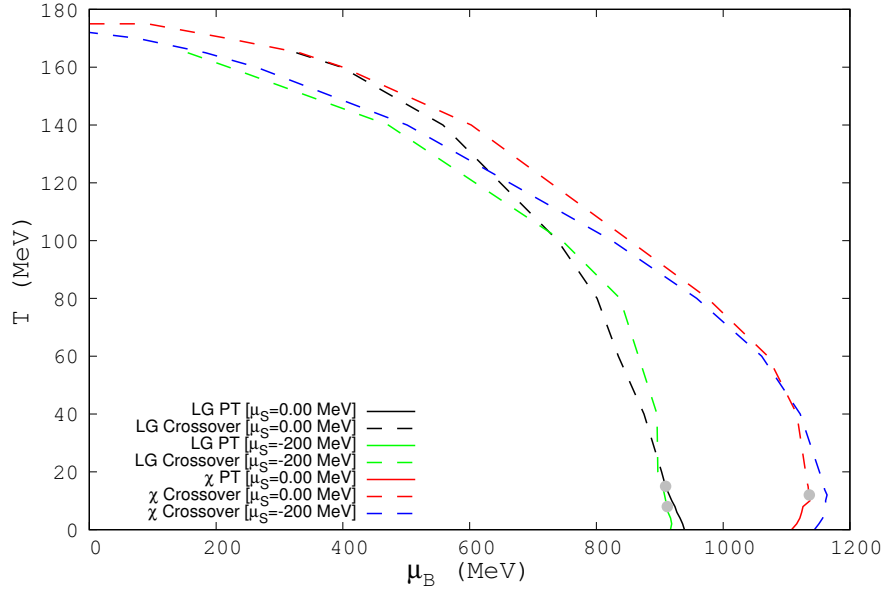
FIGURE 2.12: $T - \mu_B$ phase diagram, showing the LG and chiral transitions
at $\mu_S = 0$ and -200 MeV.

on the transitions, though, when present in considerable numbers, through the excluded-volume corrections. But in an environment filled with heavy hyperons and strange-quarks, even the full baryon octet remains unfilled. Thus, to simplify the discussion; without major quantitative changes; the higher resonances are excluded, as they can be considered non-existent for all practical purposes, under the current circumstances.

2.4 Results for isospin-symmetric, strange nuclear matter

In this section, an investigation into the effects of a non-zero μ_S on the QCD phase-diagram is conducted and the results are discussed at length.

2.4.1 Effects on the phase boundary

As can be seen from Eqn. (2.23), due to a non-zero μ_S, depending on the sign, hyperon thresholds are lowered to values below, or close to, the masses of the non-strange baryons. Thus, the hyperonic particles appear in the system at smaller values of μ_B, as compared to the case of $\mu_S = 0$. The hyperons produced have two non-zero quantum numbers (B_j and S_j) and chemical potentials (μ_{B_j} and μ_{S_j}). These changes naturally drive the first-order, nuclear Liquid-Gas (LG) transition to lower values of μ_B, as shown in Fig. 2.12. At $\mu_S = -200$ MeV, not only is the LG transition line shifted to the left, but also its critical end-point ($T_{\text{CEP}},\mu_{B_{\text{CEP}}}$) is lowered along the $T-$axis; from 15 MeV (for $\mu_S = 0$ MeV) to 8
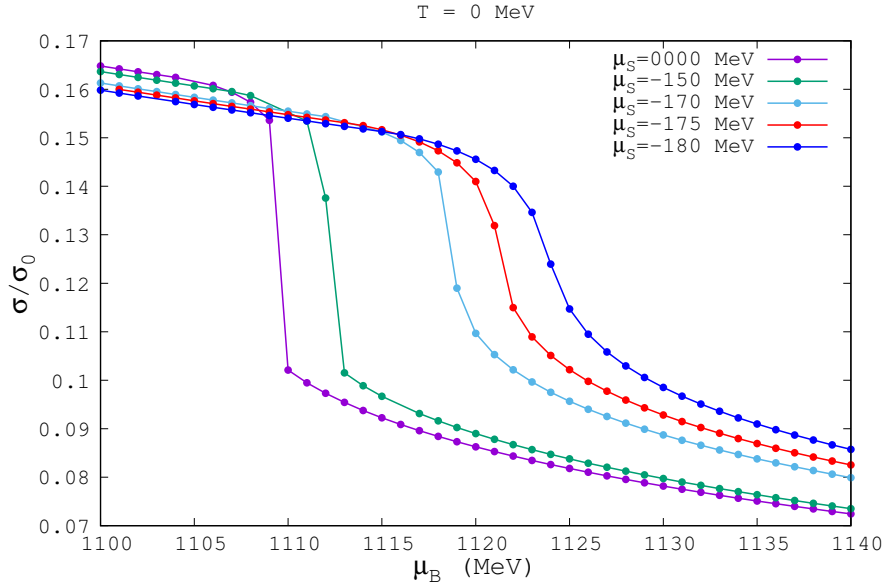
FIGURE 2.13: Normalised chiral condensate, as a function of μ_B, for different values of μ_S, at $T = 0$.

MeV (for $\mu_S = -200$ MeV), weakening the phase boundary to a crossover, earlier than that with a vanishing μ_S. It is also evident from the figure that the chiral first-order transition weakens with larger negative values of μ_S and disappears completely below $\mu_S = -200$ MeV, giving way to a smooth crossover transition, for the full range of temperatures.

In Fig. 2.13 the normalised scalar field (σ/σ_0) is plotted as a function of μ_B at $T = 0$ MeV. One can observe that the chiral first-order transition actually vanishes at $\mu_S = -175$ MeV. As can be seen in Figs. 2.14, 2.15, 2.16 and 2.17, the chiral condensate is intimately related to the net-baryon density, and hence, the change in either variable can be used to define the transition (Mukherjee, Steinheimer, and Schramm, 2017; Walecka, 1974; Bender, Heenen, and Reinhard, 2003; Cohen, Furnstahl, and Griegel, 1992). From the figures, one arrives at the immediate conclusion that, with increasing $|\mu_S|$, these quantities exhibit progressively shallower jumps near the transition, pointing to a weakening of the first-order phase transition. The increase of higher-mass hyperons in the hadronic phase reduces the relative abundance of the lower-mass, non-strange baryons (Figs. 2.14 and 2.15). Fig. 2.16 shows that the strange-quark degrees-of-freedom, already present in the system before the transition (in the hadronic phase), increase, with an increase in $|\mu_S|$; causing the relative contribution of the lighter, non-strange quark degrees-of-freedom to decrease (Fig. 2.17). By significant couplings to the much stiffer strange-quark condensate ζ, the hyperons gradually push the chiral transition to higher values of μ_B. Since the transition is signalled by an abrupt decrease in σ, to which the nucleons exhibit a stronger coupling, a lower concentration of these non-strange baryons at moderate μ_B causes the hadronic phase to survive much longer than that for a vanishing μ_S. Moreover, this suppression of the non-strange baryons causes a smoothing of the transition, even at lower values of $|\mu_S|$, as seen
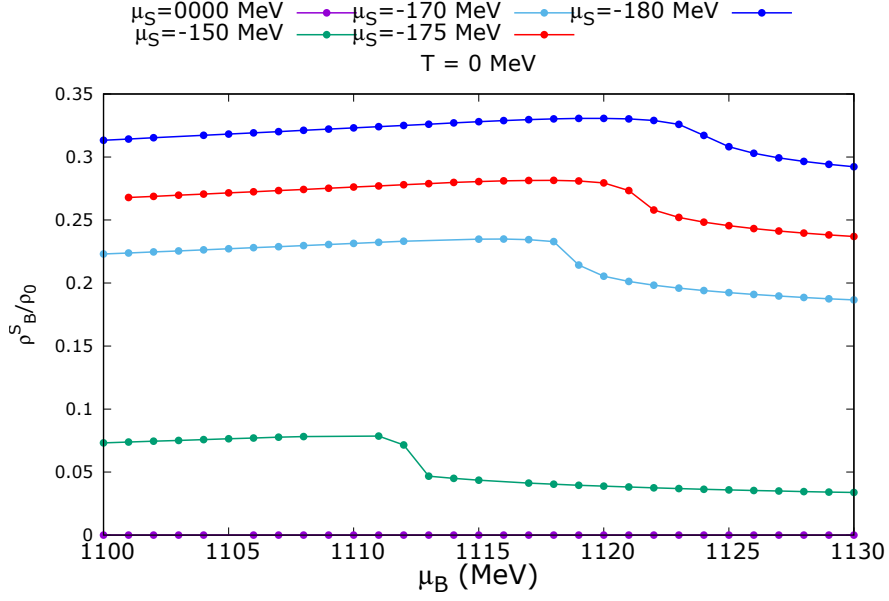
FIGURE 2.14: Relative abundance of hyperons, as a function of μ_B, for different values of μ_S, at $T = 0$.
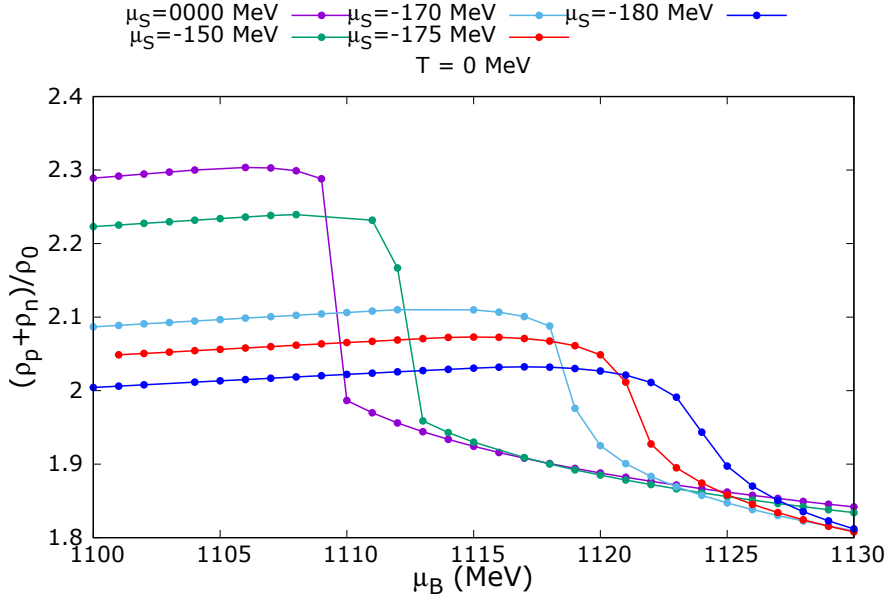
FIGURE 2.15: Relative abundance of non-strange baryons, as a function of μ_B, for different values of μ_S, at $T = 0$.
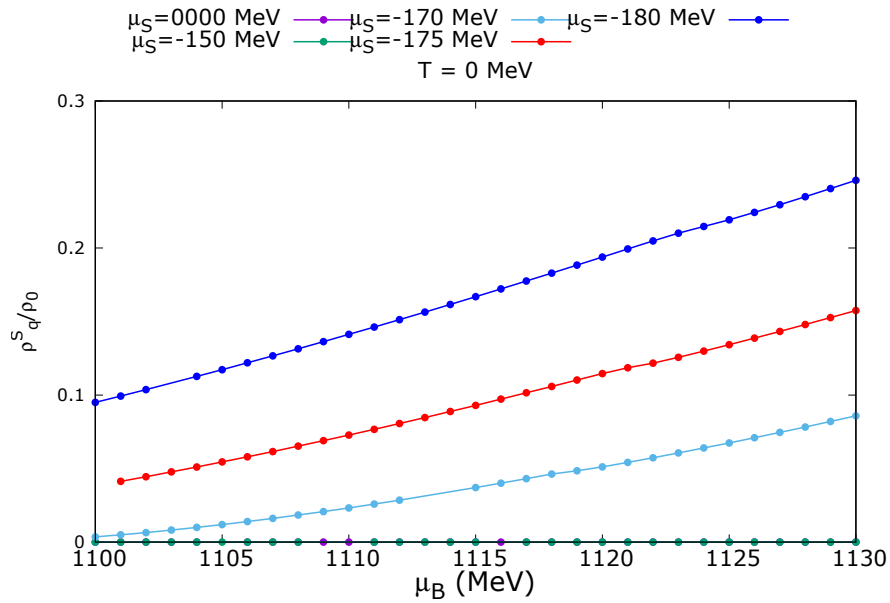
FIGURE 2.16: Relative abundance of strange-quarks, as a function of μ_B, for different values of μ_S, at $T = 0$.
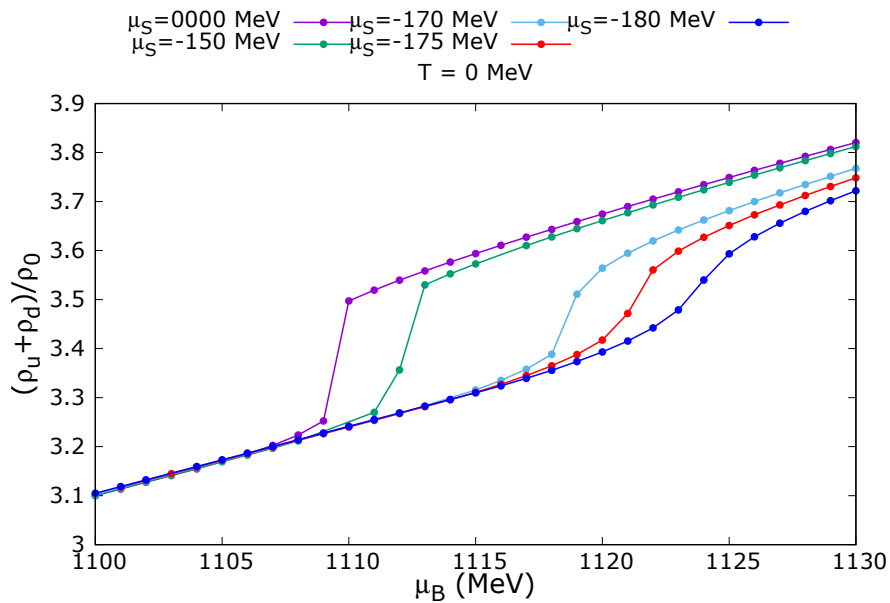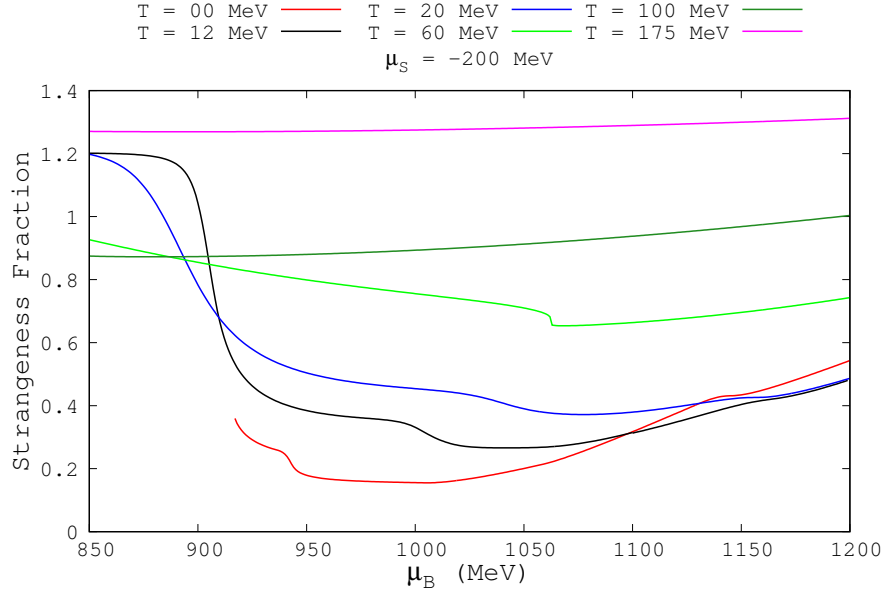

FIGURE 2.17: Relative abundance of non-strange quarks, as a function of μ_B, for different values of μ_S, at $T = 0$.

FIGURE 2.18: Strangeness fraction, as a function of μ_B, for different values of T, at $\mu_S = -200$ MeV.

in Fig. 2.13. When the concentration of strange-quarks in the hadronic phase increases further, with higher values of $|\mu_S|$ (Fig. 2.16), the degrees-of-freedom do not change as drastically across the chiral transition, resulting in a smooth crossover, instead of a sharp first-order, for all strangeness-chemical potentials ≤ -175 MeV and temperatures ≥ 0 MeV.

2.4.2 Fraction of strangeness and the particle cocktail

In Figs. 2.18 and 2.19, the strangeness fraction (f_S); defined as:

$$f_S = \frac{\rho_B^S}{\rho_B} \; ; \tag{2.24}$$

is plotted against μ_B, at different temperatures, for $\mu_S = -200$ MeV and 0 MeV, respectively. The baryon number density ρ_B^S includes contributions from both quarks and baryons. In Figs. 2.20 and 2.21, the relative abundances of the strange-quarks and hyperons are plotted, while in Figs. 2.22 and 2.23, the normalised particle-number-densities; for all quarks and baryons, at different temperatures; are plotted against μ_B, for constant values of μ_S (-200 MeV and 0 MeV, respectively).

As is amply evident from Fig. 2.19, for $\mu_S = 0$, the system lacks the rich structure, at lower temperatures, visible in Fig. 2.18. Moreover, the curve for $T = 0$ MeV in this figure is buried beneath the $T = 20$ MeV curve. So there is no evidence of any structure between the temperatures 0 and 20 MeV; as corroborated by Fig. 2.21.
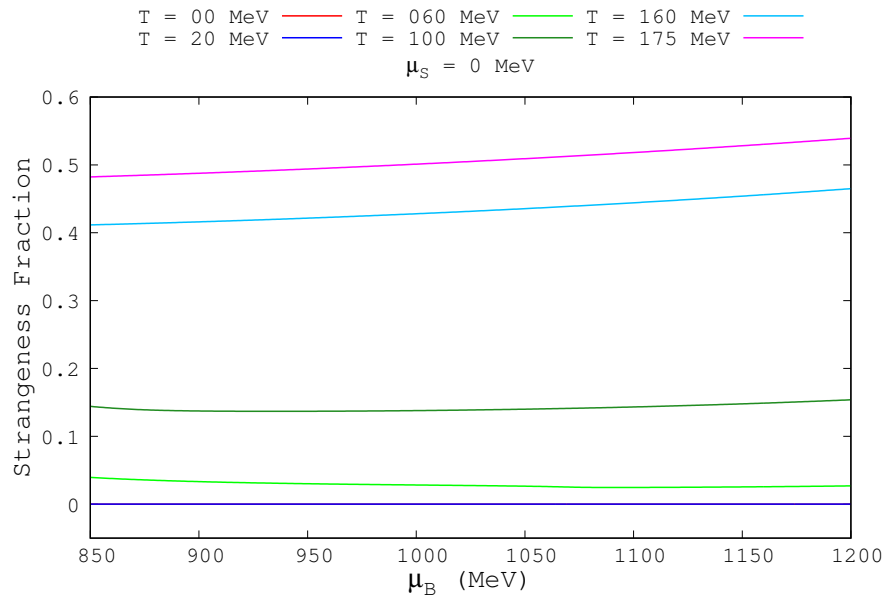
FIGURE 2.19: Same as Fig. 2.18, at $\mu_S = 0$ MeV.
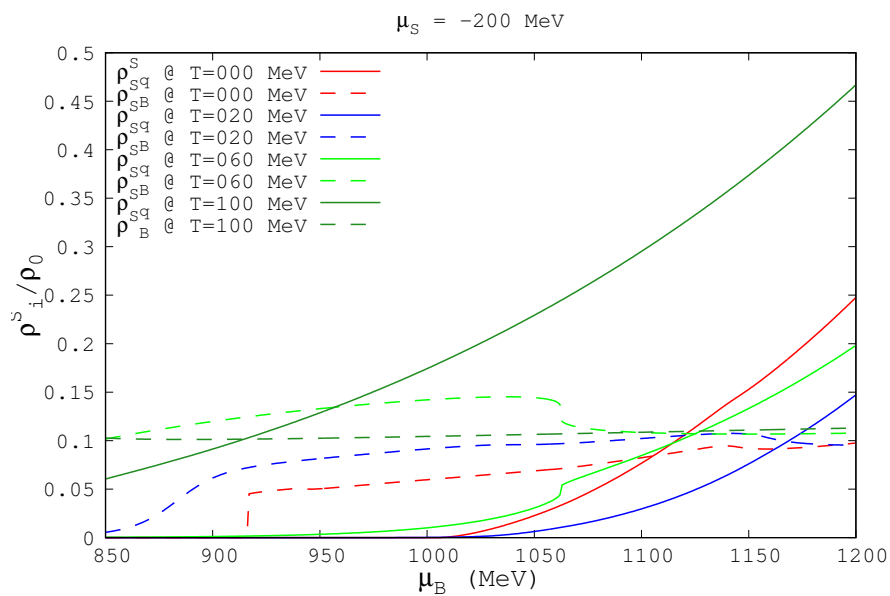
FIGURE 2.20: Relative abundances of strange-quarks and hyperons, as functions of μ_B, for different values of T, at $\mu_S = -200$ MeV.
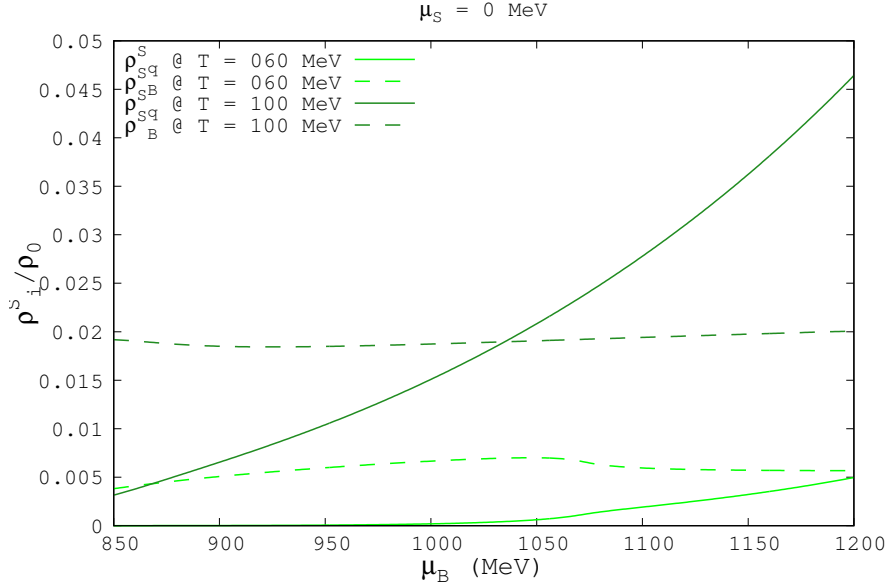
FIGURE 2.21: Same as Fig. 2.20, at $\mu_S = 0$ MeV. The curves corresponding to temperatures less than 60 MeV are negligibly close to zero and have, therefore, not been shown.
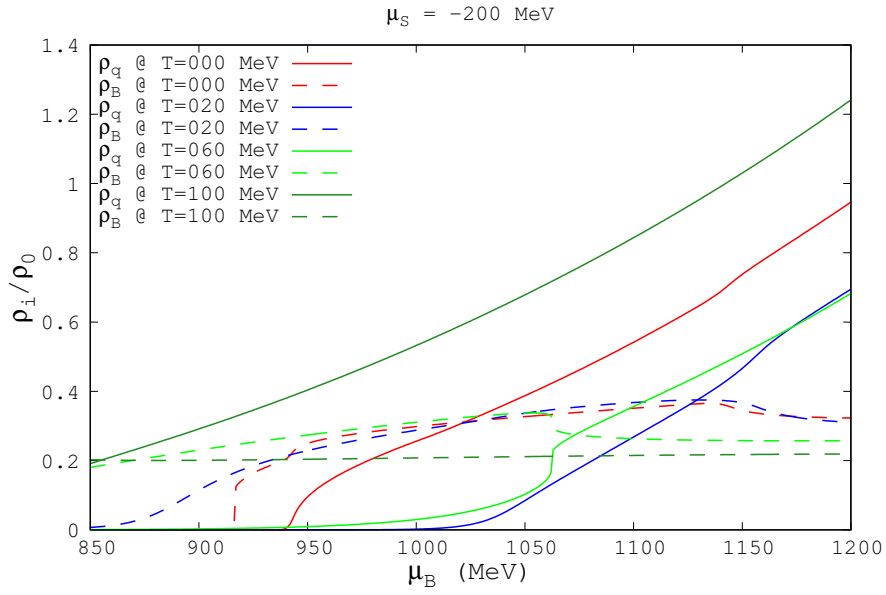

FIGURE 2.22: Relative abundances of quarks and baryons, as functions of μ_B, for different values of T, at $\mu_S = -200$ MeV.

In Fig. 2.18, the $T = 0$ MeV curve begins exactly after the first-order LG transition, at
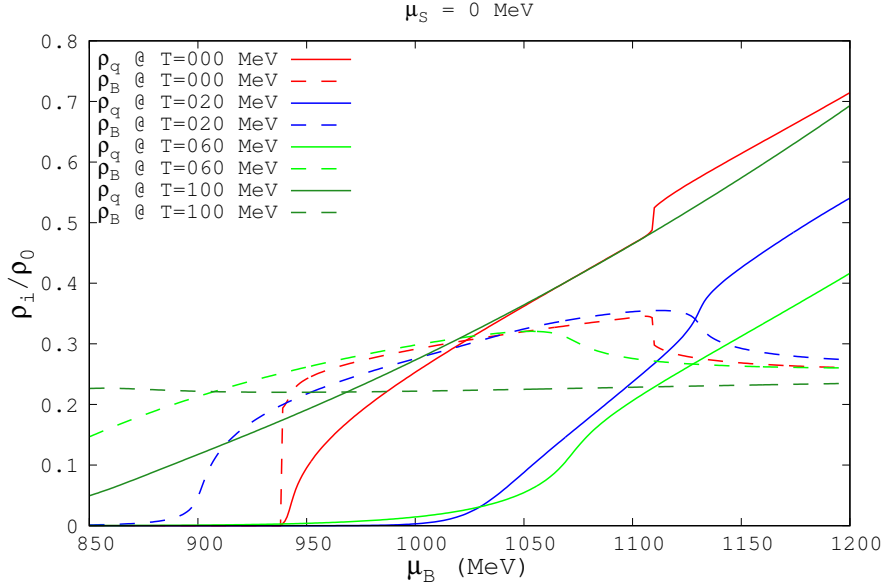
FIGURE 2.23: Same as Fig. 2.20, at $\mu_S = 0$ MeV.

$\mu_B \sim 920$ MeV. This sudden appearance of strangeness can be attributed to the introduction of the Λ and Ξ hyperons to the system - along with other baryons - as can be seen in Fig. 2.20, thereby making both ρ_B^S and ρ_B non-zero. The shoulder-like dip at $\mu_B \sim 940$ MeV is the result of the early onset of the up- and down-quarks, as seen in Fig. 2.22.

For the $T = 12$ and 20 MeV curves in Fig. 2.18, f_S decreases drastically after the LG transition. This is because, right after the transition, there is a sudden rise in ρ_B, while the strange-particle contribution ρ_B^S does not rise as much, due to the higher masses of the hyperons, which change relatively less strongly across the transition. This drives down the fraction of strangeness in the system, which is slowly revived as the hyperons start increasing in abundance with increasing μ_B, as is evident from the gradual rise of ρ_B^S, for $T = 12$ and 20 MeV, in Fig. 2.20. With the appearance of the up- and down-quarks (Fig. 2.22), at around $\mu_B \sim 1000$ MeV, f_S again experiences a slight dip in value. The third and final dips, observed at $\mu_B \sim 1140$ MeV, are caused by the chiral first-order transition (Fig. 2.12), which is not as sharp compared to the nuclear LG transition. As seen in Figs. 2.20 and 2.22, the quarks start dominating the composition of the system, as μ_B increases, from this point onward.

The kink in the $T = 60$ MeV curve (Fig. 2.18) is caused by the chiral crossover transition, as evident from Figs. 2.12, 2.20 and 2.22. Expectedly, after the transition into the quark sector, the relative abundance of baryons decreases w.r.t. quarks; only in this case, the decrement is much smoother, and smaller, as compared to a first-order transition.

For $T = 100$ and 175 MeV, the respective chiral crossover transitions occur at $\mu_B \sim 840$ and 0 MeV (cf. Fig. 2.12). As expected, the corresponding f_S curves in Fig. 2.18 are monotonously increasing functions of μ_B, for the range of values $(850-1200$ MeV) considered.

The figures, in addition to showing the disappearance of the chiral first-order transition at higher μ_S values, showcase the effect that μ_S has on the system as a whole. The fraction of strangeness in the system, driven by the growing relative abundance of the hyperons and strange-quarks, increases rapidly with μ_B in Figs. 2.18, 2.20 and 2.22. They also grow to much higher values, as compared to what they attained with a zero strangeness-chemical potential, for similar values of μ_B (Figs. 2.21 and 2.23). A non-zero μ_S also results in an early onset of the aforementioned strange-particles, as evidenced by the shifting of the kink; corresponding to the chiral transition; in Fig. 2.18, to progressively lower values of μ_B, with an increase in temperature.

In the case of $\mu_S = 0$ MeV, the strangeness-fraction is observed to be either monotonously increasing, or remaining fairly constant, with μ_B; for all temperatures in Fig. 2.19. This is to be expected, however, since from Figs. 2.21 and 2.23, it is clear that the transitions are primarily driven by the changes in the relative abundances of the non-strange quarks and baryons. But, even in this case, with an increase in temperature, strange-particles with baryon numbers do start to come in due to strange-mesons, and in particular, the kaons. This explains the existence of a non-zero f_S, which increases with an increase in temperature of the system, for a zero strangeness-chemical potential. The slight dip in f_S, at $T = 60$ MeV, is again caused by a sudden increase in ρ_B across the chiral transition (Fig. 2.12), with ρ_B^S not being able to change as rapidly.
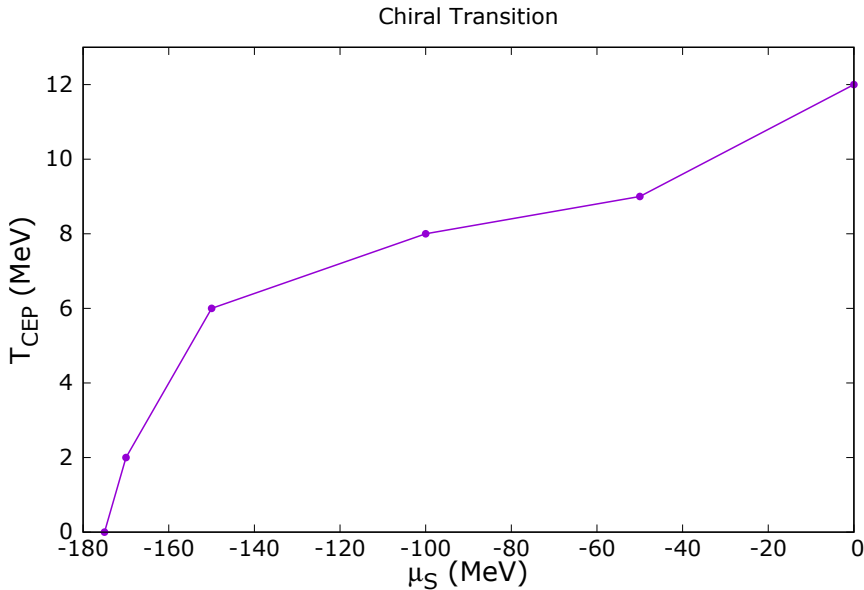
FIGURE 2.24: Critical end-point temperature, for the chiral transition, as a function of μ_S.

In Fig. 2.24, the critical end-point temperature is plotted as a function of μ_S. As expected, a considerable, gradual decrease in T_{CEP} is observed, with an increase in the magnitude of μ_S. This re-emphasises the fact that the strangeness-chemical potential directly affects the LG and chiral transitions. The hadronic phase is dominated by hyperons, as μ_S increases

in magnitude, suppressing other baryons and resulting in an early onset of both light ($u-$ and $d-$) and strange quarks; which go on to become a quark state at high densities.

This model investigation of quark-hadron systems shows that the QCD phase diagram can be significantly affected by a non-zero strangeness-chemical potential, changing the chiral transition from a first-order to a smooth crossover. The critical end-point in this model appears at low temperatures, which makes such an effect difficult to be directly observed in heavy-ion collisions, but it could have an impact in the higher-temperature smooth transition region as well. Another strangeness-enriched situation is the beta-equilibrated matter in a neutron star, which is investigated in the next chapter, following Mukherjee et al., 2017.

Chapter 3

Neutron Stars

We explored the properties of isospin-symmetric nuclear matter, with the QχP model, in the previous chapters. In this chapter, we intend to apply the model to neutron stars. But before we do that, a brief introduction to neutron stars; adapted from Dexheimer, 2009; is in order.

3.1 A brief introduction

The matter inside neutron stars is isospin-asymmetric, i.e., it has many more neutrons than protons. This asymmetry is controlled by the isovector mesons δ and ρ which are crucial to neutron star calculations. Neutron stars are also charge neutral:

$$\sum_i \rho_{B_i} Q_i = 0 \ , \tag{3.1}$$

where ρ_B is the number density and Q the electric charge of the different baryonic and leptonic species i. The number density is given by:

$$\rho_{B_i} = \int d\rho_{B_i} = \int \frac{g}{(2\pi\hbar)^3} f_i d^3 k \ , \tag{3.2}$$

where:

$$\frac{d\rho_{B_i}}{d^3 k} = \frac{g}{(2\pi\hbar)^3} f_i \ , \tag{3.3}$$

with g being the number of states of a particle with momentum k, f being the distribution function, and $(2\pi\hbar)^3$ being the unit volume of a cell in phase space.
The distribution function is defined as:

$$f_i = \frac{1}{e^{\left(E_i^* - \mu_i^*\right)/k_B T} + 1} \ , \tag{3.4}$$

where $E_i^*(k) = \sqrt{k^2 + m_i^{*2}}$ is the energy and $\mu_i^* = \mu_i - g_{i\omega}\omega - g_{i\phi}\phi - g_{i\rho}\tau_3\rho$ is the chemical potential of the different species modified by the medium and k_B is the Boltzmann constant.

The chemical equilibrium conditions determine the particle composition at each layer of the star; and due to the strangeness S being unconstrained as a consequence of the large time-scales associated with a neutron star's evolution; the only remaining conserved charges are the baryon-number, $\sum_i B_i = B = \text{constant}$, and the electric charge, $\sum_i Q_i = 0$. Therefore, the total chemical potential, for any particle, can be written as:

$$\mu_i = B_i \mu_B + Q_i \mu_Q \ ; \tag{3.5}$$

where μ_B is the baryochemical potential and μ_Q is the charge- (a.k.a. electron-) chemical potential.

Contrary to isospin symmetric nuclear matter in HIC's, neutron stars are massive objects; where the influence of gravity on the evolution and composition of the system can not be ignored. For stable, non-rotating neutron stars, the stability is ensured by the hydrostatic equilibrium between the inward gravitational pull and the outward neutron degeneracy pressure, expressed mathematically as:

$$dF_G = dF_P \ , \tag{3.6}$$

where F_P is related to the pressure P as $dF_P = dPdA$; with A being the surface area; and F_G is related to the mass M as $dF_G = -\frac{MdM}{r^2}$. The mass of the star is given by:

$$M = \int_0^r \rho dV = \int_0^r \rho 4\pi r^{'2} dr^{'} \ , \tag{3.7}$$

where ρ is the density and r is the radius of the star. Combining Eqns. (3.6) and (3.7); and using the expressions for $dV = r^2 dr \sin\phi d\phi d\theta$ and $dA = r^2 \sin\phi d\phi d\theta$ in spherical polar coordinates; we can write:

$$\frac{dP}{dr} = -\frac{M\rho}{r^2} \tag{3.8}$$

which, when relativistic effects are taken into account, yields the Tolman-Oppenheimer-Volkoff (TOV) equations (Oppenheimer and Volkoff, 1939; Tolman, 1939):

$$\frac{dP}{dr} = -\frac{M\rho}{r^2} \left(1 + \frac{P}{\varepsilon} \right) \left(1 + \frac{4\pi r^3 P}{M} \right) \left(1 - \frac{2M}{r} \right)^{-1} \ , \tag{3.9}$$

where ε is the energy density. We use the QχP model EoS, in conjunction with these TOV equations, to produce the results in Sec. 3.3.

3.2   Modifying the QχP

A slight modification to the model is required in order for it to be applicable to isospin-asymmetric matter in a way that produces an EoS which, consequently, gives a reasonable value for the symmetry energy. As has been pointed out in Horowitz and Piekarewicz, 2002; Dexheimer, Negreiros, and Schramm, 2015 (and references therein) and discussed

in general in Schramm, 2003, a coupling term between the ω and ρ mesons leads to a reduced value of the slope parameter of the symmetry energy. Without this coupling, the slope parameter is close to a value of 100 MeV, which is rather large compared to current estimates. We introduce such a term in the model as:

$$V_{\omega\rho} = \beta\omega^2\rho^2 \ . \tag{3.10}$$

k_0 $(242.61 \text{ MeV})^2$	k_1 4.818	k_2 -23.357
k_6 $(0.276)^6 \text{ MeV}^{-2}$	ε $(75.98 \text{ MeV})^4$	$g_\sigma^{1,1}$ -8.239296
$g_{N\rho}$ 4.55	δm_q 6	δm_s 150
$g_\sigma^{1,8}$ -0.936200	α_σ^1 2.435059	$g_{N\omega}$ 5.45
$g_{q\sigma}$ 2.5	$g_{s\zeta}$ 2.5	β 900

TABLE 3.1: Modified model parameters: the SU(3) couplings $g_\sigma^{1,1}$, $g_\sigma^{1,8}$ and α_σ^1 determine the baryonic coupling strengths $g_{\sigma i}^{(1)}$ and $g_{\zeta i}^{(1)}$ as in Papazoglou et al., 1999.

For the sake of simplicity, we did not add this term in an SU(3) invariant way, although it is possible to do so in principle. This is reasonable because the strange-vector field necessary for the invariance, ϕ, is effectively zero, as no hyperons occur in the system at relevant densities. The modified parameters are summarised in Table 3.1.

3.3 Results for isospin-asymmetric, strange nuclear matter

In this section, in order to investigate neutron stars, i.e., highly isospin-asymmetric matter, we first determine the basic isospin-dependent coefficients around the nuclear matter saturation density (ρ_0).

3.3.1 Isospin-asymmetric matter

To that end, we calculate the value of the isospin-asymmetry energy S_v, given by:
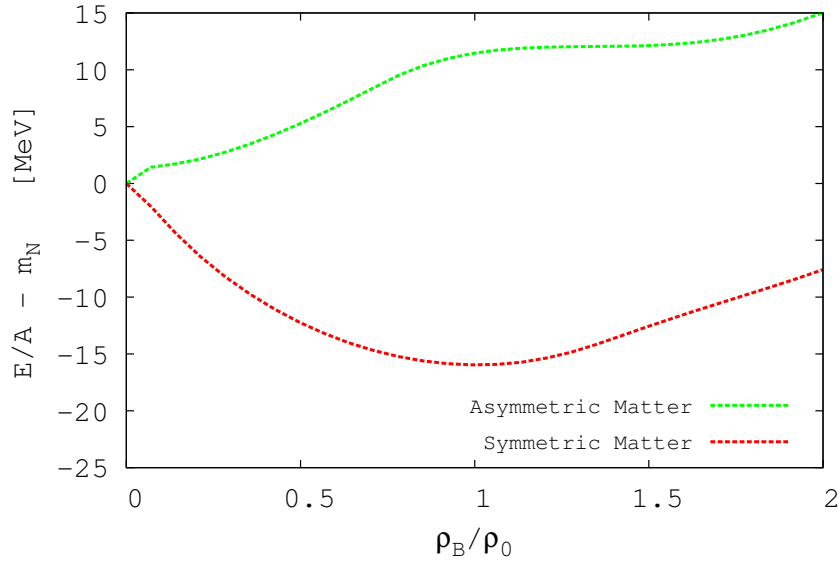
FIGURE 3.1: Binding energies for symmetric and asymmetric nuclear matter, as functions of the baryon-number density, which is normalised to nuclear matter saturation density ρ_0.

$$S_v = \frac{1}{8} \left[\frac{d^2(\varepsilon/\rho_B)}{d(I_3/B)^2} \right]_{\rho_B = \rho_0} , \tag{3.11}$$

where ε is the energy density, ρ_B the baryon-number density, I_3 the isospin 3-component, and B the net baryon-number. The density dependence of S_v is usually parametrized by the slope parameter:

$$L = 3\rho_0 \left[\frac{dS}{d\rho_B} \right]_{\rho_B = \rho_0} . \tag{3.12}$$

Using our model, we obtain $S_v = 30.02$ MeV and $L = 56.86$ MeV; which are in agreement with ranges of L and S_v obtained from various experiments and analyses (Lattimer and Lim, 2013).

The binding energy per baryon of asymmetric star matter is shown in Fig. 3.1. In this case, the energy is determined self-consistently by the imposition of electric charge neutrality and chemical equilibrium, including free, charged leptons. In addition, we show the square of the speed of sound for star matter in Fig. 3.2. It is calculated from our equation of state as:

$$c_s^2 = dP/d\varepsilon|_{T=0} , \tag{3.13}$$

where P is the pressure and ε the energy density. The sharp decrease in the speed of sound around $\rho_B \approx 3\rho_0$ signals the appearance of the parity partner, N^{*0}, of the neutron, as it starts to be populated. The smaller sharp decrease in the speed of sound just before $\rho_B \approx 2\rho_0$ signals the appearance of the down quarks, although only a few quarks contribute
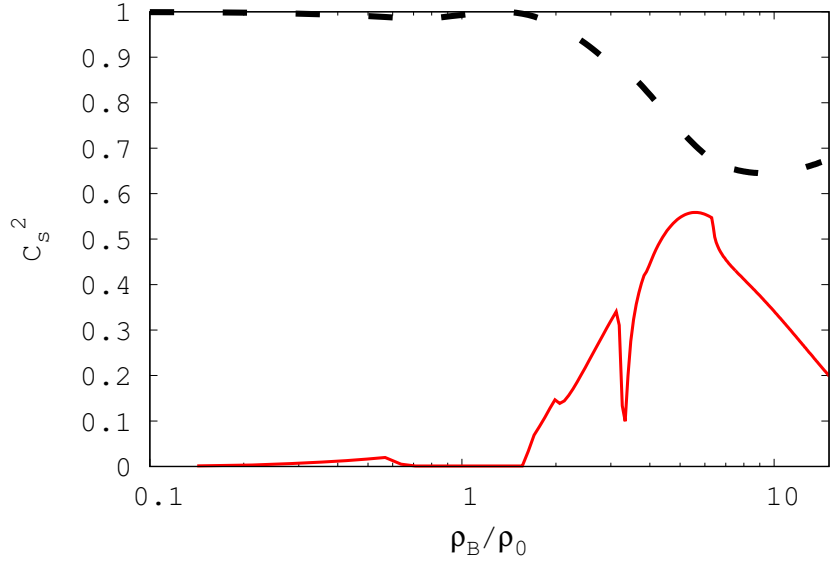
FIGURE 3.2: Speed of sound squared as a function of normalised baryon-number density (on a logarithmic scale), with the dashed, black line representing the kinetic-theory-bound on c_s^2 (cf. Moustakidis et al., 2017).
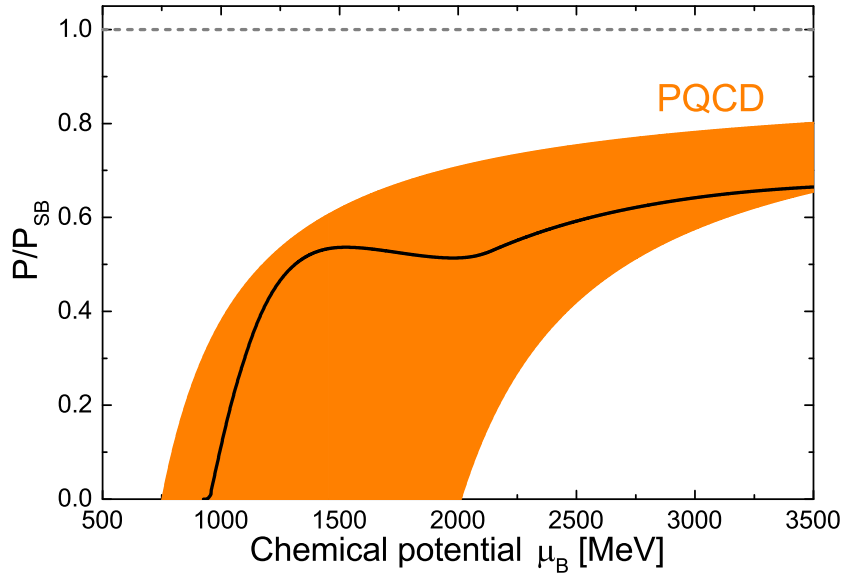
FIGURE 3.3: Comparison between the pressure, normalised to the Stefan-Boltzmann pressure, P/P_{SB} obtained from QχP (Mukherjee et al., 2017) and PQCD calculations (Fraga, Kurkela, and Vuorinen, 2014).

to the particle cocktail at low density. Fig. 3.2 also shows that, in our model, the speed of sound never crosses the boundary established by kinetic theory (Moustakidis et al., 2017):

$$\frac{c_s^2}{c} = \frac{\varepsilon - P/3}{\varepsilon + P}. \tag{3.14}$$

In addition, for very large densities, our speed of sound remains around $\sqrt{1/3}$, as expected. The pressure of star matter, divided by the Stefan-Boltzmann pressure (ideal-gas limit), as a function of baryo-chemical potential is shown in Fig. 3.3. We compare our results with star-matter, perturbative-QCD (PQCD) calculations at zero temperature from Fraga, Kurkela, and Vuorinen, 2014, which can be considered a constraint on the high density QCD equation of state (cf. Kurkela et al., 2014). Our EoS falls inside the band in Fig. 3.3, which represents their uncertainty estimates. One should note, however, that the agreement of our model with the PQCD result gets worse for very large values of chemical potential. This is because we have assumed the quark mass parameter (m_{0q} in Eqn. (2.8)) to remain constant for all densities. In reality, we expect that, as the dilaton field melts slowly at large values of chemical potential, the quark mass also slowly approaches the current quark mass value, i.e., the quark mass parameter should vanish. Thus, for high values of the chemical potential, our model shows a rise in pressure that is too slow near the Stefan-Boltzmann limit.

In order to better understand the chemical composition of our asymmetric EoS, we determined the corresponding particle populations. Fig. 3.4 shows the number densities of various particle species normalised to the total baryon-number, where quark number densities are divided by 3. At low densities, as expected, we only observe neutrons. An increase in density is followed by the appearance of protons, leptons and, soon after, down-quarks. Later, the up-quarks start appearing, followed by the chiral partner of the neutrons. The latter appears rather suddenly and causes the rapid decrease of the speed of sound mentioned earlier (cf. Fig. 3.2). Finally, the chiral partner for the protons, and afterwards the strange quarks, appear. Although the hyperons are included in the model, they are completely absent from the particle cocktail shown in Fig. 3.4. The chiral partners of the nucleons have lower masses than the hyperons and owing to the crossover formalism, quarks can also appear very early. In addition, the hyperons are suppressed by the appearance of the other light quark states through the excluded volume formalism. Eventually the strange quarks appear in the cocktail, however, only at much higher densities.

As we have already mentioned, the isospin asymmetry of charge neutral and chemically equilibrated matter is self-consistently determined. In this case, we show in Fig. 3.5 how the pressure to energy density ratio P/ε changes as a function of isospin per baryon, which is defined as:

$$\frac{I_3}{B} = \sum_i \frac{(I_3)_i \rho_i}{\rho_B} \ , \tag{3.15}$$

and the normalised baryon density. The colours in the figure show regions where the pressure is positive (red) and negative (blue). All the unstable and meta-stable states of the nuclear liquid-gas transition fall into the blue region at small baryon-number densities.
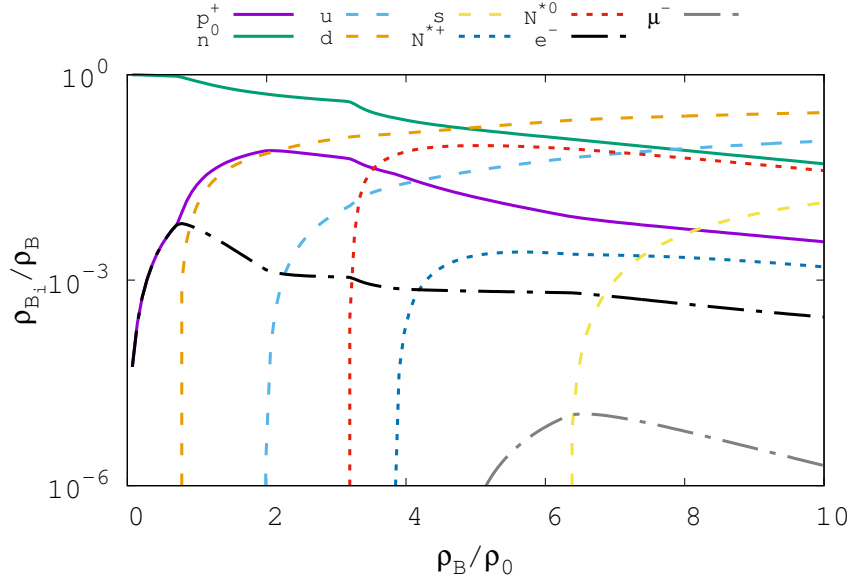
FIGURE 3.4: Normalised baryon-number densities of various particle species as functions of the normalised baryon-number density.
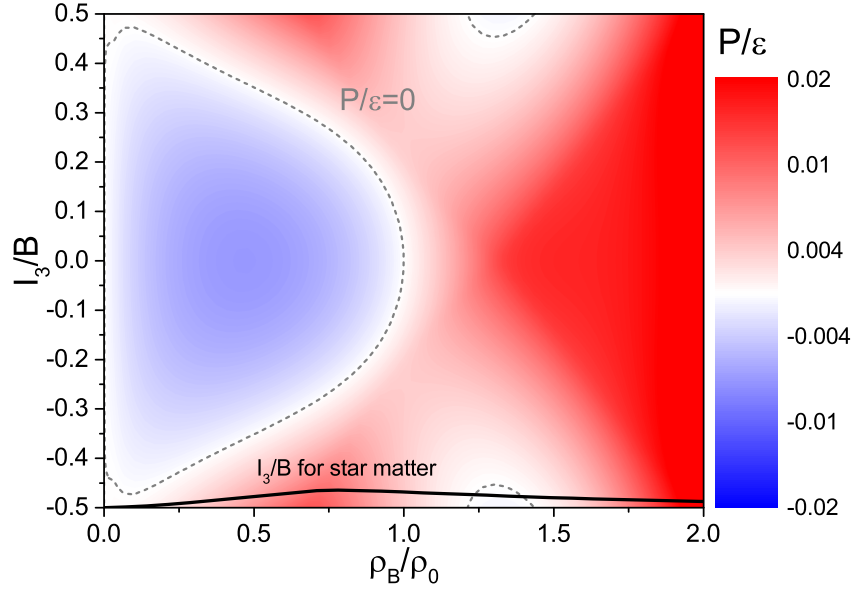

FIGURE 3.5: Contour plot of the ratio P/ε on a normalised $I_3 - \rho_B$ plane, showing regions of stability in red and those of instability in blue. The bold, black line represents the isospin-per-baryon for charge-neutral and chemically equilibrated matter .

We also observe small regions, both at large and small values of isospin-per-baryon, where the pressure decreases as function of density, or in other words, where the speed of sound

becomes imaginary and matter becomes mechanically unstable. This region corresponds to the spinodal region of a first-order phase transition, which appears only for large isospin asymmetries. The bold, black line corresponds to the EoS of neutron star matter, where the isospin per baryon is fixed by condition of beta-equilibrium.

3.3.2   The M-R diagram, rotating NS's and compactness

In order to describe neutron stars we make use of a Maxwell construction around the first-order phase transition to avoid thermodynamic instabilities, i.e., we guarantee that the pressure increases as a function of energy density in our EoS. We also add a standard result for the crust to our EoS, originally calculated by Baym, Pethick, and Sutherland, 1971. The mass-radius diagram for the resulting compact stars, as shown in Fig. 3.6, is determined using TOV equations for a range of central pressures. The most massive star of the family has a mass of 1.98 $M_\odot$ ($M_\odot$ = the solar mass) and a radius of 10.25 km. The canonical 1.4 $M_\odot$ star has a radius of 11.10 km. This radius value, which is small for models of hybrid or other exotic matter, is in agreement with a number of observational studies, particularly of low-mass X-ray binaries that point to small neutron star radii in the range of about 9 km to 11 km (Guillot et al., 2013; Guillot, Rutledge, and Brown, 2011; Ozel and Freire, 2016; Ozel and Psaltis, 2015). Since most of the stellar cores we reproduce contain some amount of quarks, we choose to mark the stars from the family that contain 20%, 25%, and 30% of baryon mass coming from quarks (blue dots in Fig. 3.6). For the most massive star of the family 35% of its baryon mass is generated by quark matter.

When we include rotation effects, Fig. 3.8 shows how the stellar maximum mass increases as a function of rotational frequency in two cases, keeping a fixed central pressure or the number of baryons in the star. In the second case, we describe the evolution of an isolated star, as the frequency of rotation decreases over time, which has a Kepler frequency of 1606 Hz. Here, we considered monopole and quadrupole corrections to the metric due to the rotation, as was derived in Glendenning and Weber, 1994. The higher the rotational frequency, the more massive and larger the stars become. The increase in mass of the most massive star of the family is about 5% for a star with fixed baryon-number rotating at its Kepler frequency (compared to a non-rotating star). This kind of calculation differs by about 1% from full general relativity results from Stergioulas and Friedman, 1995.

Usually, the effect of rotation in hybrid stars is to suppress their quark phase (cf. Wei et al., 2017 for a recent discussion on the topic). A phase transition to deconfined matter can only take place when heavy stars spin down and their central densities increase. In our case, the situation is different because the quarks occupy a fraction of almost all stars, heavy and light, that rotate with any allowed frequency and only the quark fraction (compared to hadrons) increases as the stars spin down.
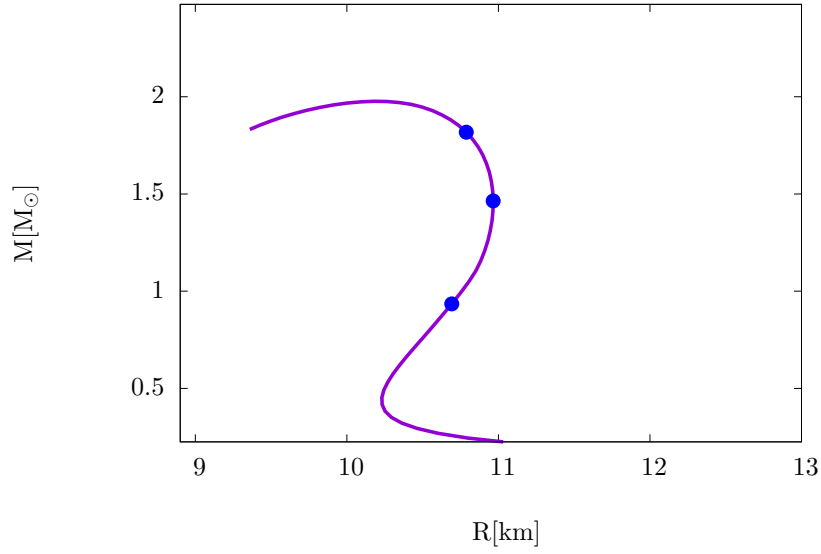
FIGURE 3.6: Mass-radius diagram. The blue dots indicate stars with a fraction of 20%, 25%, and 30% of the baryon mass coming from quarks.
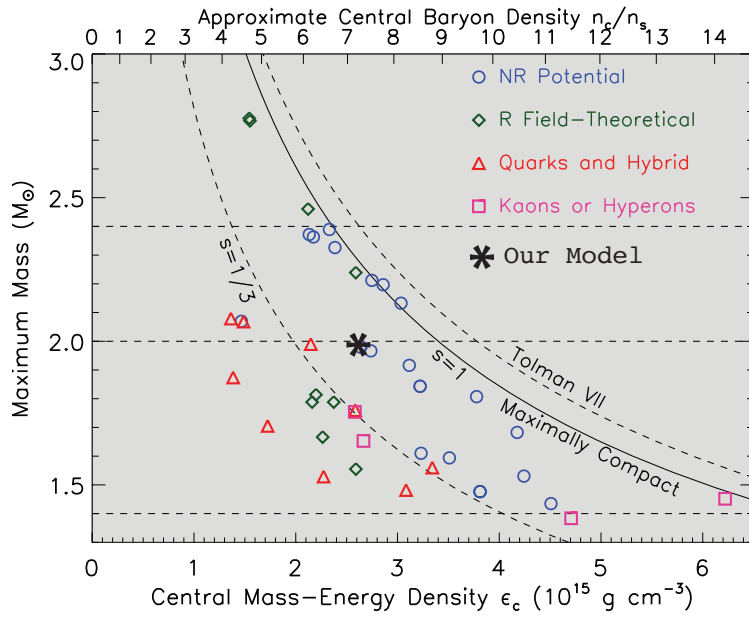

FIGURE 3.7: Compactness (stellar mass vs. central density) of the most massive star generated by the QχP EoS.
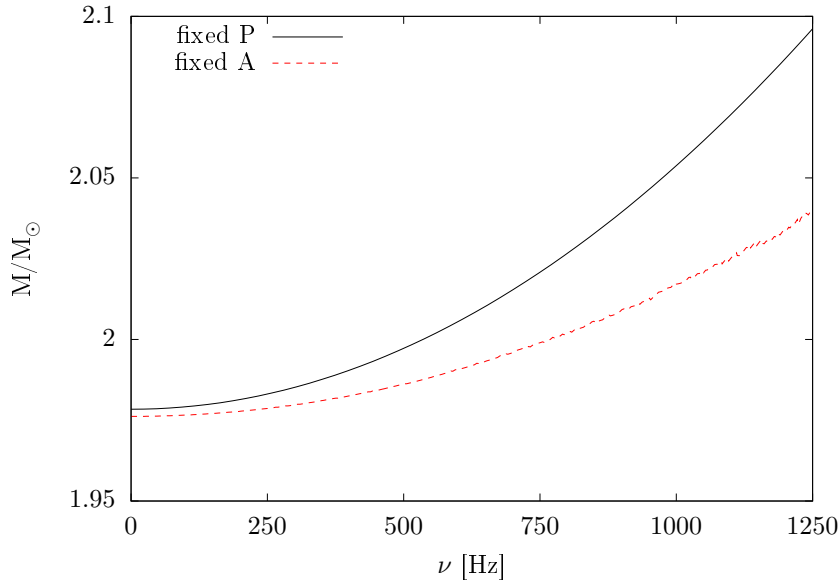
FIGURE 3.8: Mass of the most massive star of the family as a function of rotational frequency. The two cases correspond to a fixed central pressure (bold, black) and a fixed number of baryons (dotted, red) in the star.

The term "compactness" refers to how packed together matter is in a star. Our QχP equation of state is shown in Fig. 3.7 together with other equations of state calculated using non-relativistic models, relativistic models, models containing quarks, and models containing strange hadrons. It is interesting to see that the star we generate is very compact, and is more compact than all the massive exotic stars shown in the figure. Naturally, the maximum-mass star we reproduce is between the line that represent EoS with constant speeds-of-sound, equal to $\sqrt{1/3}$ or 1.

Concerning star cooling, our EoS does not allow the hadronic direct Urca process. This is the case because, although a large fraction of the star core contains nucleons and their parity partners, there are not enough electrons to complete the reactions. For a more detailed study of the role of chiral partners in neutron star cooling, see Lattimer, 2012. For quarks, we assumed that all flavours are paired and as such the quark direct Urca process is heavily suppressed (Blaschke, Voskresensky, and Grigorian, 2006; Page, Geppert, and Weber, 2006; Alford et al., 2005; Negreiros, Dexheimer, and Schramm, 2012). The absence of the direct Urca process is a large advantage of our EoS, as it prevents the enhanced cooling of heavy stars, as discussed in Page et al., 2004; Negreiros, Schramm, and Weber, 2013.

An important outcome of this section is that we have at hand a single model for the description of hybrid stars with a hadronic and a quark phase. The properties of the EoS are different from most simpler models, which usually incorporate the phase transition from a hadronic to a quark phase through an artificial construction. However, we present a hybrid EoS that leads to more compact stars and still allows for a large quark fraction, while not forbidding the appearance of hyperons.

The application of the QχP EoS to dynamic simulations for HIC can be used to study observables for the QCD phase transition in isospin symmetric matter. At the same time, numerical studies of neutron-star mergers can be conducted with the same model EoS in a consistent manner. This enables us to study nuclear matter in very different environments and in systems of vastly different scales using a single EoS; as shown in Sec. 3.4.

3.4 NS mergers and the Taub adiabat

As seen in the previous sections, the properties of elementary matter at high temperatures ($T \approx 100$ MeV) and densities ($\rho \approx 3\rho_0$) can be studied in two different physical scenarios: in high energy heavy ion collision experiments; where we try do determine the phase structure of the isospin-symmetric QCD EoS, and in computer simulations of binary neutron star mergers; where the knowledge of the isospin-asymmetric QCD EoS is required. These two different fields of physics, *viz.* elementary particle physics and astrophysics, combine when two neutron stars collide. It is therefore possible to study the properties of dense QCD for systems of different size, time-scales and chemical composition. By studying the properties of this QCD matter in a single, consistent approach; we can address one of the most relevant challenges of high-energy nuclear theory: the determination of the properties and phase structure of QCD at large densities and temperature. But, before attempting to do that, a short recapitulation of neutron star mergers, black hole mergers and recent LIGO detector results are in order.

3.4.1 The set-up

Gravitational waves (GW's) have been recently observed from a pair of merging black holes (BH's) by the LIGO detectors (Abbott et al., 2016b; Abbott et al., 2016a) and from merging neutron star binaries in the GW170817 event. The main difference between the GW's originating from a merger of two BH's and those originating from a merger of two NS's, is the possibility of an existence of a post-merger phase after the collisions of the two objects: it can only be present in the case of NS mergers. Depending on a variety of parameters, e.g. the initial mass of the two stars, the product right after the merger could be a prompt collapse to a BH, a meta-stable hyper-massive NS or a stable supra-massive NS. The GW's produced by a merger of NS's are by far more interesting than the GW's resulting from a BH-merger, as, in the case of the existence of a post-merger phase, the EoS of elementary matter might be deduced by a frequency analysis of the GW (Rezzolla and Takami, 2016; Takami, Rezzolla, and Baiotti, 2015; Takami, Rezzolla, and Baiotti, 2014). This is insofar interesting, as the EoS until now is mainly understood by high energy heavy ion collisions and only coarse constraints are available from astrophysical observations, like the current observational constraint on the observed maximum mass in neutron stars, i.e., 2.01 ± 0.04 M$_\odot$ (Antoniadis et al., 2013). In the subsequent section, following Hanauske et al., 2017, we compare the results of numerical simulations of merging NS binaries with simulations of high energy heavy ion collisions. In the cited study, we also discuss how
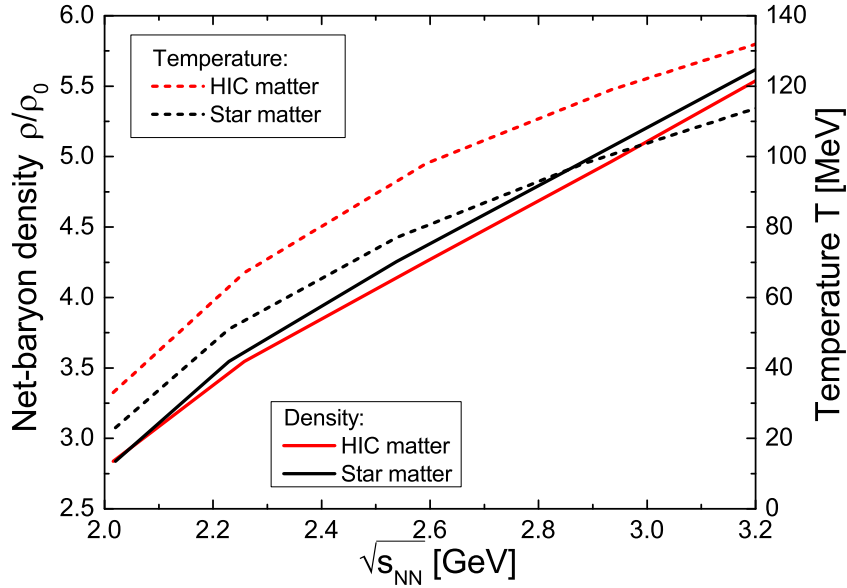
FIGURE 3.9:   Largest net-baryon density (solid lines) and temperatures (dashed lines) achieved in collisions of heavy ions and compact stars at a given centre of mass beam energy $\sqrt{s_{\mathrm{NN}}} = 2 \cdot \gamma_{\mathrm{c.m.}} \cdot m_N$. To calculate the densities and temperatures, we used the Taub Adiabat with the $\mathrm{Q}\chi\mathrm{P}$ EoS. Due to the different properties of the EoS as function of isospin, the temperatures in heavy ion collisions are larger and densities slightly smaller, at the same relative velocities.

one can create a similar state of hot and dense nuclear matter in two seemingly different "experimental" set-ups.

3.4.2   Results from the Taub adiabat

As seen in Hanauske et al., 2017, the densities created in the mergers of compact stars can exceed several times the nuclear ground state density. Furthermore, we have shown that in the early time of the merger, high temperatures ($T \leq 100$ MeV) are obtained. We know that similar densities and temperatures can be created in the relativistic collisions of heavy nuclei at different particle accelerators.

The properties of the QCD EoS are the links connecting the neutron star mergers and relativistic nuclear collisions. Consequently, the goal of such studies has to be to find a description for the EoS that is able to describe neutron star merger and nuclear collision observables and therefore establish the connection. It is, thus, very important to employ a model that produces an EoS that entails a realistic set of degrees of freedom, as well as interactions. The $\mathrm{Q}\chi\mathrm{P}$ model is highly qualified for studying said properties since, within the same parameter set we can use this model to calculate the EoS and chemical properties of QCD matter, as evident from the earlier chapters. A straightforward way of connecting
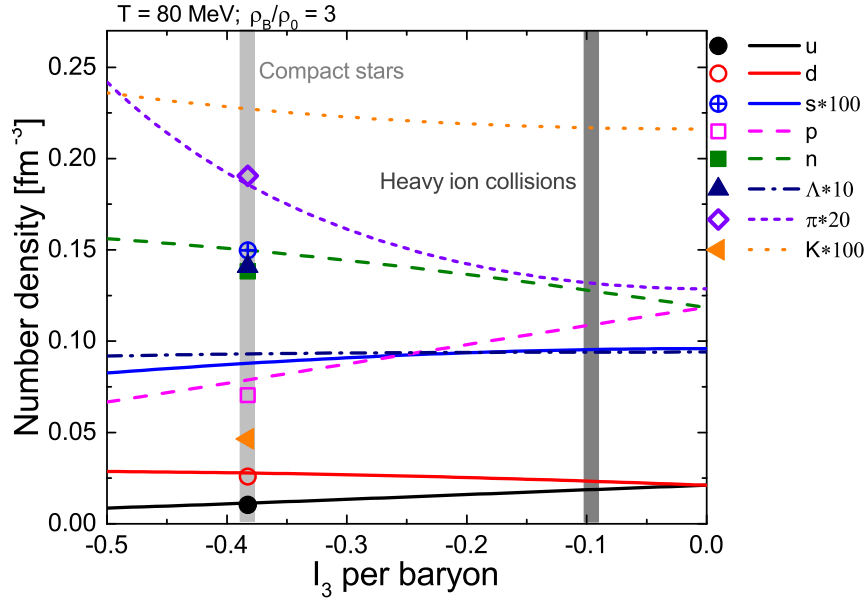
FIGURE 3.10: Number densities of different hadronic and free quark species (re-scaled for visibility) as functions of the isospin per baryon at a fixed temperature T=80 MeV and net-baryon density $\rho = 3\rho_0$. The lines correspond to matter with conserved net strangeness, as expected for heavy-ion collisions, while the symbols represent results where the matter is in β-equilibrium (as expected for neutron star matter).

the features of the EoS with the maximally achievable compression of a relativistic collision is by employing the so called Rankine-Hugoniot-Taub Adiabat (Taub, 1948; cf. Appendix B for more details).

The Taub adiabat is essentially a shock wave solution for two colliding infinite slabs of matter. If the EoS, i.e. the connection between pressure, energy density and baryon density is known (as $p(\epsilon, \rho)$), then one can calculate the maximum compression in a collision by solving the following Taub-equation:

$$(\rho_0 \cdot X_0)^2 - (\rho \cdot X)^2 - (p_0 - p)(X_0 + X) = 0 \qquad (3.16)$$

where $X = (\epsilon + p)/\rho^2$, is the generalised volume. For simplicity we assume $p_0 = 0$.

One can furthermore connect the centre of mass gamma factor $\gamma_{\text{c.m.}}$ of the colliding slabs to the densities created using:

$$\gamma_{\text{c.m.}}^2 = \left(\frac{\epsilon \, \rho_0}{\rho \, \epsilon_0}\right)^2 \qquad (3.17)$$

The resulting beam energy dependence of the net-baryon density and temperatures reached is shown in Fig. 3.9 for two different scenarios:

1. the EoS for heavy ion collisions, with conserved strangeness and no beta-equilibrium and

2. the EoS for compact stars, in beta-equilibrium.

We observe that the densities and temperatures achieved in this consistent approach to be similar to those discussed earlier. We also observe, from Fig. 3.10, that the maximum density compression is independent of the chemical composition of the system. Another important observation is that the density compression is independent of the isospin content, i.e., it is very similar in isospin-symmetric matter and NS matter, but the actual temperature is quite different. This difference is a result of the additional degrees of freedom; *viz.* the leptons in beta equilibrium and the non-conserved strangeness; which decrease the temperature at a given compression. It also highlights the importance of employing a consistent and realistic temperature-dependent EoS for the description of NS matter; an EoS that can be used in full 3+1D fluid dynamical simulations of heavy ion collisions (cf. Chap. 4). The ultimate goal of these calculations is to find observables for a (non-equilibrium) first-order phase transition in dense QCD matter (Steinheimer and Randrup, 2012).

Chapter 4

Relativistic Heavy-ion Collisions

Through the study of the beam energy dependence of various observables in a heavy-ion collision (HIC), one hopes to find unambiguous signals for the appearance of a phase transformation of hadrons to their quark and gluon constituents. It is very important to ascertain the order of the phase transition at large densities experimentally. To this end, a focus has been put on possible observables for a phase transition and the associated critical end-point: the fluctuations of conserved charges (Gupta et al., 2011; Luo and Xu, 2017; Herold et al., 2016; Wang and Yang, 2012; Karsch and Redlich, 2011a; Schaefer and Wagner, 2012; Chen et al., 2011; Fu, Liu, and Wu, 2010; Cheng et al., 2009). As explained earlier, in a grand canonical thermodynamic ensemble, the cumulants of the net-charge distribution functions should diverge at the critical point of the phase transition, due to the divergence of the correlation length. It was therefore suggested, that the measurement of the net-proton-number fluctuations; as a proxy for the net-baryon-number fluctuations; in a fixed rapidity interval could reveal the onset of deconfinement and/or the critical endpoint of QCD. The measured rapidity interval has to be much smaller than the total systems rapidity width and larger than the correlation length (Jeon and Koch, 2000; Koch, 2010). However, the system created in heavy-ion collisions can hardly be treated as a grand canonical system in thermal equilibrium, thus the measured cumulants are also affected by other aspects of the dynamical evolution, many of which have been discussed in recent literature (Bzdak and Koch, 2012; Bzdak, Holzmann, and Koch, 2016; Kitazawa, 2016; Feckova et al., 2015; Begun et al., 2004; Bzdak, Koch, and Skokov, 2013; Gorenstein et al., 2009; Gorenstein and Gazdzicki, 2011; Sangaline, 2015; Tarnowsky and Westfall, 2013; Xu, 2014; Adamczyk, 2014a; Adamczyk, 2014b). The systems created in these nuclear collisions are very small, rapidly expanding and therefore a detailed understanding and interpretation of the measured moments is difficult due to uncertainties in the centrality determination, efficiency corrections and acceptance cuts. To address these experimental uncertainties one employs models to simulate the dynamical expansion of the system created in the heavy ion collision.

There are two main approaches: a fluid dynamical (or interchangeably, hydrodynamical) description and/or a microscopic transport description. The fluid dynamical description has the advantage that any equation of state can be easily introduced and effects of spinodal decomposition due to a phase transition can be described in a controlled manner (Steinheimer and Randrup, 2012; Chomaz, Colonna, and Randrup, 2004; Randrup, 2004;

Sasaki, Friman, and Redlich, 2007a). On the other hand, thermal fluctuations, which are an important ingredient for the formation of critical fluctuations near the critical endpoint (Stephanov, Rajagopal, and Shuryak, 1998; Stephanov, 2009; Koch, 2010), as well as the production of discrete particles from the fluid (Steinheimer and Koch, 2017) cannot be easily introduced.

Alternatively, one can use a microscopic transport model, which naturally includes thermal fluctuations and usually describes the evolution of discrete particles. On the downside, it is very challenging to introduce the dynamics of a phase transition and critical point in such a transport approach. Especially a change of the effective degrees of freedom, as expected at the deconfinement transition, is not easily introduced in a consistent manner. Brief introductions to both ideal hydrodynamics (adapted from Jaiswal and Roy, 2016; Romatschke and Romatschke, 2017 and references therein) and basic microscopic transport models (adapted from Steinheimer-Froschauer, 2011) are provided in the following sections.

4.1   A brief introduction to hydrodynamics

In order to handle the rapid temporal evolution of a system of strongly-interacting matter formed in high-energy heavy-ion collisions; close to equilibrium; a formulation of hydrodynamics, based on the special theory of relativity is required. This formulation is called the ideal relativistic fluid dynamics. It is a macroscopic description of an ideal fluid, where it is assumed that the microscopic variables fluctuate so rapidly with space-time, that only their average values are relevant at a macroscopic scale. The conserved quantities, however, vary much more slowly and play an important role in the effective description of the system; at the long-wavelength and low-frequency limit of its underlying microscopic dynamics.

An ideal fluid is defined as a continuous system of infinitesimal volume elements, each of which are assumed to be very close to thermodynamic equilibrium. Thus, in the neighbourhood of each point in space, these infinitesimal volumes - called fluid elements - are defined with the matter in them assumed to be homogeneous i.e., without any spatial gradients, and consequently, can be described by thermodynamic variables. Mathematically, for each space-time coordinate of the fluid, $x \equiv x^\mu$; a temperature $T(x)$, a chemical potential $\mu(x)$ and a collective four-velocity field $u^\mu(x) \equiv dx^\mu/d\tau$ can be assigned to the fluid element; where the proper time τ is defined as:

$$(d\tau)^2 = g_{\mu\nu}dx^\mu dx^\nu = (dt)^2[1 - (\mathbf{v})^2] \ , \tag{4.1}$$

with $\mathbf{v} \equiv d\mathbf{x}/dt$ and $g^{\mu\nu}$ being the metric tensor:

$$g^{\mu\nu} = \begin{pmatrix} 1 & 0 & 0 & 0 \\ 0 & -1 & 0 & 0 \\ 0 & 0 & -1 & 0 \\ 0 & 0 & 0 & -1 \end{pmatrix} = \mathrm{diag}(1, -1, -1, -1) \ . \tag{4.2}$$

The state of such an ideal fluid can be completely specified by the densities and currents associated with the conserved quantities: energy, momentum and net particle-number. In

the relativistic case, the energy-momentum tensor $T^{\mu\nu}$ and the net particle four-current N^μ become the state variables. In the local rest-frame (LRF), with $\mathbf{v} = 0 \implies u^\mu = (1, \mathbf{0})$, they can be written as:

$$
\begin{aligned}
T_{\text{LRF}}^{00} &= \epsilon &,\quad T_{\text{LRF}}^{ij} &= \delta^{ij} P \ , \\
N_{\text{LRF}}^0 &= n &,\quad \mathbf{N}_{\text{LRF}} &= 0 \ , \\
S_{\text{LRF}}^0 &= s &,\quad \mathbf{S}_{\text{LRF}} &= 0 \ ,
\end{aligned}
\tag{4.3}
$$

with δ^{ij} being the Kronecker delta, s being the entropy, ϵ being the energy density and P being the pressure.

The state variables are built out of the hydrodynamic tensor degrees-of-freedom: u^μ and $g^{\mu\nu}$. Since, for an ideal (or, zeroth-order) fluid, $T_{(0)}^{\mu\nu}$ needs to be symmetric and transform as a tensor, while $N_{(0)}^\mu$ and $S_{(0)}^\mu$ need to transform as vectors under Lorentz transformations, one can write, in the most general form:

$$
T_{(0)}^{\mu\nu} = a_1 u^\mu u^\nu + a_2 g^{\mu\nu} \ , \ N_{(0)}^\mu = a_3 u^\mu \text{ and } S_{(0)}^\mu = a_4 u^\mu \ .
\tag{4.4}
$$

Combining Eqns. (4.3) and (4.4), the coefficients turn out to be:

$$
a_1 = \epsilon + P \ , \ a_2 = -P \ , \ a_3 = n \text{ and } a_4 = s \ .
\tag{4.5}
$$

For the dynamics of an ideal fluid, the conservation laws can be used; in the absence of sources:

$$
\nabla_\mu T_{(0)}^{\mu\nu} = 0 \ , \ \partial_\mu N_{(0)}^\mu = 0 \ ;
\tag{4.6}
$$

where ∇_μ is the covariant derivative; along with the short-hand notations:

$$
D \equiv u^\mu \nabla_\mu \ , \ \Delta^{\mu\nu} = g^{\mu\nu} - u^\mu u^\nu \ , \ \theta^\alpha \equiv \Delta^{\alpha\mu} \nabla_\mu \ ,
\tag{4.7}
$$

and Eqns. (4.3) - (4.5) to give the equations of motion:

$$
\begin{aligned}
D\epsilon + (\epsilon + P)\theta_\mu u^\mu &= 0 \ , \\
(\epsilon + P)Du^\alpha + c_s^2 \theta^\alpha \epsilon &= 0 \ , \\
Dn + n\partial_\mu u^\mu &= 0 \ ;
\end{aligned}
\tag{4.8}
$$

where

$$
c_s(\epsilon) = \sqrt{\frac{\partial P(\epsilon)}{\partial \epsilon}} \ ,
\tag{4.9}
$$

also known as the speed of sound; is a zeroth-order transport coefficient.

With the four fields - ϵ , P , n and u^μ - corresponding to six degrees-of-freedom, and the conservation laws providing only five equations of motion, another equation is required

to close this set of equations and determine the value of the transport coefficient. That equation, relating the pressure of the fluid to other thermodynamic quantities $P = P(n, \epsilon)$, is called the Equation of State (EoS) and is derived, as a parametric relationship, from the underlying microscopic theory of strong interactions. The numerical scheme used to solve Eqns. (4.8) is the SHASTA algorithm (Rischke, Bernard, and Maruhn, 1995; Rischke, Pursun, and Maruhn, 1995; Petersen et al., 2008), which is part of the UrQMD algorithm, based on the UrQMD hybrid model, explained below.

4.2 A brief description of the UrQMD hybrid model

A relativistic HIC can be generally split into three, relatively distinct, phases:

1. An initial pre-equilibrium phase:
   Beginning in the immediate aftermath of the collision between the projectile and target nuclei, this phase can be described by binary collisions of two nucleons. The kinetic energy of these collisions is then transferred to the produced particles and fields; both of the partonic (quark) and hadronic type. Following this, the produced particles and fields start interacting with the reaction products of other constituent collisions, thereby producing more particles and resulting in a system with high enough energy and particle density for the second phase to set in.

2. An equilibrium expansion phase:
   After the initial product particles scatter multiple times, the system reaches a local thermal equilibrium, such that it exhibits collective behaviour and can be characterised by intensive quantities like pressure, energy density and particle-number density. This phase can therefore be modelled in a hydrodynamic/fluid-dynamic, or microscopic transport, approach.

3. A final decoupling phase:
   Following the hydrodynamic expansion, the system dilutes to an extent that local or chemical equilibrium conditions are no longer fulfilled. The hadrons are formed at these stage, and having decoupled from the system, they start flying into the detectors to be measured.

Barring the intermediate equilibrium expansion phase − which can be described with hydrodynamics, the system's evolution is governed by non-equilibrium dynamics. Therefore, a relativistic, microscopic transport approach, based on the Boltzmann equations is used to describe the initial and final, non-equilibrium phases(Molnar and Huovinen, 2004; Burau et al., 2004; Xu and Greiner, 2004). However, a model that aims to describe a heavy-ion collision should be able to reproduce all the three aforementioned phases. This requires a physically consistent model that incorporates a hydrodynamic description of the intermediate phase with the transport description of the initial and final phases. The ultra-relativistic quantum molecular dynamics (UrQMD) is one such model (Bass, 1998;

Bleicher, 1999). The UrQMD starts with an effective solution of the relatvistic Boltzmann equation:

$$p^\mu \cdot \partial_\mu f_i(x^\nu, p^\nu) = \mathcal{C}_i \; ; \qquad (4.10)$$

where f_i are the distribution functions of particle species i, the time-evolution of which are described by this equation. The term on the right-hand side of the equation is the full collision term. The presence of an external potential results in an additional term on the left-hand side. Hadrons and strings, excited in high-energy binary collisions, form the underlying degrees-of-freedom and the projectile, and target, nuclei are initialised with a Woods-Saxon profile in coordinate space, with Fermi momenta being randomly assigned to each nucleon in the rest-frame of its corresponding nucleus. The collision criterion is as follows:

$$d_{\mathrm{trans}} \leq d_0 = \sqrt{\frac{\sigma_{\mathrm{tot}}}{\pi}} \; , \; \sigma_{\mathrm{tot}} = \sigma\left(\sqrt{s}, \mathrm{type}\right) \; ; \qquad (4.11)$$

where d_{trans} is the covariant relative distance and d_0 is the critical distance given by the corresponding total cross-section, σ_{tot}, of the collision. Although each collision process is calculated in the rest-frame of the binary collision; the nucleus-nucleus equal-speed system is used as a reference frame for time ordering the collisions.

Over 50 different baryon and 40 different meson species, with their ground-states and higher resonances with masses up to 2.25 GeV, are included in the UrQMD. Additionally, full particle-antiparticle symmetry is applied, isospin-symmetry is assumed and only flavour-SU(3) states are considered. The principle of detailed balance, or the additive quark model, or fitting to available experimental data is used to calculate the elementary cross-sections. The resonance excitations and decays are handled using the Breit-Wigner formalism.

There are two stages during the evolution of the system where the non-equilibrium descriptions need to couple to the equilibrium (hydrodynamic) description of the system. The first of these couplings happens when the two Lorentz-contracted nuclei have passed through each other, i.e., all the initial collisions have proceeded and the baryon currents have de-coupled from each other to an extent where the system has achieved local thermodynamic equilibrium or thermalisation. The 'point-like' hadrons are consistently and numerically stably mapped from their transport descriptions to the 3D hydrodynamic spatial grid via corresponding Gaussian representations of finite width, i.e., each particle is described by a Gaussian distribution of the total energy, momentum and baryon-number density carried by the particle.

The second coupling takes place at a stage called the freeze-out; where the dilution of the system leads to a decoupling of the particles. At this point, a hypersurface needs to be found where all the existing fluid elements can be transformed back to known hadrons, which are then propagated via the hadronic cascade of UrQMD. A necessary condition for freeze-out is that both the fluid-dynamic and transport approaches be valid in this transition region. A standard procedure is to use the Cooper-Frye prescription (Cooper and Frye, 1974) to map the fluid-dynamic fields to the hadrons:

$$E\frac{dN}{d^3p} = \int_\sigma f(x,p)p^\mu d\sigma_\mu \; ; \tag{4.12}$$

where $f(x,p)$ denote the boosted Fermi, or Bose, distributions of the respective particle species and $d\sigma_\mu$ is a vector normal to the hypersurface. On the predefined transition hypersurface, a Monte Carlo sampling of Eqn. (4.12) is carried out to produce the hadronic particles post freeze-out. However, in the context of this work, the freeze-out stage is skipped, since; as will be apparent in the next section; the plan is to compare di-lepton yields from the UrQMD hybrid model simulations to those from actual experimental data obtained by the HADES collaboration.

4.3   Di-leptons & the HADES

As a result of a heavy-ion collision, the system evolves into a fireball up until the freeze-out, when the outgoing particles decouple from the system and move towards the detectors. The hadronic particles; their yield and transverse momentum spectra; are used to describe the system near chemical and kinetic freeze-out. But, photons and di-leptons are also emitted from this rapidly evolving and strongly interacting system (cf. Rapp and Hees, 2016b; Rapp and Hees, 2016a and references therein). These, however, only undergo electromagnetic (EM) interactions, and given the evolution timescale of a strongly interacting system, get essentially decoupled from the system pretty early in its evolution (Galatyuk et al., 2016). As a result, their phase space distributions can provide valuable insights into the temperature, collectivity and spectral structure of the medium during these early stages. Given the emissivity (ε) of the matter over the full reaction volume:

$$\varepsilon = \frac{dN_{\text{ee}}}{dV\,dt\,d^4q} \; ; \tag{4.13}$$

which denotes the radiation rate of virtual photons from a cell of strongly interacting matter per unit time and 4-momentum; the invariant mass spectra of the di-leptons can be obtained by integrating ε over space-time. In thermal equilibrium (Gale and Kapusta, 1991; Pisarski, 1982; McLerran and Toimela, 1985):

$$\varepsilon = \frac{Kf^B(q_0, T)\rho_{\text{EM}}}{M^2} \; ; \tag{4.14}$$

where K is a constant, ρ_{EM} is the EM spectral function, f^B is the thermal Bose distribution and M is the invariant di-lepton mass.

Some experimental data, from HIC's at the Scherionensynchroton (SIS) 18 of the Gesellschaft für Schwerionenforschung (GSI), has already been made available as part of the HADES (High Acceptance Di-electron Spectrometer) collaboration results. Theoretical conclusions, drawn from simulations of HIC's, about modifications to the properties of hadrons in a QCD system and their deconfinement/chiral parity restoration can be tested against the available di-lepton yield data. To that end; in collaboration with Dr. Tetyana Galatyuk's
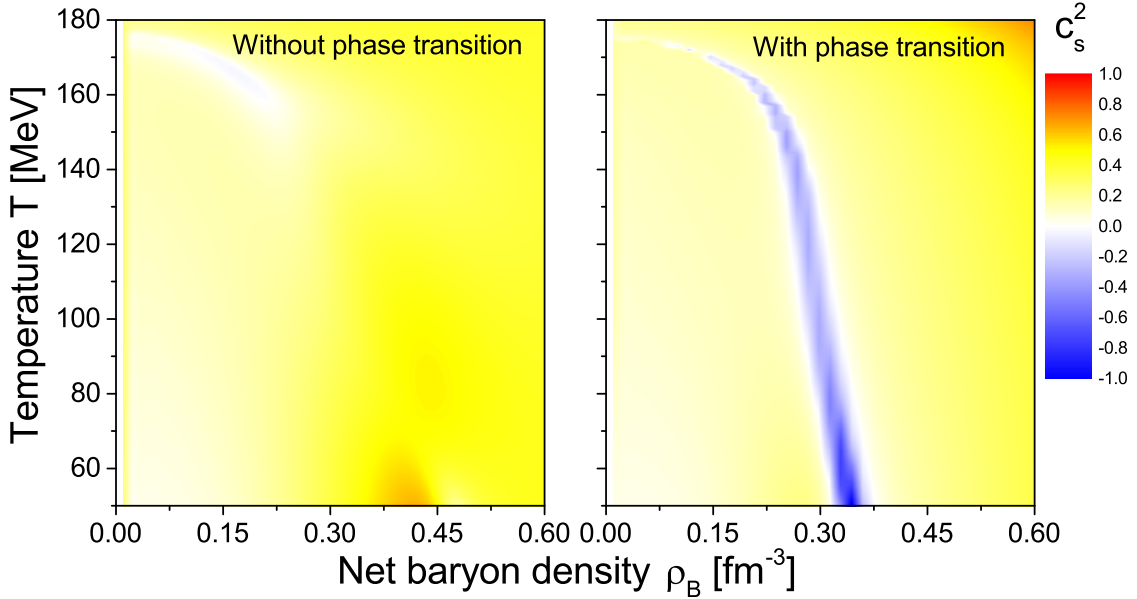
FIGURE 4.1: Two different equations of state generated by the QχP. The left pane denotes the reasonable EoS, with $T_c < 50$ MeV, while the right pane denotes the non-physical, full first-order EoS.

HADES group at GSI; the UrQMD hybrid (v3.4) algorithm is used, with two EoS's from the QχP as input (cf. Fig. 4.1), to simulate Au-Au (gold-on-gold) collisions at a beam energy $E_{\mathrm{lab}} = 1.23$ AGeV, for three different impact parameters (b) of 2 fm, 4 fm and 7 fm. Using the speed-of-sound, defined previously as $\sqrt{\partial P(\epsilon)/\partial \epsilon}$, on a temperature−baryon-number density ($T - \rho_B$) plane, Fig. 4.1 illustrates the equations of state with and without the first-order chiral/deconfinement phase transition. In order to facilitate comparison with HADES data, results below $T = 50$ MeV were not considered, and although the first (left panel) EoS has a first-order transition, its T_c is below 50 MeV, and it can therefore be considered as representing a system with a "full" or "pure" crossover phase boundary.

As a control to check whether the phase transition has any effect on the system's di-lepton production, the second (right panel) EoS; representing an unrealistic system with a "pure" first-order phase boundary; is used. It is obtained by modifying the strength of the quark couplings to the chiral fields ($g_{q\sigma} = -5.2$ and $g_{s\zeta} = -4.2$); and by decreasing the Polyakov loop parameter (T_0) from 200 MeV to 120 MeV.

The HIC simulations run with the aforementioned EoS's, under the aforementioned conditions, produce data for T and ρ_B as functions of space ($\mathbf{x}$) and time (t), which are then used in Eqn. 4.14 to calculate the emissivity, from which the invariant-mass spectrum of the di-leptons is obtained.

Figs. 4.2, 4.3 and 4.4 show the simulation results, obtained with the two different equations of state and the three different impact parameters, for the weighted averages of temperature, baryon-number density and quark fraction as functions of time; while Fig. 4.5 shows the average temperature as a function of average baryon-number density. The averages are
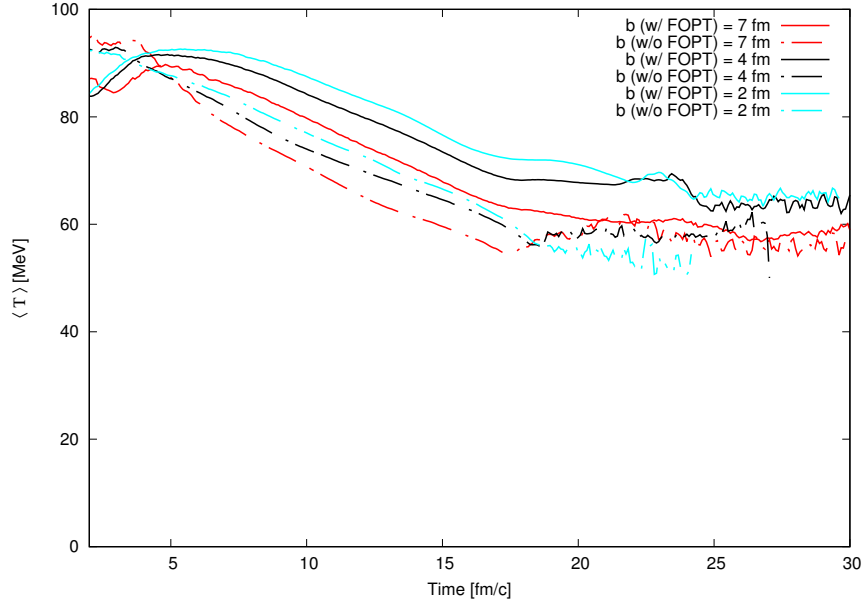
FIGURE 4.2: Average temperature as a function of time for two different
HIC simulations with different equations of state and impact parameters.
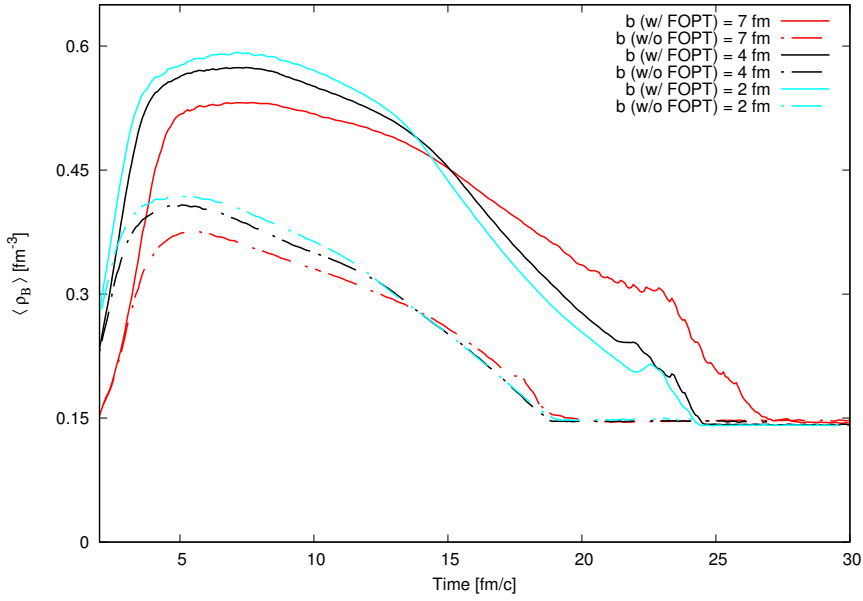
FIGURE 4.3: Average baryon-number density as a function of time for two
different HIC simulations with different equations of state and impact pa-
rameters.

defined as:

$$\langle A \rangle = \frac{\sum\limits_{i=1}^{200} A_i (\rho_B)_i}{\sum\limits_{i=1}^{200} (\rho_B)_i} \; ; \qquad (4.15)$$
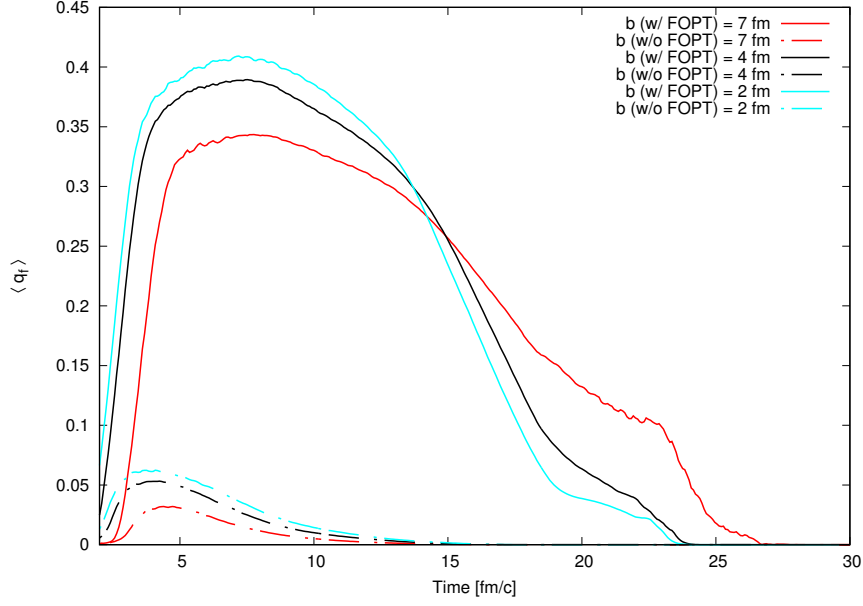
FIGURE 4.4: Average quark fraction as a function of time for two different HIC simulations with different equations of state and impact parameters.
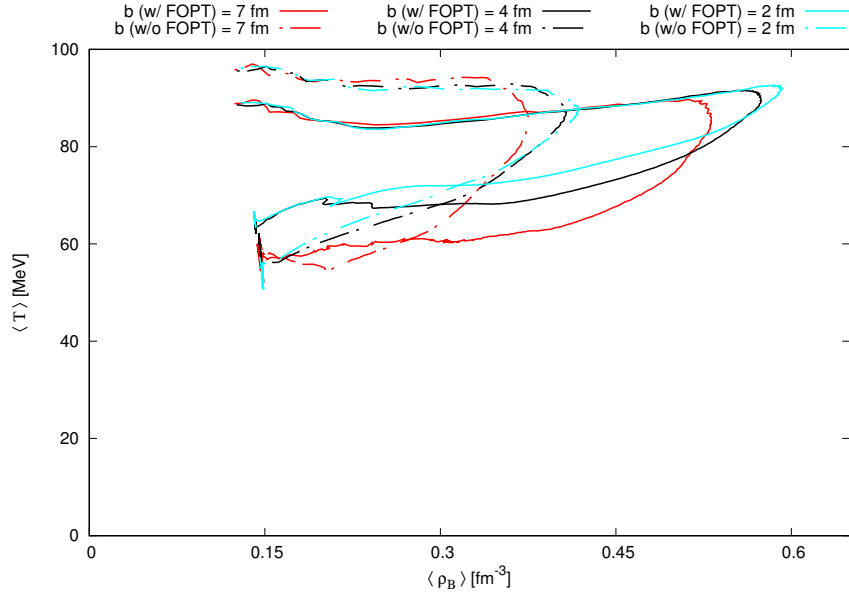
FIGURE 4.5: Average temperature as a function of average baryon-number density for two different HIC simulations with different equations of state and impact parameters.

where A is the quantity to be averaged and $(\rho_B)_i$, the baryon-number density of each cell, is the weighting function for the 3D $200 \times 200 \times 200$ grid over which the simulation is

performed.

The figures clearly demonstrate the effects of a first-order transition on the averaged quantities. In Fig. 4.2, the bold curves exhibit a saddle-like feature in the $20-25$ fm/c time-range; which denotes the first-order transition; and this feature is consequently absent in the dotted curves. In Fig. 4.3, it can be observed that the average densities increase by almost 150% in the "pure" first-order case and the knee-like shape to the right of the bold curves results from the transition occurring during that time. The same can be said about the quark fraction curves in Fig. 4.4, with the transition resulting in an almost 1000% (or, tenfold) increase in the average quantity of quarks in the system. The phase-space distribution in Fig. 4.5 amply illustrates the effects of a first-order chiral/deconfinement transition on the system; effects that are conjectured to be supported by experimental data on di-lepton yields, on comparison.

The figures also illustrate the expected influence of an increase in the impact parameter, with peak temperatures, baryon-number densities and quark fractions increasing as the collision is changed from a grazing collision to one where its almost head-on. The marked difference observed in the quark fractions and baryon-number densities in the two different cases is, however, the most important outcome of this part of the project; an outcome that is likely to be confirmed by a noticeable difference in the di-lepton yields obtained in the two different scenarios. Dr. Galatyuk's HADES group is currently hard at work, calculating the di-lepton yields from the simulation results and comparing them to available experimental data.

4.4   Nuclear interactions and the UrQMD

In Section 2.2.3, with grand canonical models of dense QCD, it was observed that the interactions of nucleons can have a significant impact on the measured net-proton cumulants at low ($\sqrt{s_{NN}} < 20$ GeV) beam energies (Fukushima, 2015; Vovchenko et al., 2015; Vovchenko, Gorenstein, and Stoecker, 2017; Mukherjee, Steinheimer, and Schramm, 2017). In the following, we will investigate how important the effect of the nuclear interactions on the measured proton-number fluctuations really is, within a microscopic transport approach. A similar study, but at a higher beam energy ($\sqrt{s_{NN}} = 5$ GeV) came to the conclusion that no effect of the nuclear interactions could be found (He et al., 2016). We will study this effect for fixed target experiments at a beam energy of $E_{lab} = 1.23$ AGeV which corresponds to the current SIS18 HADES experiment. Here the effect of nuclear interactions should be much stronger and therefore is more likely to be observed.

4.4.1   Adding nuclear potentials

Nuclear interactions have been introduced to the UrQMD model some time ago (Bass, 1998; Li et al., 2006). In the case where nuclear interactions are taken into account, each hadron is represented by Gaussian wave packet with the width parameter L in phase space (Bass,

1998). The Wigner distribution function f_i of the hadron i reads

$$f_i(\mathbf{r}, \mathbf{p}, t) = \frac{1}{(\pi\hbar)^3} e^{-\frac{[\mathbf{r}-\mathbf{r}_i(t)]^2}{2L}} e^{-\frac{[\mathbf{p}-\mathbf{p}_i(t)]^2 \cdot 2L}{\hbar^2}}, \tag{4.16}$$

where $L = 2$ fm^2 is usually chosen for simulating collision with heavy nuclei like Au. $\mathbf{r}_i$ and $\mathbf{p}_i$ are the centroids of coordinate and momentum of hadron i, respectively. The equations of motion for $\mathbf{r}_i$ and $\mathbf{p}_i$ read as:

$$\dot{\mathbf{r}}_i = \frac{\partial\langle H\rangle}{\partial\mathbf{p}_i} \text{ and } \dot{\mathbf{p}}_i = -\frac{\partial\langle H\rangle}{\partial\mathbf{r}_i}. \tag{4.17}$$

Here, $\langle H\rangle$ is the total Hamiltonian function of the system, it comprises the kinetic energy and the effective interaction potential energy. The importance of the mean field potential for describing HICs has been extensively studied (Stoecker and Greiner, 1986; Bertsch and Das Gupta, 1988). For studying HICs at intermediate energies, the following density and momentum dependent potential has been widely used in QMD-like models (Aichelin, 1991; Hartnack et al., 1998; Li et al., 2006),

$$\begin{aligned} U &= \alpha(\rho/\rho_0) + \beta(\rho/\rho_0)^\gamma \\ &+ t_{md}\ln^2[1 + a_{md}(\mathbf{p}_i - \mathbf{p}_j)^2]\rho/\rho_0. \end{aligned} \tag{4.18}$$

Here α=-393 MeV, β=320 MeV, γ=1.14, t_{md}=1.57 MeV, and $a_{md} = 500$ GeV^{-2} are chosen, which yields the (in)compressibility κ_0=200 MeV for isospin-symmetric nuclear matter. This set of parameters does give a good description of the azimuthal correlations of charged particles (the so called v_n) at SIS18 beam energy range (Hillmann, Steinheimer, and Bleicher, 2018). In recent years, in order to follow present progress on determining the nuclear symmetry energy and better describe the recent experimental data for HICs at SIS energies, the surface and surface asymmetry terms, as well as the bulk symmetry energy term obtained from the Skyrme potential energy density functional have been further considered in the present version. Details about these terms can be found in Wang et al., 2014a; Wang et al., 2015. Since they are expected to be less important for bulk properties of HICs, the chosen of those parameters will not significantly influence our results. Besides the nuclear potential, the Coulomb potential for all charged particles is also taken into account. It has been further found that with an appropriate choice of the in-medium elastic nucleon-nucleon cross-section, some recent published experimental data, especially the collective flows of light clusters, can be reproduced reasonably well. See Refs. Wang et al., 2014a; Wang et al., 2014b; Wang et al., 2015 for more details.

4.4.2 Method

In the following, results for head-on (b=0 fm) Au+Au collisions at a fixed target beam energy of $E_{\text{lab}} = 1.23A$ GeV, with the UrQMD model, will be presented. In particular we will compare results where the model is used in its cascade mode with results where the
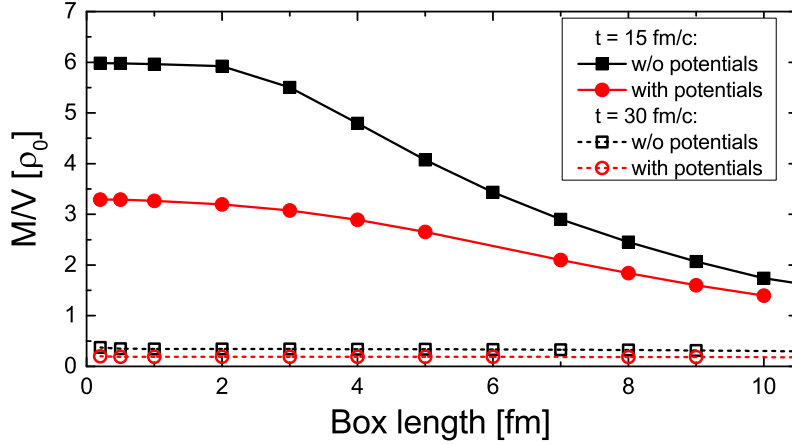
FIGURE 4.6: Baryon number density in a cubic box with of l. The box is centred at the center of mass of the collisions, i.e. $x = y = z = 0$. Two time steps are compared, t=15 and 30 fm/c. The density is given in units of the nuclear ground state density $\rho_0 \approx 0.16\text{fm}^{-3}$

long range nuclear interactions are explicitly taken into account. Note that we will treat all baryons as free baryons, i.e. they are not bound in nuclear clusters. In general this is not true and one usually applies an afterburner to calculate the cluster abundances on an event-by-event basis (Li et al., 2016a; Li et al., 2016b). Using such an afterburner it would be very interesting to study the effect of nuclear clustering on the baryon number fluctuations in more detail (Feckova et al., 2015). However in this paper we will focus only on the effect of potential interactions and leave the cluster study to future publications. The importance of taking into account the nuclear interactions can already be observed from the time evolution of the baryon number density. Fig. 4.6 shows the average net-baryon number density in a box, centered around the collision point $x = y = z = 0$ with a given length l, at two different times t. The times are chosen to correspond to the time of largest compression $t \approx 15$ fm/c and the time at which inelastic processes cease $t \approx 30$ fm/c. Note that we have chosen to treat baryons as point like particles to calculate the average density in the box as there should only be integer numbers of baryon in a given volume for a single event. We have also neglected the effect that baryons may coalesce and form nuclei at a late time which will influence the extracted cumulants (Feckova et al., 2015). This effect will be studied in a forthcoming paper in more detail.

It can be clearly observed that the compression in the case of the cascade version is larger than in the case where nuclear potentials are taken into account. This is mainly due to the repulsive nature of the nuclear interaction at high density.

In addition, Fig. 4.7 shows the total fraction of baryons within the described box. Since the total number of baryons is conserved to be 394 this fraction must be between 0 and 1. At early times it varies between 0% and 80%, while at late times at most 10% of all the baryons are in the box of length 10 fm. This ratio will become important later on, in the discussion of baryon number fluctuations as effects of global baryon conservation laws are
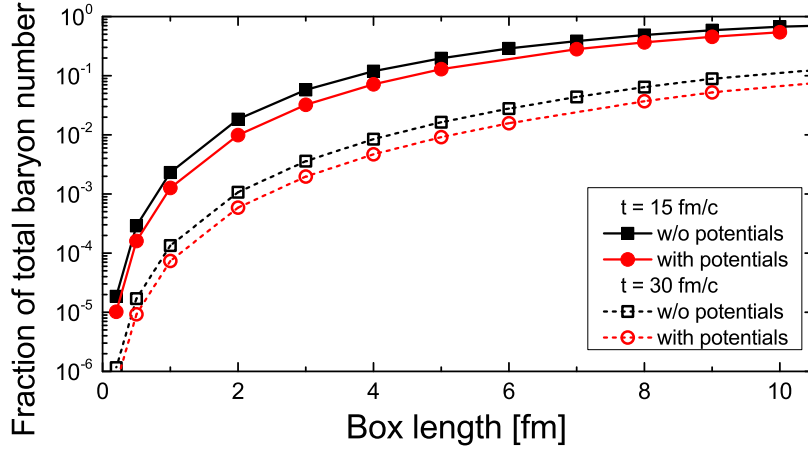
FIGURE 4.7: Fraction of baryons in the cubic box of length l (see text for description). At an early time t=15 fm/c, for a box length of 10 fm about 70-80% of the baryons are enclosed within the box. At later times only about 10% are in the same box, due to the rapid expansion of the system.

important. These effects should depend on the fraction of the total baryon number in a given acceptance/box.

In order to quantify a possible enhancement of fluctuations one usually studies ratios of cumulants of the multiplicity distributions. This is done, because the cumulants C_n depend explicitely on the volume and therefore effects of the total volume cancel when the ratio is taken. Furthermore, for a Poisson distribution all cumulant ratios will be unity and the cumulant ratios for a Binomial distribution are also well known. The cumulants in the following will be defined as:

$$
\begin{aligned}
C_1 &= M = \langle \mathrm{N} \rangle \\
C_2 &= \sigma^2 = \left\langle (\delta \mathrm{N})^2 \right\rangle \\
C_3 &= S\sigma^3 = \left\langle (\delta \mathrm{N})^3 \right\rangle \\
C_4 &= \kappa\sigma^4 = \left\langle (\delta \mathrm{N})^4 \right\rangle - 3 \left\langle (\delta \mathrm{N})^2 \right\rangle^2
\end{aligned}
\tag{4.19}
$$

where $\delta \mathrm{N} = \mathrm{N} - \langle \mathrm{N} \rangle$ with N being the net-proton or net-baryon number in a given acceptance for a single event and the brackets denote an event average. Here M is the Mean, σ^2 the variance, S the Skewness and κ the Kurtosis of the underlying multiplicity distribution. Usually one takes the following appropriate ratios of these cumulants:

$$
\begin{aligned}
C_2/C_1 &= \sigma^2/M & (4.20) \\
C_3/C_2 &= S\sigma & (4.21) \\
C_4/C_2 &= \kappa\sigma^2 & (4.22)
\end{aligned}
$$

The statistical errors in our simulations are estimated according to the delta-theorem (Luo, 2012). The errors of the cumulant ratios then are:

$$
\mathrm{error}(C_r/C_2) \propto \sigma^{r-2}/\sqrt{n} , \tag{4.23}
$$

where n is the number of events and $\sigma^2 = C_2$ the variance of the observable.
For reference we also cite the corresponding cumulant ratios for a Binomial distribution, which would be the correct description of uncorrelated baryons where the total baryon number is conserved globally.

$$
\begin{aligned}
C_2/C_1{}^{\text{Binomial}} &= 1 - p \\
C_3/C_2{}^{\text{Binomial}} &= 1 - 2p \\
C_4/C_2{}^{\text{Binomial}} &= 1 - 6p(1 - p)
\end{aligned}
\tag{4.24}
$$

where p is the fraction of the total baryon number within a given acceptance/box.

4.4.3   Results in co-ordinate space

Fluctuations and correlations due to a phase transition and critical behaviour usually are manifested in coordinate space. For example the spinodal decomposition creates clumps of matter in coordinate space and at the critical endpoint, correlations can extend over large spatial distances. To verify that indeed fluctuations are affected by nuclear interactions, we first have to study the cumulant ratios for a fixed spatial volume, during the dynamical evolution of the system. Figs. 4.8 and 4.9 show the cumulant ratios, for the net-baryon number, calculated as a function of the box length as defined in the previous section. Again two different times, $t = 15$ fm/c and $t = 30$ fm/c, are shown. At the early time one can clearly observe a suppression of all cumulant ratios in the case where nuclear potential interactions are taken into account. The suppression is strongest for the fourth order cumulant, as expected. As the density at this early time is still large, the suppression is due to the short range repulsive force between nucleons and therefore only occurs for boxes of length smaller than 2 fm. For larger boxes the effect of baryon number conservation begin to dominate and all cumulant ratios decrease.

At the later time the suppression of the cumulant ratios, in coordinate space, is all but gone. This can be understood as a result of the much lower density (sub-saturation density) at the late time. One should kepp in mind that at such a late time, most baryons are not within this small box anymore, mayn of them have already decoupled from the system. The cumulant ratios of the baryons at a late time therefore should be defined over their freeze-out hypersurface or, as is done by experiments, within a finite acceptance window in momentum space.

4.4.4   Results in momentum space

Heavy ion experiments cannot measure coordinate space distributions of baryons during the time evolution of the fireball. They measure momentum space distributions of protons after the final kinetic freeze-out of all particles. Furthermore it is not clear that the coordinate space correlations which appear due to the nuclear interactions (or critical phenomena) will translate into momentum space correlation at the end of the systems evolution.

In the following we will therefore present results of our simulations for baryons and protons in the HADES transverse momentum acceptance ($0.4 < p_T < 1.6$ GeV) (Agakishiev, 2009) and for a given interval in rapidity, around the centre of mass rapidity. The results for the cumulant rations will again be for head on ($b = 0$ fm) collisions, to avoid strong contributions from volume fluctuations. Fig. 4.11 shows the average net-baryon number rapidity distributions for most central Au+Au events. Here we compare cascade mode results with simulations that include nuclear potentials. One can see that the average rapidity distributions are very similar for the two cases, even though the maximum compression varies quite significantly as was shown in Fig. 4.6.
Finally, Fig. 4.10 shows the results of the net-baryon and net-proton cumulant ratios as function of the rapidity interval Δy. Here several interesting observations can be made.

1. The cumulant ratios for net-baryons are enhanced, in the case where nuclear interactions are enabled, for a small rapidity window $\Delta y < 0.3$.

2. For larger rapidity windows all cumulant ratios are suppressed due to the effect of conservation laws, especially baryon number conservation.

3. The effect of the enhancement is much smaller for net-protons, as compared to net-baryons, due to the random exchange of isospin with neutrons and pions, which are produced abundantly already at this beam energy (Reisdorf, 2010).

4. The cascade mode (black lines with squares) agrees rather well with a simple binomial distribution for the net-baryons. As an input p for the binomial cumulant ratios in equations (4.24) we simply use the fraction of total baryons in the given rapidity interval.
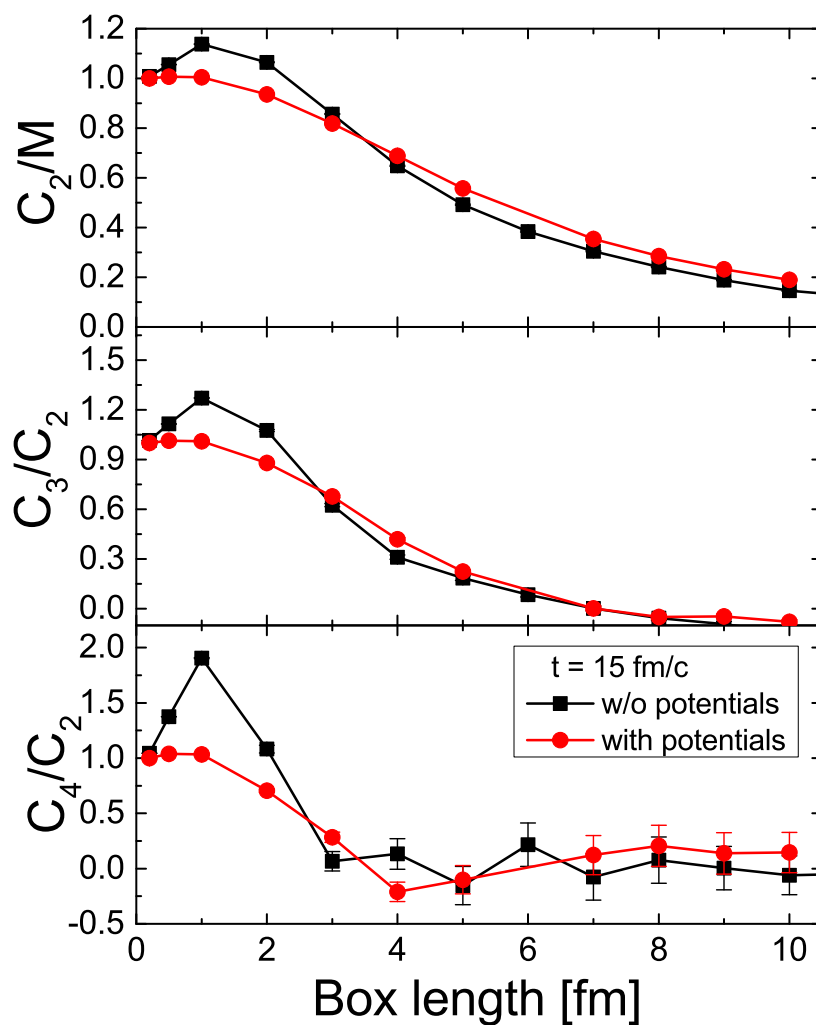
FIGURE 4.8: Ratios of cumulants of the baryon-number as function of the box length (see Figs. 4.6 and 4.7). Only the results for the early time (t=15 fm/c) are shown, with and without potentials.
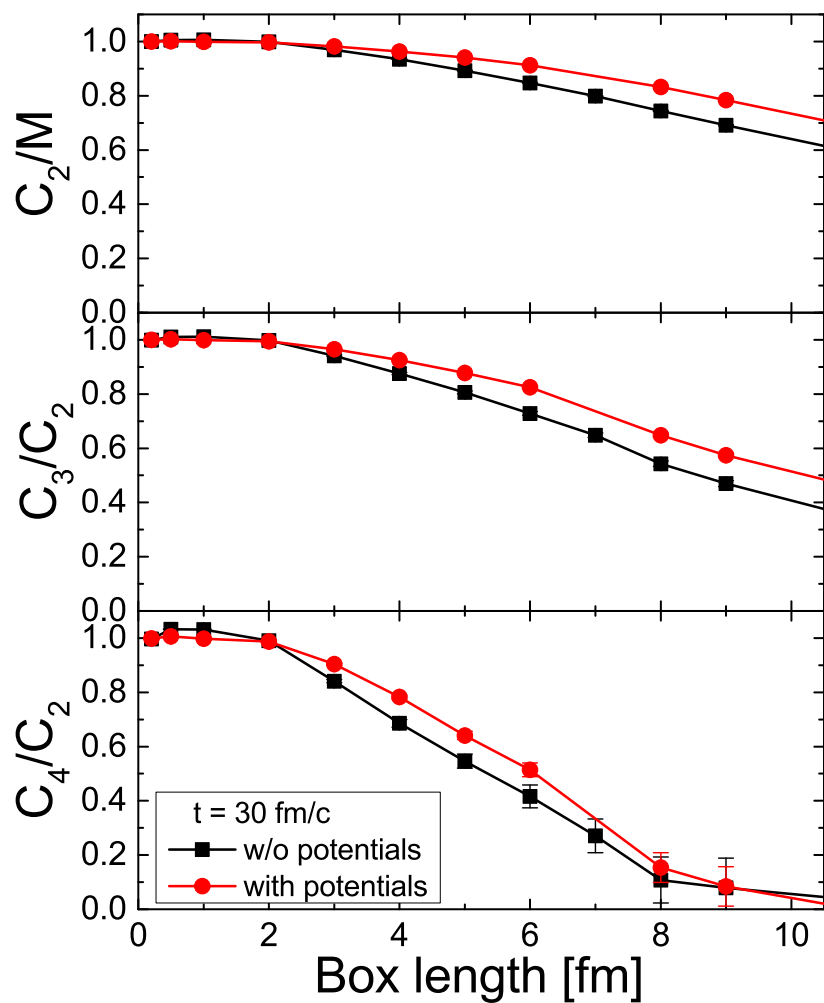
FIGURE 4.9: Ratios of cumulants of the baryon-number as function of the box length (see Figs. 4.6 and 4.7). Only the results for the late time (t=30 fm/c) are shown, with and without potentials.
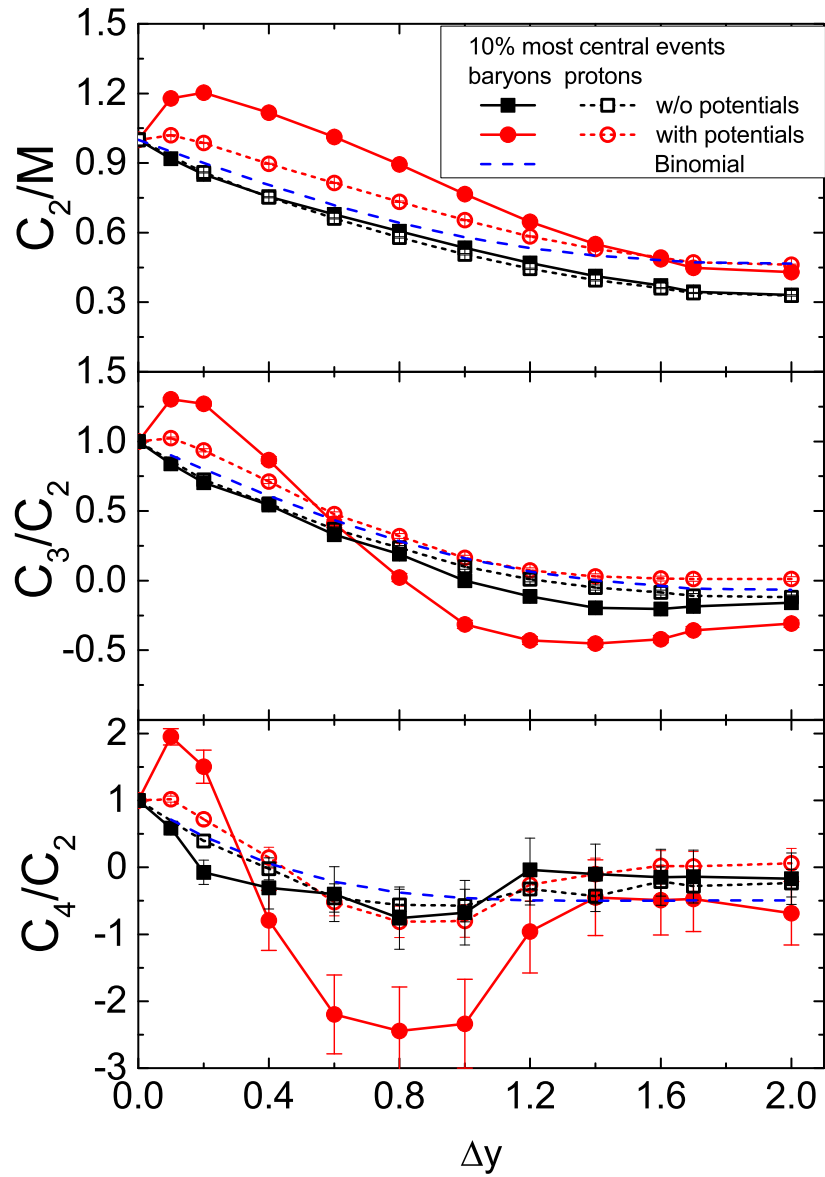
FIGURE 4.10: Comparison of final proton- and baryon-number cumulant ratios with acceptance cuts, for head on collisions, as function of the rapidity window Δy, around mid-rapidity.
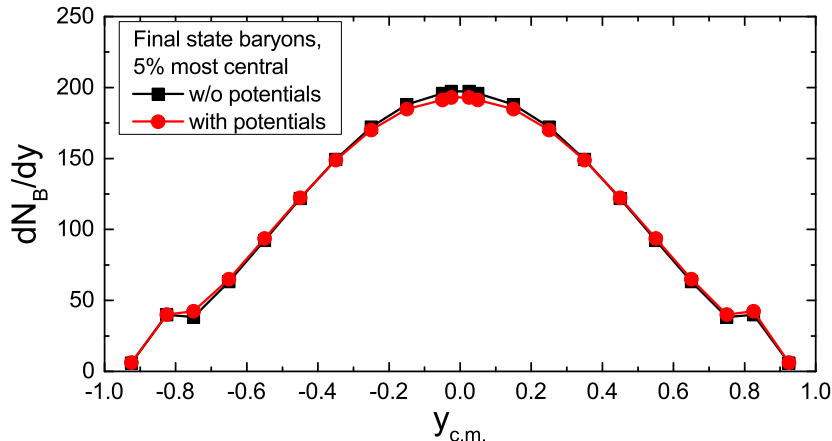
FIGURE 4.11: Final rapidity distribution of baryons in most central collisions ($b < 3.4$ fm). Compared are the results for the calculation with and without nuclear potentials. Only a small difference in the mean rapidity distribution is observed.

4.4.5 Discussion

We have shown that nuclear interactions can have a significant effect on the net-baryon number cumulant ratios in heavy ion collisions at SIS18 beam energies. This is true for the cumulant ratios in coordinate and momentum space. At early times the repulsive interaction dominates and all cumulant ratios are suppressed. Furthermore, it was shown that an enhancement of the final cumulant ratios, after freeze out and in momentum space, is only observed for a small acceptance window and that larger windows are dominated by conservation laws. Finally, we have also shown that the effect is diminished if only net-protons are measured, due to the fact that isospin is randomly distributed amongst the baryons.

Even though the qualitative effect of the nuclear interactions is in agreement with predictions from grand canonical models (Vovchenko et al., 2015; Mukherjee, Steinheimer, and Schramm, 2017), the quantitative signal is significantly smaller. This can be explained by the following factors:

1. The system in heavy ion collisions is small and short lived. Therefore the correlation length is limited not only by the system size but also the short time period the system spends in a dense phase.

2. Coordinate space correlations $\neq$ Momentum space correlations. The increase/decrease of the cumulants usually originates from correlations in coordinate space induced by attractive and repulsive interactions. It is not clear that these coordinate correlations completely translate to momentum space correlations which can be measured.

3. Calculations in a grand canonical ensemble do not take into account the conservation of the net baryon number as it occurs in nuclear collisions. In a microscopic transport model this is taken into account.

In conclusion, it was shown that the above discussed factors make it much harder for long range correlations from nuclear interactions or critical behaviour to be measured through the proton-number cumulants in heavy ion collisions.

Chapter 5

Summary

Theoretical implications of the quark-gluon plasma (QGP) have been around since the 1970's. Trying to locate said plasma, or the phase transition to it, by identifying the fluctuations of a hot, dense fireball produced by a heavy-ion collision (HIC), is also not a new idea. The problem, however, is that the theory used to describe systems that are so hot and dense, viz., quantum chromodynamics (QCD) has a coupling constant that goes to infinity for small values of Q^2; thereby requiring numerical analysis methods, like lattice QCD, to be predominant. But, the fact that lattice calculations require humongous computational resources; and that they are plagued by the familiar fermion sign problem; prevents them from analysing dynamic observables and progressing beyond the scope of vanishing baryochemical potentials. Under such circumstances, the only viable solution is to formulate an effective Lagrangian - which has some properties of QCD - and use it to delve into the fundamentals of the QCD theory. The models that use these effective Lagrangians are aptly called "Effective Models".

The flavour SU(3) quark-hadron chiral parity-doublet model (QχP) is one such model (Steinheimer, Schramm, and Stocker, 2011b), which was later extended to include a deconfinement transition to a gas of quarks and gluons. The calculations were done using a scalar meson self-interaction potential which incorporated several important properties of QCD. A drawback of this particular model was that the excluded-volume corrections led to nuclear matter (in)compressibility values much higher than the experimentally observed upper bounds.

In the present work, the aforementioned model was modified by changing the mesonic self-interaction potential; following Motohiro, Kim, and Harada, 2015; and by revising both physical and numerical parametrisations. The resulting new (in)compressibility value of 267 MeV - calculated by imbibing the excluded-volume corrections - was found to be well within the phenomenological range of $200 - 280$ MeV.

Regarding the experimental impact of these modifications, it is generally accepted that the matter produced in the aftermath of the initial pre-equilibrium stage of an HIC is in a state of thermodynamic equilibrium, and as such, thermal fluctuations can be utilised to detect the presence and ascertain the properties, of the QGP. But, before devoting large sums of money in conducting experiments to that effect, a theoretical/numerical calculation; involving a medium in local thermal equilibrium at moderate-to-high temperatures and high densities; is necessary to enable the success of such experiments. Some of the commonly
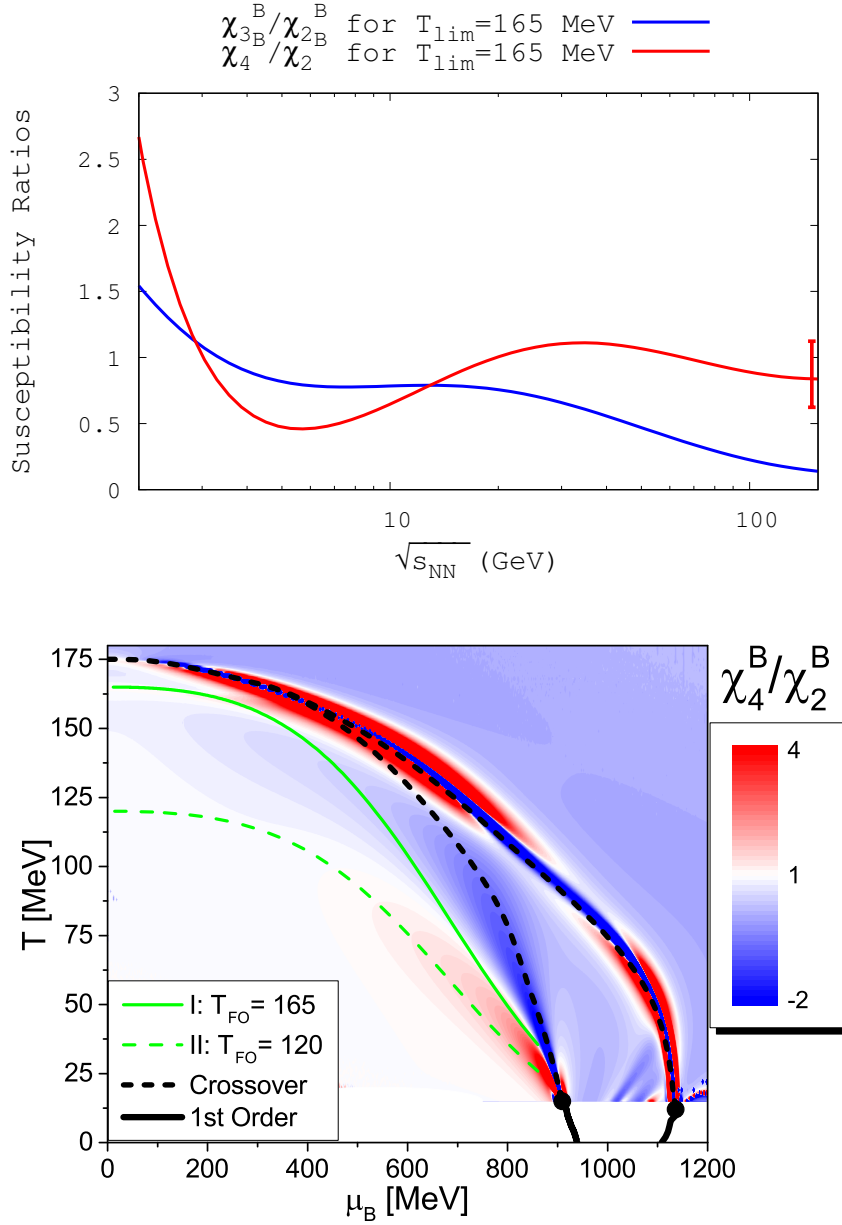
FIGURE 5.1: The dependence of the susceptibility ratios on nuclear interactions.

used quantities; born out of the aforementioned fluctuations in model simulations; that can be transformed into measurable experimental observables are the cumulants, also called the susceptibilities, of the conserved charges of the system. The fluctuations caused during the transition of the system from a broken chiral symmetry to a restored one may survive through all the intermediate states of the system. Consequently, the susceptibility ratios; which are shown in Fig. 5.1 (upper panel); were observed straying away from their pure-hadron-gas value in the vicinity of the phase transitions (both first-order and crossover)

and may, therefore, be used to experimentally verify the existence of said transition.

In the present work, it was also shown; from the variation of the susceptibility ratios observed in the phase diagram Fig. 5.1 (lower panel); that plenty of complications can be unearthed from the region in-between the two transitions − nuclear liquid-gas and chiral/deconfinement, where an interplay of their crossover regions results in significant changes to the fluctuations of the conserved charges in the system. Moreover, a strong influence of the position of the freeze-out line in the QCD phase diagram (which is effectively the temperature at which the freeze-out occurs) on the energy dependence of the susceptibility ratios was illustrated.

By changing the overall strangeness content of the medium, it was observed that the phase diagram depends heavily on the strangeness-chemical potential. Consequently, the entire phase boundary of the quark-hadron deconfinement transition weakened from a combination of first-order and crossover to a "pure" crossover. It is not outlandish to expect such a situation arising in HIC experiments, where the temperature and density provide conditions ripe for the spontaneous production of strangeness via the formation of small, non-zero strangeness (and anti-strangeness) sub-systems (Steinheimer et al., 2009). Due to the short timescales associated with the evolution of the system, the hyperons formed in these sub-systems are not expected to decay into non-strange hadrons (Schaffner et al., 1993; Schulze et al., 1998; Nakamura and Group, 2010; Yao and Group, 2006; Beringer and Group, 2012) and can, therefore, affect the particle output detected from the collision. Tracing the particle-number distributions, and their fluctuations, back to the initial stages of the system, the conjectured influence of the strangeness, on the evolution of the system, can be confirmed. However, the critical end-point in the QχP model appears at low temperatures, which makes such an effect difficult to be directly observed in heavy-ion collisions, but it could have an impact in the higher-temperature, smooth transition region as well. Given that the strangeness-chemical potential values obtained from experimental data analysis come out to about $20-25\%$ of the baryochemical potential (Braun-Munzinger, Redlich, and Stachel, 2011; Kovács and Szép, 2008; Becattini, Gazdzicki, and Sollfrank, 1998; Braun-Munzinger, Heppe, and Stachel, 1999), the modifications induced to the phase diagram at low temperatures need to be considered when constructing facilities capable of performing beam-energy scans at progressively lower energies.

In the context of very slowly evolving, isospin-asymmetric, hot and dense systems, as found in neutron stars (NS's), the assumptions behind the QχP model become relatively more accurate and hence, these systems were studied using the equation of state (EoS) generated by the model. It was observed that the symmetry energy and slope parameter values agree exceptionally well with the experimental constraints put on astrophysical data, and the resultant mass-radius diagram obtained from solving the Tolman-Oppenheimer-Volkoff (TOV) equations with the aforementioned EoS leads to a 1.98 M$_\odot$ neutron star with a radius of 10.25 km, in accordance with recent observations. It was also observed that the maximum-mass star generated by the QχP EoS is very compact and that, the EoS does not support the hadronic direct Urca process. Extending the EoS to high chemical potentials, it was observed to meet the band of values produced by perturbative QCD calculations. Thus, this effective model can now efficiently describe stars with both a hadronic and a

quark phase; with a hybrid EoS that leads to more compact stars and still allows for a large quark fraction, while not forbidding the appearance of hyperons.

A straightforward way of connecting the features of an EoS with the maximally achievable compression of a relativistic collision is by employing the Rankine-Hugoniot-Taub-Adiabat. Since collisions of this type are commonplace not only in HIC experiments, but also in neutron star mergers, the beam-energy dependence of the net-baryon-number density and temperature was studied for these two different scenarios. It was revealed that the density compression is independent of the isospin content, and the chemical composition, of the system and that the QχP EoS is a consistent and realistic temperature-dependent EoS for describing NS matter, as observed before.

It is important to keep in mind that the QχP model is based on some basic assumptions that make a direct comparison with experimental HIC data difficult: the sub-system considered is so small w.r.t. the entire system that it can be reasonably assumed to be in thermal equilibrium, it is essentially static and it freezes out in an instant. Therefore, in order to implement the current effective EoS in a dynamical model suited for studying the evolution of a fireball created by an HIC, the SHASTA fluid-dynamic model; in conjunction with the ultra-relativistic quantum molecular dynamics (UrQMD) algorithm was used. A two-pronged approach was employed to determine whether the conclusions drawn from the QχP model were valid in case of an actual relativistic HIC.

First, the claim that the nuclear liquid-gas transition, and its interplay with the chiral/deconfinement transition, has a considerable effect on the fluctuations of the system was checked by introducing nuclear interaction potentials to UrQMD simulations of HIC's at the GSI's SIS18 accelerator and observing the measurable net-proton-number fluctuations. It was revealed that nuclear interactions can have a significant effect on the net-baryon-number cumulant ratios in heavy-ion collisions at SIS18 beam-energies. This was observed to be true for the cumulant ratios in both the co-ordinate and the momentum spaces. Moreover, it was observed that at early times, the repulsive interaction dominates and all the cumulant ratios are suppressed. Furthermore, it was shown that an enhancement of the final cumulant ratios, after freeze-out and in momentum space, is only visible for a small acceptance window and that larger windows are dominated by conservation laws. Additionally, it was shown that the effect got diminished when only the net-protons were measured, due to the fact that isospin is randomly distributed amongst the baryons. Even though the qualitative effect of the nuclear interactions was found to be in agreement with predictions from grand canonical models (Vovchenko et al., 2015; Mukherjee, Steinheimer, and Schramm, 2017), the quantitative signal was significantly smaller due to multiple factors making it difficult for the long-range correlations; born out of nuclear interactions, or critical behaviour; from getting measured through the proton-number cumulants in heavy-ion collisions.

Second, the results produced by UrQMD simulations of HIC's with two different QχP EoS's were to be compared, in collaboration with Dr. Tetyana Galatyuk's group at GSI, to the di-lepton yield obtained from the HADES experiment at the aforementioned facility, to check whether the chiral/deconfinement phase transition has any effect on the early evolution of an HIC system. Photons and di-leptons, by responding exclusively to the

long-timescale electromagnetic and electroweak interactions, lend themselves as effective probes for the early evolution of the short-timescale, strongly interacting system; since they become essentially decoupled from the system after being produced. The first of the EoS's used had a critical end-point below 50 MeV temperature and; for the purpose of comparison to HADES data, which are obtained at temperatures of approximately $100-150$ MeV; could be considered as representing a "pure" crossover system. The second of the two had a non-physical critical end-point at a baryochemical potential of 0 MeV and hence represented a "pure" first-order system. This was used as a control to ascertain whether there are any noticeable changes to the invariant-mass spectrum of the di-leptons, when the system is undergoing a first-order transition from QGP to hadrons, and/or from chirally symmetric to chirally asymmetric matter. A knowledge of the emissivity of the system; defined as the radiation rate of virtual photons from a cell of strongly interacting matter per unit time and four-momentum; is required to calculate the di-lepton yield of a medium. The emissivity, in a thermally equilibrated system, depends on intensive properties; like the temperature, the pressure and the chemical composition; of said system and can therefore be obtained as a space-time integral of these quantities over the total reaction-volume. These quantities were produced by running the UrQMD simulations of relativistic HIC's under the operational conditions of the HADES experiment and the weighted averages of temperature, baryon-number density and quark fraction were calculated, before handing over the simulation results to the HADES group at GSI, where the emissivity and di-lepton yield are to be calculated. The simulations revealed a considerable dependence of the averaged quantities on the phase transition; with the "pure" first-order EoS leading to an almost 150% increase in baryon-number density and an almost 1000% (or, tenfold) increase in quark fraction, when compared to the "pure" crossover case. These dependencies are likely to influence the invariant mass-spectrum of the di-leptons and cement its place amongst the variables used to probe critical behaviour in hot, dense, strongly interacting systems.

Overall, this work highlights the importance of consistently including the effects of nuclear interactions and modifications arising from the rapidly evolving chemical composition of a strongly interacting system; within the framework of a single effective-Lagrangian, chiral, mean-field model; in the study of both isospin-symmetric and isospin-asymmetric, hot and dense nuclear matter, and of reliably accounting for these influences during the interpretation of experimental data from relativistic heavy-ion collision experiments and observational data from neutron stars; and their mergers.

Appendix A

The PNJL Model

The PNJL model was introduced by Fukushima, 2004; Ratti, Thaler, and Weise, 2006 as an effective chiral quasi-quark model that incorporates a mean field like coupling to a colour background field. It has often been shown to reproduce many general features of lattice results at $\mu_B = 0$ (Roessner, Ratti, and Weise, 2007; Ghosh et al., 2006; cf. Chapter 2 for other references).

The thermodynamic potential for the model reads:

$$\Omega = U(\Phi, \Phi^*, T) + \sigma^2/2G_S - \omega^2/2G_V - \Omega_q \ , \tag{A.1}$$

with

$$
\begin{aligned}
\Omega_q &= 2N_f \int \frac{d^3p}{(2\pi)^3} \left\{ T \ln \left[1 + 3\Phi e^{-(E_p - \mu_q^*)/T} + 3\Phi^* e^{-2(E_p - \mu_q^*)/T} + e^{-3(E_p - \mu_q^*)/T} \right] \right. \\
&\quad + T \ln \left[1 + 3\Phi^* e^{-(E_p + \mu_q^*)/T} + 3\Phi e^{-2(E_p + \mu_q^*)/T} + e^{-3(E_p + \mu_q^*)/T} \right] \\
&\quad \left. + 3\Delta E_p \Theta(\Lambda^2 - \vec{p}^2) \right\} \ ,
\end{aligned}
\tag{A.2}
$$

where Φ is the traced Polyakov loop after averaging, written as:

$$\Phi = 1/3 \ \text{Tr} \langle L \rangle = 1/3 \ \text{Tr} \ e^{i\phi/T} \ . \tag{A.3}$$

The Wilson line, (L), is a 3×3 matrix in the fundamental representation in colour space, defined as:

$$L(\vec{x}) = \mathcal{P} \exp \left(i \int_0^\beta A_4 dx_4 \right) \ . \tag{A.4}$$

The dynamical mass of the quarks $m = m_0 - \sigma = m_0 - G_S \langle \overline{\Psi}\Psi \rangle$ is the same as in the NJL model and the vector coupling induces an effective chemical potential for the quarks $\mu_q^* = \mu_q + \omega = \mu_q + G_V \langle \Psi^\dagger \Psi \rangle$. The two auxiliary fields σ and ω are controlled by the potential terms and the last term includes the difference ΔE_p between the quasi particle energy and the energy of free quarks. The NJL part of the model has 4 parameters, the bare quark mass for the u- and d-quarks (assuming isospin symmetry), the three-momentum cut-off of the quark-loop integration λ and the coupling strengths G_S and G_V.

The thermodynamics of Φ (and Φ^*) are controlled by the effective potential $U(\Phi, \Phi^*, T)$ (Ratti et al., 2007):

$$U = -\frac{1}{2}a(T)\Phi\Phi^* + b(T)\ln[1 - 6\Phi\Phi^* + 4(\Phi^3\Phi^{*3}) - 3(\Phi\Phi^*)^2] \, , \qquad (A.5)$$

where $a(T) = a_0 T^4 + a_1 T_0 T^3 + a_2 T_0^2 T^2, \ \ b(T) = b_3 T_0^3 T$.

This choice of effective potential satisfies the $Z(3)$ centre symmetry of the pure gauge Lagrangian. In the confined phase, U has a minimum at $\Phi = 0$, while above the critical Temperature T_0 its minimum is shifted to finite values of Φ. The logarithmic term appears from the Haar measure of the group integration with respect to the SU(3) Polyakov loop matrix. The parameters a_0, a_1, a_2 and b_3 are fixed, as in Ratti et al., 2007, by demanding a first order phase transition in the pure gauge sector at $T_0 = 270$ MeV, and that the Stefan-Boltzmann limit is reached for $T \to \infty$. Self consistent solutions are obtained by minimizing the thermodynamic potential with respect to the fields σ, ω, Φ and Φ^*.

PNJL-type models have been used recently to successfully describe lattice results on bulk properties of a strongly interacting matter (Fukushima, 2004; Ratti, Thaler, and Weise, 2006). These constituent quark models seem to have the correct degrees of freedom in the asymptotic regime of free quarks and gluons, but lack the rich hadronic spectrum.

Appendix B

The Taub Adiabat

Following derivations that can be found in Rischke, Bernard, and Maruhn, 1995; Rischke, 1998; Rau, 2013 *etc*, the relativistic shock adiabat; also called the Rankine-Hugoniot-Taub adiabat; is derived here.

Consider a gas which gets perturbed by a moving shock wave. In the rest frame of the shock front, there is a flux of matter along the x-axis from the fully unperturbed region 1 into the perturbed region 2. Fig. B.1 illustrates this situation with the thermodynamic variables used in the following. On the discontinuity surface, the conservation equations for energy density, pressure and particle flux as given by the energy-momentum tensor, $[T^{\mu\nu}] = (\epsilon + p)\, u^\mu u^\nu - p g^{\mu\nu}$, are valid:

$$[T^{0x}] = [(\epsilon + p)\gamma u^x] = 0 \ , \tag{B.1}$$

$$[T^{xx}] = [(\epsilon + p)u^x u^x + p] = 0 \ , \tag{B.2}$$

$$[n u^x] = 0 \ ; \tag{B.3}$$

with the conserved particle/baryon number n and $x = 1[1]3$. Here, the square brackets denote the difference of the specific quantities on the discontinuity $[O] = O_1 - O_2$.

By using the definition of the enthalpy $w = \epsilon + p$ and the four velocity $u = \gamma(1, \mathbf{v})$ the above equations can be written in the form:

$$w_1 v_1 \gamma_1^2 = w_2 v_2 \gamma_2^2 \ , \tag{B.4}$$

$$w_1 v_1^2 \gamma_1^2 + p_1 = w_2 v_2^2 \gamma_2^2 + p_2 \ , \tag{B.5}$$

$$j = n_1 v_1 \gamma_1 = n_2 v_2 \gamma_2 \ ; \tag{B.6}$$

with the Lorentz gamma factor $\gamma = (1 - v^2)^{-1/2}$.

From Eqn. (B.6), the relation:

$$\frac{j^2}{n_i^2} = v_i^2 \gamma_i^2 \tag{B.7}$$

can be derived. This, together with the conservation of the pressure flux (B.5) and the definition $x_i = w_i/n_i^2$ leads to:
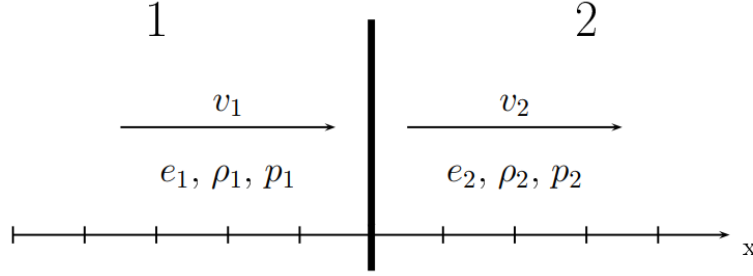
FIGURE B.1: Properties of the matter on both sides of a shock front as seen in the rest frame of the shock front. In this representation, unperturbed quantities carry the index 1 and all variables perturbed by the shock are denoted by index 2. In this illustration the medium is characterised by the energy density e, the density ρ, and the pressure p. Instead of the density, the conserved baryon, or particle, number n can also be used (figure adapted from Rau, 2013).

$$j^2 = \frac{p_2 - p_1}{x_1 - x_2} \; ; \tag{B.8}$$

which, using the particle flux (B.6) can be transformed into:

$$\left(\frac{w_2}{n_2} v_2 \gamma_2\right)^2 - \left(\frac{w_1}{n_1} v_1 \gamma_1\right)^2 = (p_1 - p_2)(x_1 + x_2) \; . \tag{B.9}$$

Furthermore, using the particle flux (B.6) again, the conservation equation for the energy (B.4) can be rewritten in the form:

$$\left(\frac{w_2 \gamma_2}{n_2}\right)^2 - \left(\frac{w_1 \gamma_1}{n_1}\right)^2 = 0 \tag{B.10}$$

By subtracting (B.10) - (B.9), one obtains the final expression for the relativistic shock adiabat, also called the Taub adiabat:

$$\left(\frac{w_1}{n_1}\right)^2 - \left(\frac{w_2}{n_2}\right)^2 + (p_2 - p_1)\left(\frac{w_1}{n_1^2} + \frac{w_2}{n_2^2}\right) = 0 \; , \tag{B.11}$$

using the relation $\gamma_i^2 - v_i^2 \gamma_i^2 = 1$.

The Taub adiabatic describes the behaviour of a shock wave using the thermodynamic quantities on both sides of the shock front. The full dynamics of the shock wave are defined by the initial quantities $e_{1,2}, n_{1,2}$ and $p_{1,2}$; although the pressure itself is not a free variable, but is defined by the other parameters via the underlying EoS $p(\epsilon, n)$.

In the non-relativistic limiting case which assumes $e \approx mn$ and $e \gg p$, the Taub adiabat goes over into its classical counterpart, the Rankine-Hugoniot equation:
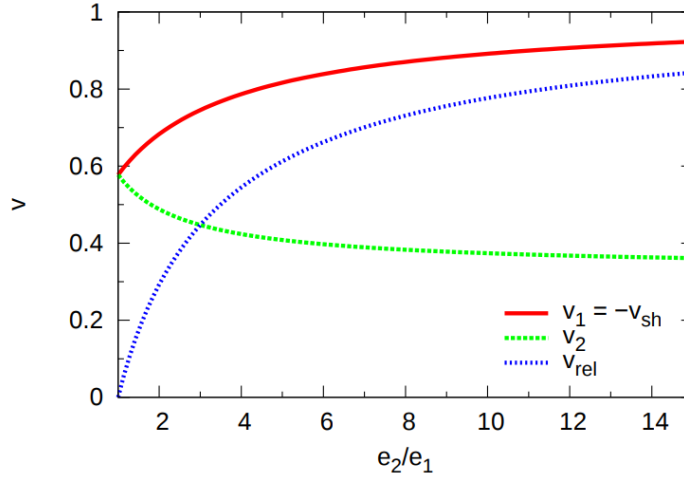
FIGURE B.2: Flow velocities of the unperturbed and perturbed medium, v_1 and v_2 respectively, from the relativistic Taub adiabat in the rest frame of the shock front (cf. Fig. B.1). The velocities are given as functions of the ratio of the energy densities on both sides of the shock front using an ideal gas EoS ($p = e/3$). The relative velocity between the two systems is denoted by $v_{\rm rel}$ (figure adapted from Rau, 2013).

$$2\left(w_1 - w_2\right) + \left(p_2 - p_1\right)\left(\frac{1}{n_1} + \frac{1}{n_2}\right) = 0 \tag{B.12}$$

Using the conservation equation for the energy flux (B.1), the velocities on both sides of the shock front can be derived from the Taub adiabat. In the rest frame of the discontinuity, the flow velocity in the unperturbed region is given by:

$$v_1 = \left[\frac{(p_2 - p_1)(\epsilon_2 + p_1)}{(\epsilon_2 - \epsilon_1)(\epsilon_1 + p_2)}\right]^{1/2} \quad ; \tag{B.13}$$

and in the perturbed region behind the shock front, the velocity is:

$$v_2 = \left[\frac{(p_2 - p_1)(\epsilon_1 + p_2)}{(\epsilon_2 - \epsilon_1)(\epsilon_1 + p_1)}\right]^{1/2} \quad . \tag{B.14}$$

When changing the reference frame, from the resting shock front into the unperturbed medium 2, the shock front moves with a velocity $v_{\rm sh} = v_1$ towards the observer. This is due to the fact that, the relative velocity only changes sign when changing the reference frame.

Adding both velocities v_1 and v_2 relativistically yields the relative velocity of the flow between the two regions as:

$$v_{\rm rel} = \left[\frac{(p_2 - p_1)(\epsilon_2 - \epsilon_1)}{(\epsilon_2 + p_1)(\epsilon_1 + p_2)}\right]^{1/2} . \tag{B.15}$$

Fig. B.2 shows the velocities v_1, v_2 and $v_{\rm rel}$ for an ultra-relativistic ideal gas with pressure defined by $p = \epsilon/3$. In the limit of a vanishing intensity of the shock front $(\epsilon_2 \to \epsilon_1)$, one has $v_1 = v_2 = c_s = \sqrt{1/3}$; which is the smallest possible shock velocity corresponding to the velocity of sound in the medium. Strictly speaking, such a small perturbation is not a shock wave but, a sound wave and contrastingly, in this specific case, there is no discontinuity in any quantities at the position of the medium perturbation. With very strong perturbations of the medium, (i.e.; $\epsilon_2 \to \infty$), v_1 increases to approach 1 and v_2 approaches $1/3$.

Bibliography

Aarts, Gert et al. (2017). "Light baryons below and above the deconfinement transition: medium effects and parity doubling". In: *JHEP* 06, p. 034. DOI: 10.1007/JHEP06(2017)034. arXiv: 1703.09246 [hep-lat].

Abbott, B. P. et al. (2016a). "Astrophysical Implications of the Binary Black-hole Merger GW150914". In: *The Astrophysical Journal Letters* 818.2, p. L22. URL: http://stacks.iop.org/2041-8205/818/i=2/a=L22.

Abbott, B. P. et al. (2016b). "Observation of Gravitational Waves from a Binary Black Hole Merger". In: *Phys. Rev. Lett.* 116 (6), p. 061102. DOI: 10.1103/PhysRevLett.116.061102. URL: https://link.aps.org/doi/10.1103/PhysRevLett.116.061102.

Abuki, H. et al. (2008a). "Chiral crossover, deconfinement and quarkyonic matter within a Nambu-Jona Lasinio model with the Polyakov loop". In: *Phys. Rev.* D78, p. 034034. DOI: 10.1103/PhysRevD.78.034034. arXiv: 0805.1509 [hep-ph].

Abuki, H. et al. (2008b). "Electrical neutrality and pion modes in the two flavor PNJL model". In: *Phys. Rev.* D78, p. 014002. DOI: 10.1103/PhysRevD.78.014002. arXiv: 0801.4254 [hep-ph].

Abuki, H. et al. (2008c). "Enforced neutrality and color-flavor unlocking in the three-flavor Polyakov-loop NJL model". In: *Phys. Rev.* D77, p. 074018. DOI: 10.1103/PhysRevD.77.074018. arXiv: 0802.2396 [hep-ph].

Adamczyk, L. et al. (2014a). "Beam energy dependence of moments of the net-charge multiplicity distributions in Au+Au collisions at RHIC". In: *Phys. Rev. Lett.* 113, p. 092301. DOI: 10.1103/PhysRevLett.113.092301. arXiv: 1402.1558 [nucl-ex].

– (2014b). "Energy Dependence of Moments of Net-Proton Multiplicity Distributions at RHIC". In: *Phys. Rev. Lett.* 112 (3), p. 032302. DOI: 10.1103/PhysRevLett.112.032302. URL: https://link.aps.org/doi/10.1103/PhysRevLett.112.032302.

Agakishiev, G. et al. (2009). "The High-Acceptance Dielectron Spectrometer HADES". In: *Eur. Phys. J.* A41, pp. 243–277. DOI: 10.1140/epja/i2009-10807-5. arXiv: 0902.3478 [nucl-ex].

Aichelin, J. (1991). "'Quantum' molecular dynamics: A Dynamical microscopic n body approach to investigate fragment formation and the nuclear equation of state in heavy ion collisions". In: *Phys. Rept.* 202, pp. 233–360. DOI: 10.1016/0370-1573(91)90094-3.

Alford, Mark et al. (2005). "A Hot water bottle for aging neutron stars". In: *Phys. Rev.* D71, p. 114011. DOI: 10.1103/PhysRevD.71.114011. arXiv: astro-ph/0411560 [astro-ph].

Alford, Mark G., Anton Kapustin, and Frank Wilczek (1999). "Imaginary chemical potential and finite fermion density on the lattice". In: *Phys. Rev.* D59, p. 054502. DOI: 10.1103/PhysRevD.59.054502. arXiv: hep-lat/9807039 [hep-lat].

Allton, C. R. et al. (2002). "The QCD thermal phase transition in the presence of a small chemical potential". In: *Phys. Rev.* D66, p. 074507. DOI: 10.1103/PhysRevD.66.074507. arXiv: hep-lat/0204010 [hep-lat].

Andronic, A., P. Braun-Munzinger, and J. Stachel (2009). "Thermal hadron production in relativistic nuclear collisions: The Hadron mass spectrum, the horn, and the QCD phase transition". In: *Phys. Lett.* B673. [Erratum: Phys. Lett.B678,516(2009)], pp. 142–145. DOI: 10.1016/j.physletb.2009.02.014,10.1016/j.physletb.2009.06.021. arXiv: 0812.1186 [nucl-th].

Antoniadis, John et al. (2013). "A Massive Pulsar in a Compact Relativistic Binary". In: *Science* 340.6131. ISSN: 0036-8075. DOI: 10.1126/science.1233232. eprint: http://science.sciencemag.org/content/340/6131/1233232.full.pdf. URL: http://science.sciencemag.org/content/340/6131/1233232.

Aoki, Y. et al. (2006). "The Order of the quantum chromodynamics transition predicted by the standard model of particle physics". In: *Nature* 443, pp. 675–678. DOI: 10.1038/nature05120. arXiv: hep-lat/0611014 [hep-lat].

Aoki, Y. et al. (2009). "The QCD transition temperature: results with physical masses in the continuum limit II." In: *JHEP* 06, p. 088. DOI: 10.1088/1126-6708/2009/06/088. arXiv: 0903.4155 [hep-lat].

Asakawa, Masayuki, Ulrich W. Heinz, and Berndt Muller (2000). "Fluctuation probes of quark deconfinement". In: *Phys. Rev. Lett.* 85, pp. 2072–2075. DOI: 10.1103/PhysRevLett.85.2072. arXiv: hep-ph/0003169 [hep-ph].

Baacke, Jurgen (1977). "Thermodynamics of a Gas of MIT Bags". In: *Acta Phys. Polon.* B8, p. 625.

Barducci, A. et al. (2003). "Ladder QCD at finite isospin chemical potential". In: *Phys. Lett.* B564, pp. 217–224. DOI: 10.1016/S0370-2693(03)00705-6. arXiv: hep-ph/0304019 [hep-ph].

Bass, S. A. et al. (1998). "Microscopic models for ultrarelativistic heavy ion collisions". In: *Prog. Part. Nucl. Phys.* 41. [Prog. Part. Nucl. Phys.41,225(1998)], pp. 255–369. DOI: 10.1016/S0146-6410(98)00058-1. arXiv: nucl-th/9803035 [nucl-th].

Bass, S. A. et al. (1999). "Signatures of quark gluon plasma formation in high-energy heavy ion collisions: A Critical review". In: *J. Phys.* G25, R1–R57. DOI: 10.1088/0954-3899/25/3/013. arXiv: hep-ph/9810281 [hep-ph].

Bass, Steffen A, Pawel Danielewicz, and Scott Pratt (2000). "Clocking hadronization in relativistic heavy-ion collisions with balance functions". In: *Physical Review Letters* 85.13, p. 2689.

Baym, Gordon, Christopher Pethick, and Peter Sutherland (1971). "The Ground state of matter at high densities: Equation of state and stellar models". In: *Astrophys. J.* 170, pp. 299–317. DOI: 10.1086/151216.

Bazavov, A. et al. (2012a). "Fluctuations and Correlations of net baryon number, electric charge, and strangeness: A comparison of lattice QCD results with the hadron resonance gas model". In: *Phys. Rev.* D86, p. 034509. DOI: 10.1103/PhysRevD.86.034509. arXiv: 1203.0784 [hep-lat].

Bazavov, A et al. (2012b). "Freeze-out conditions in heavy ion collisions from QCD thermodynamics". In: *Physical review letters* 109.19, p. 192302.

Bazavov, Alexei and Peter Petreczky (2010). "Deconfinement and chiral transition with the highly improved staggered quark (HISQ) action". In: *J. Phys. Conf. Ser.* 230, p. 012014. DOI: 10.1088/1742-6596/230/1/012014. arXiv: 1005.1131 [hep-lat].

– (2011). "Chiral transition and deconfinement transition in QCD with the highly improved staggered quark (HISQ) action". In: *Phys. Part. Nucl. Lett.* 8, pp. 860–864. DOI: 10.1134/S1547477111080024. arXiv: 1009.4914 [hep-lat].

Becattini, F., M. Gazdzicki, and J. Sollfrank (1998). "On chemical equilibrium in nuclear collisions". In: *Eur. Phys. J.* C5, pp. 143–153. DOI: 10.1007/s100529800831, 10.1007/s100520050256. arXiv: hep-ph/9710529 [hep-ph].

Begun, V. V. et al. (2004). "Particle number fluctuations in canonical ensemble". In: *Phys. Rev.* C70, p. 034901. DOI: 10.1103/PhysRevC.70.034901. arXiv: nucl-th/0404056 [nucl-th].

Bellwied, R. et al. (2015). "Fluctuations and correlations in high temperature QCD". In: *Phys. Rev.* D92.11, p. 114505. DOI: 10.1103/PhysRevD.92.114505. arXiv: 1507.04627 [hep-lat].

Bender, Michael, Paul-Henri Heenen, and Paul-Gerhard Reinhard (2003). "Self-consistent mean-field models for nuclear structure". In: *Rev. Mod. Phys.* 75, pp. 121–180. DOI: 10.1103/RevModPhys.75.121.

Beringer, J., P. D. Group, et al. (2012). "Review of Particle Physics". In: *Phys. Rev. D* 86 (1), p. 010001. DOI: 10.1103/PhysRevD.86.010001. URL: https://link.aps.org/doi/10.1103/PhysRevD.86.010001.

Bertsch, G. F. and S. Das Gupta (1988). "A Guide to microscopic models for intermediate-energy heavy ion collisions". In: *Phys. Rept.* 160, pp. 189–233. DOI: 10.1016/0370-1573(88)90170-6.

Bhattacharyya, Abhijit et al. (2014). "Fluctuations and correlations of conserved charges in an excluded volume hadron resonance gas model". In: *Phys. Rev.* C90.3, p. 034909. DOI: 10.1103/PhysRevC.90.034909. arXiv: 1310.2793 [hep-ph].

Blaschke, D. et al. (2010). "Preface". In: *European Physical Journal Web of Conferences*. Vol. 7. European Physical Journal Web of Conferences, p. 00001. DOI: 10.1051/epjconf/20100700001.

Blaschke, David, Dmitri N. Voskresensky, and Hovik Grigorian (2006). "Cooling of neutron stars with color superconducting quark cores". In: *Nucl. Phys.* A774, pp. 815–818. DOI: 10.1016/j.nuclphysa.2006.06.142. arXiv: hep-ph/0510368 [hep-ph].

Bleicher, M. et al. (1999). "Relativistic hadron hadron collisions in the ultrarelativistic quantum molecular dynamics model". In: *J. Phys.* G25, pp. 1859–1896. DOI: 10.1088/0954-3899/25/9/308. arXiv: hep-ph/9909407 [hep-ph].

Boguta, J (1983). "A saturating chiral field theory of nuclear matter". In: *Physics Letters B* 120.1-3, pp. 34–38.

Borsanyi, S. et al. (2013). "Freeze-out parameters: lattice meets experiment". In: *Phys. Rev. Lett.* 111, p. 062005. DOI: 10.1103/PhysRevLett.111.062005. arXiv: 1305.5161 [hep-lat].

Borsanyi, Szabocls et al. (2014). "Full result for the QCD equation of state with 2+1 flavors". In: *Phys. Lett.* B730, pp. 99–104. DOI: 10.1016/j.physletb.2014.01.007. arXiv: 1309.5258 [hep-lat].

Borsanyi, Szabolcs et al. (2010a). "Is there still any T_c mystery in lattice QCD? Results with physical masses in the continuum limit III". In: *JHEP* 09, p. 073. DOI: 10.1007/JHEP09(2010)073. arXiv: 1005.3508 [hep-lat].

Borsanyi, Szabolcs et al. (2010b). "The QCD equation of state with dynamical quarks". In: *JHEP* 11, p. 077. DOI: 10.1007/JHEP11(2010)077. arXiv: 1007.2580 [hep-lat].

Borsanyi, Szabolcs et al. (2012). "Fluctuations of conserved charges at finite temperature from lattice QCD". In: *JHEP* 01, p. 138. DOI: 10.1007/JHEP01(2012)138. arXiv: 1112.4416 [hep-lat].

Braun-Munzinger, P., I. Heppe, and J. Stachel (1999). "Chemical equilibration in Pb + Pb collisions at the SPS". In: *Phys. Lett.* B465, pp. 15–20. DOI: 10.1016/S0370-2693(99)01076-X. arXiv: nucl-th/9903010 [nucl-th].

Braun-Munzinger, Peter, Krzysztof Redlich, and Johanna Stachel (2011). "PARTICLE PRODUCTION IN HEAVY ION COLLISIONS". In: *Quark–Gluon Plasma 3*. WORLD SCIENTIFIC, pp. 491–599. DOI: 10.1142/9789812795533_0008. URL: https://www.worldscientific.com/doi/abs/10.1142/9789812795533_0008.

Braun-Munzinger, Peter et al. (2016). "Properties of hot and dense matter from relativistic heavy ion collisions". In: *Phys. Rept.* 621, pp. 76–126. DOI: 10.1016/j.physrep.2015.12.003. arXiv: 1510.00442 [nucl-th].

Bugaev, K. A. et al. (2000). "Van der Waals excluded volume model for Lorentz contracted rigid spheres". In: *Phys. Lett.* B485, pp. 121–125. DOI: 10.1016/S0370-2693(00)00690-0. arXiv: nucl-th/0004061 [nucl-th].

Bugaev, Kyrill A. (2008). "The Van-der-Waals Gas EOS for the Lorentz Contracted Spheres". In: *Nucl. Phys.* A807, pp. 251–268. DOI: 10.1016/j.nuclphysa.2008.04.007. arXiv: nucl-th/0611102 [nucl-th].

Burau, G. et al. (2004). "Anisotropic flow of charged and identified hadrons in the quark-gluon string model for Au+Au collisions at sqrt(s) = 200 GeV". In: *Phys.Rev. C71 (2005) 054905*. DOI: 10.1103/PhysRevC.71.054905. arXiv: nucl-th/0411117v2 [nucl-th].

Bzdak, Adam, Romain Holzmann, and Volker Koch (2016). "Multiplicity dependent and non-binomial efficiency corrections for particle number cumulantsMultiplicity-dependent and nonbinomial efficiency corrections for particle number cumulants". In: *Phys. Rev.* C94.6, p. 064907. DOI: 10.1103/PhysRevC.94.064907. arXiv: 1603.09057 [nucl-th].

Bzdak, Adam and Volker Koch (2012). "Acceptance corrections to net baryon and net charge cumulants". In: *Phys. Rev.* C86, p. 044904. DOI: 10.1103/PhysRevC.86.044904. arXiv: 1206.4286 [nucl-th].

Bzdak, Adam, Volker Koch, and Vladimir Skokov (2013). "Baryon number conservation and the cumulants of the net proton distribution". In: *Phys. Rev.* C87.1, p. 014901. DOI: 10.1103/PhysRevC.87.014901. arXiv: 1203.4529 [hep-ph].

Chen, Jiunn-Wei et al. (2017). "Universal relations between nongaussian fluctuations in heavy-ion collisions". In: *Phys. Rev.* D95.1, p. 014038. DOI: 10.1103/PhysRevD.95.014038. arXiv: 1603.05198 [hep-ph].

Chen, Lizhu et al. (2011). "Statistical and dynamical fluctuations in the ratios of higher net-proton cumulants in relativistic heavy-ion collisions". In: *J. Phys.* G38, p. 115004. DOI: 10.1088/0954-3899/38/11/115004.

Cheng, M et al. (2009). "Baryon number, strangeness, and electric charge fluctuations in QCD at high temperature". In: *Physical Review D* 79.7, p. 074505.

Chomaz, Philipe, Maria Colonna, and Jorgen Randrup (2004). "Nuclear spinodal fragmentation". In: *Phys. Rept.* 389, pp. 263–440. DOI: 10.1016/j.physrep.2003.09.006.

Ciminale, M. et al. (2008). "Three flavor Nambu-Jona Lasinio model with Polyakov loop and competition with nuclear matter". In: *Phys. Rev.* D77, p. 054023. DOI: 10.1103/PhysRevD.77.054023. arXiv: 0711.3397 [hep-ph].

Cleymans, J. et al. (1993). "Excluded volume effect and the quark - hadron phase transition". In: *Phys. Scripta* 48, pp. 277–280. DOI: 10.1088/0031-8949/48/3/004.

Cohen, Thomas D., R. J. Furnstahl, and David K. Griegel (1992). "Quark and gluon condensates in nuclear matter". In: *Phys. Rev.* C45, pp. 1881–1893. DOI: 10.1103/PhysRevC.45.1881.

Contrera, G. A., D. Gomez Dumm, and Norberto N. Scoccola (2010). "Meson properties at finite temperature in a three flavor nonlocal chiral quark model with Polyakov loop". In: *Phys. Rev.* D81, p. 054005. DOI: 10.1103/PhysRevD.81.054005. arXiv: 0911.3848 [hep-ph].

Contrera, G. A., M. Orsaria, and N. N. Scoccola (2010). "Nonlocal Polyakov-Nambu-Jona-Lasinio model with wavefunction renormalization at finite temperature and chemical potential". In: *Phys. Rev.* D82, p. 054026. DOI: 10.1103/PhysRevD.82.054026. arXiv: 1006.4639 [hep-ph].

Cooper, Fred and Graham Frye (1974). "Comment on the Single Particle Distribution in the Hydrodynamic and Statistical Thermodynamic Models of Multiparticle Production". In: *Phys. Rev.* D10, p. 186. DOI: 10.1103/PhysRevD.10.186.

Costa, Pedro et al. (2009a). "Scalar-pseudoscalar meson behavior and restoration of symmetries in SU(3) PNJL model". In: *Phys. Rev.* D79, p. 116003. DOI: 10.1103/PhysRevD.79.116003. arXiv: 0807.2134 [hep-ph].

Costa, Pedro et al. (2009b). "The QCD critical end point in the PNJL model". In: *EPL* 86.3, p. 31001. DOI: 10.1209/0295-5075/86/31001. arXiv: 0801.3616 [hep-ph].

DeTar, Carleton and Teiji Kunihiro (1989). "Linear sigma model with parity doubling". In: *Phys. Rev. D* 39 (9), pp. 2805–2808. DOI: 10.1103/PhysRevD.39.2805. URL: https://link.aps.org/doi/10.1103/PhysRevD.39.2805.

Dexheimer, V, R Negreiros, and S Schramm (2015). "Reconciling nuclear and astrophysical constraints". In: *Physical Review C* 92.1, p. 012801.

Dexheimer, V., S. Schramm, and D. Zschiesche (2008). "Nuclear matter and neutron stars in a parity doublet model". In: *Phys. Rev.* C77, p. 025803. DOI: 10.1103/PhysRevC.77.025803. arXiv: 0710.4192 [nucl-th].

Dexheimer, V. et al. (2008). "Neutron stars within the SU(2) parity doublet model". In: *Eur. Phys. J.* A38, pp. 105–113. DOI: 10.1140/epja/i2008-10652-0. arXiv: 0805.3301 [nucl-th].

Dexheimer, Verônica Antocheviz (2009). "Chiral symmetry restoration and deconfinement in neutron stars". Frankfurt (Main), Univ., Diss., 2009. PhD thesis. URL: http://d-nb.info/994757387/34.

Dumitru, Adrian, Robert D. Pisarski, and Detlef Zschiesche (2005). "Dense quarks, and the fermion sign problem, in a SU(N) matrix model". In: *Phys. Rev.* D72, p. 065008. DOI: 10.1103/PhysRevD.72.065008. arXiv: hep-ph/0505256 [hep-ph].

Endrodi, G. et al. (2011). "The QCD phase diagram at nonzero quark density". In: *JHEP* 04, p. 001. DOI: 10.1007/JHEP04(2011)001. arXiv: 1102.1356 [hep-lat].

Feckova, Zuzana et al. (2015). "Net-proton number kurtosis and skewness in nuclear collisions: Influence of deuteron formation". In: *Phys. Rev.* C92.6, p. 064908. DOI: 10.1103/PhysRevC.92.064908. arXiv: 1510.05519 [nucl-th].

Ferreira, Márcio et al. (2014). "Deconfinement and chiral restoration within the SU(3) Polyakov–Nambu–Jona-Lasinio and entangled Polyakov–Nambu–Jona-Lasinio models in an external magnetic field". In: *Phys. Rev.* D89.1. [Addendum: Phys. Rev.D89,no.1,019902(2014)], p. 016002. DOI: 10.1103/PhysRevD.89.016002,10.1103/PhysRevD.89.019902. arXiv: 1305.4751 [hep-ph].

Ferroni, L. and V. Koch (2011). "Mean field approach to flavor susceptibilities with a vector interaction". In: *Phys. Rev.* C83, p. 045205. DOI: 10.1103/PhysRevC.83.045205. arXiv: 1003.4428 [nucl-th].

Fodor, Z. and S. D. Katz (2002). "Lattice determination of the critical point of QCD at finite T and mu". In: *JHEP* 03, p. 014. DOI: 10.1088/1126-6708/2002/03/014. arXiv: hep-lat/0106002 [hep-lat].

– (2004). "Critical point of QCD at finite T and mu, lattice results for physical quark masses". In: *JHEP* 04, p. 050. DOI: 10.1088/1126-6708/2004/04/050. arXiv: hep-lat/0402006 [hep-lat].

Forcrand, Philippe de and Owe Philipsen (2008). "The Chiral critical point of N(f) = 3 QCD at finite density to the order (mu/T)**4". In: *JHEP* 11, p. 012. DOI: 10.1088/1126-6708/2008/11/012. arXiv: 0808.1096 [hep-lat].

Fraga, Eduardo S., Aleksi Kurkela, and Aleksi Vuorinen (2014). "Interacting quark matter equation of state for compact stars". In: *Astrophys. J.* 781.2, p. L25. DOI: 10.1088/2041-8205/781/2/L25. arXiv: 1311.5154 [nucl-th].

Fu, Wei-jie, Yu-xin Liu, and Yue-Liang Wu (2010). "Fluctuations and Correlations of Conserved Charges in QCD at Finite Temperature with Effective Models". In: *Phys. Rev.* D81, p. 014028. DOI: 10.1103/PhysRevD.81.014028. arXiv: 0910.5783 [hep-ph].

Fu, Wei-jie, Zhao Zhang, and Yu-xin Liu (2008). "2+1 flavor Polyakov-Nambu-Jona-Lasinio model at finite temperature and nonzero chemical potential". In: *Phys. Rev.* D77, p. 014006. DOI: 10.1103/PhysRevD.77.014006. arXiv: 0711.0154 [hep-ph].

Fukushima, Kenji (2004). "Chiral effective model with the Polyakov loop". In: *Phys. Lett.* B591, pp. 277–284. DOI: 10.1016/j.physletb.2004.04.027. arXiv: hep-ph/0310121 [hep-ph].

– (2008a). "Critical surface in hot and dense QCD with the vector interaction". In: *Phys. Rev.* D78, p. 114019. DOI: 10.1103/PhysRevD.78.114019. arXiv: 0809.3080 [hep-ph].

– (2008b). "Phase diagrams in the three-flavor Nambu-Jona-Lasinio model with the Polyakov loop". In: *Phys. Rev.* D77. [Erratum: Phys. Rev.D78,039902(2008)], p. 114028. DOI: 10.1103/PhysRevD.77.114028,10.1103/PhysRevD.78.039902. arXiv: 0803.3318 [hep-ph].

– (2009). "Isentropic thermodynamics in the PNJL model". In: *Phys. Rev.* D79, p. 074015. DOI: 10.1103/PhysRevD.79.074015. arXiv: 0901.0783 [hep-ph].

– (2015). "Hadron resonance gas and mean-field nuclear matter for baryon number fluctuations". In: *Phys. Rev.* C91.4, p. 044910. DOI: 10.1103/PhysRevC.91.044910. arXiv: 1409.0698 [hep-ph].

Fukushima, Kenji and Yoshimasa Hidaka (2007). "A Model study of the sign problem in the mean-field approximation". In: *Phys. Rev.* D75, p. 036002. DOI: 10.1103/PhysRevD.75.036002. arXiv: hep-ph/0610323 [hep-ph].

Galatyuk, Tetyana et al. (2016). "Thermal Dileptons from Coarse-Grained Transport as Fireball Probes at SIS Energies". In: *Eur. Phys. J.* A52.5, p. 131. DOI: 10.1140/epja/i2016-16131-1. arXiv: 1512.08688 [nucl-th].

Gale, Charles and Joseph I. Kapusta (1991). "Vector dominance model at finite temperature". In: *Nucl. Phys.* B357, pp. 65–89. DOI: 10.1016/0550-3213(91)90459-B.

Gallas, Susanna, Francesco Giacosa, and Dirk H. Rischke (2010). "Vacuum phenomenology of the chiral partner of the nucleon in a linear sigma model with vector mesons". In: *Phys. Rev.* D82, p. 014004. DOI: 10.1103/PhysRevD.82.014004. arXiv: 0907.5084 [hep-ph].

Gell-Mann, Murray and M Levy (1960). "The axial vector current in beta decay". In: *Nuovo Cim.* 16, p. 705. DOI: 10.1007/BF02859738.

Ghosh, Sanjay K. et al. (2006). "Susceptibilities and speed of sound from PNJL model". In: *Phys. Rev.* D73, p. 114007. DOI: 10.1103/PhysRevD.73.114007. arXiv: hep-ph/0603050 [hep-ph].

Glendenning, N. K. and F. Weber (1994). "Impact of frame dragging on the Kepler frequency of relativistic stars". In: *Phys. Rev.* D50, pp. 3836–3841. DOI: 10.1103/PhysRevD.50.3836.

Glendenning, Norman K (1986). "Phase transitions in a saturating chiral theory of nuclear matter". In: *Annals of Physics* 168.1, pp. 246–269.

Gorenstein, M. I. and M. Gazdzicki (2011). "Strongly Intensive Quantities". In: *Phys. Rev.* C84, p. 014904. DOI: 10.1103/PhysRevC.84.014904. arXiv: 1101.4865 [nucl-th].

Gorenstein, M. I. et al. (2009). "Fluctuations of the K/pi Ratio in Nucleus-Nucleus Collisions: Statistical and Transport Models". In: *Phys. Rev.* C79, p. 024907. DOI: 10.1103/PhysRevC.79.024907. arXiv: 0811.3089 [nucl-th].

Gorenstein, Mark I., V. K. Petrov, and G. M. Zinovev (1981). "Phase Transition in the Hadron Gas Model". In: *Phys. Lett.* 106B, pp. 327–330. DOI: 10.1016/0370-2693(81)90546-3.

Greiner, Carsten and Stefan Leupold (2001). "Anti-hyperon production in relativistic heavy ion collision". In: *J. Phys.* G27, pp. L95–L102. DOI: 10.1088/0954-3899/27/9/102. arXiv: nucl-th/0009036 [nucl-th].

Greiner, Carsten et al. (1988). "Creation of strange-quark-matter droplets as a unique signature for quark-gluon plasma formation in relativistic heavy-ion collisions". In: *Physical Review D* 38.9, p. 2797.

Guillot, Sebastien, Robert E. Rutledge, and Edward F. Brown (2011). "Neutron Star Radius Measurement with the Quiescent Low-Mass X-ray Binary U24 in NGC 6397". In: *Astrophys. J.* 732, p. 88. DOI: 10.1088/0004-637X/732/2/88. arXiv: 1007.2415 [astro-ph.GA].

Guillot, Sebastien et al. (2013). "Measurement of the Radius of Neutron Stars with High S/N Quiescent Low-mass X-ray Binaries in Globular Clusters". In: *Astrophys. J.* 772, p. 7. DOI: 10.1088/0004-637X/772/1/7. arXiv: 1302.0023 [astro-ph.HE].

Gupta, Sourendu et al. (2011). "Scale for the Phase Diagram of Quantum Chromodynamics". In: *Science* 332, pp. 1525–1528. DOI: 10.1126/science.1204621. arXiv: 1105.3934 [hep-ph].

Hagedorn, R. (1983). "The Pressure Ensemble as a Tool for Describing the Hadron - Quark Phase Transition". In: *Z. Phys.* C17, p. 265. DOI: 10.1007/BF01578153.

Hagedorn, R. and Johann Rafelski (1980). "Hot Hadronic Matter and Nuclear Collisions". In: *Phys. Lett.* 97B, p. 136. DOI: 10.1016/0370-2693(80)90566-3.

Hanauske, Matthias et al. (2017). "Concluding Remarks: Connecting Relativistic Heavy Ion Collisions and Neutron Star Mergers by the Equation of State of Dense Hadron- and Quark Matter as signalled by Gravitational Waves". In: *J. Phys. Conf. Ser.* 878.1, p. 012031. DOI: 10.1088/1742-6596/878/1/012031.

Hansen, H. et al. (2007). "Mesonic correlation functions at finite temperature and density in the Nambu-Jona-Lasinio model with a Polyakov loop". In: *Phys. Rev.* D75, p. 065004. DOI: 10.1103/PhysRevD.75.065004. arXiv: hep-ph/0609116 [hep-ph].

Harris, John W. and Berndt Müller (1996). "THE SEARCH FOR THE QUARK-GLUON PLASMA". In: *Annual Review of Nuclear and Particle Science* 46.1, pp. 71–107. DOI: 10.1146/annurev.nucl.46.1.71. eprint: https://doi.org/10.1146/annurev.nucl.46.1.71. URL: https://doi.org/10.1146/annurev.nucl.46.1.71.

Hartnack, C. et al. (1998). "Modeling the many body dynamics of heavy ion collisions: Present status and future perspective". In: *Eur. Phys. J.* A1, pp. 151–169. DOI: 10.1007/s100500050045. arXiv: nucl-th/9811015 [nucl-th].

He, Shu et al. (2016). "Effects of Nuclear Potential on the Cumulants of Net-Proton and Net-Baryon Multiplicity Distributions in Au+Au Collisions at $\sqrt{s_{NN}} = 5\,\mathrm{GeV}$". In: *Phys. Lett.* B762, pp. 296–300. DOI: 10.1016/j.physletb.2016.09.053. arXiv: 1607.06376 [nucl-ex].

Heide, Erik K., Serge Rudaz, and Paul J. Ellis (1994). "An Effective Lagrangian with broken scale and chiral symmetry applied to nuclear matter and finite nuclei". In: *Nucl. Phys.* A571, pp. 713–732. DOI: 10.1016/0375-9474(94)90717-X. arXiv: nucl-th/9308002 [nucl-th].

Hell, T. et al. (2009). "Dynamics and thermodynamics of a non-local PNJL model with running coupling". In: *Phys. Rev.* D79, p. 014022. DOI: 10.1103/PhysRevD.79.014022. arXiv: 0810.1099 [hep-ph].

Hell, T. et al. (2010). "Thermodynamics of a three-flavor nonlocal Polyakov-Nambu-Jona-Lasinio model". In: *Phys. Rev.* D81, p. 074034. DOI: 10.1103/PhysRevD.81.074034. arXiv: 0911.3510 [hep-ph].

Hempel, Matthias et al. (2013). "Noncongruence of the nuclear liquid-gas and deconfine-ment phase transitions". In: *Phys. Rev.* C88.1, p. 014906. DOI: 10.1103/PhysRevC.88.014906. arXiv: 1302.2835 [nucl-th].

Herbst, Tina Katharina, Jan M. Pawlowski, and Bernd-Jochen Schaefer (2011). "The phase structure of the Polyakov–quark–meson model beyond mean field". In: *Phys. Lett.* B696, pp. 58–67. DOI: 10.1016/j.physletb.2010.12.003. arXiv: 1008.0081 [hep-ph].

Herold, Christoph et al. (2016). "Dynamical net-proton fluctuations near a QCD critical point". In: *Phys. Rev.* C93.2, p. 021902. DOI: 10.1103/PhysRevC.93.021902. arXiv: 1601.04839 [hep-ph].

Hillmann, Paula, Jan Steinheimer, and Marcus Bleicher (2018). "Direct, elliptic and trian-gular flow of protons in Au+Au reactions at 1.23 AGeV: A theoretical analysis of the recent HADES data". In: arXiv: 1802.01951 [nucl-th].

Horowitz, C. J. and J. Piekarewicz (2002). "Constraining URCA cooling of neutron stars from the neutron radius of Pb-208". In: *Phys. Rev.* C66, p. 055803. DOI: 10.1103/PhysRevC.66.055803. arXiv: nucl-th/0207067 [nucl-th].

Huovinen, Pasi and P. Petreczky (2011). "Equation of state at finite baryon density based on lattice QCD". In: *J. Phys.* G38, p. 124103. DOI: 10.1088/0954-3899/38/12/124103. arXiv: 1106.6227 [nucl-th].

Huovinen, Pasi and Pter Petreczky (2010). "QCD Equation of State and Hadron Resonance Gas". In: *Nucl. Phys.* A837, pp. 26–53. DOI: 10.1016/j.nuclphysa.2010.02.015. arXiv: 0912.2541 [hep-ph].

Jaiswal, Amaresh and Victor Roy (2016). "Relativistic hydrodynamics in heavy-ion col-lisions: general aspects and recent developments". In: *Adv. High Energy Phys.* 2016, p. 9623034. DOI: 10.1155/2016/9623034. arXiv: 1605.08694 [nucl-th].

Jeon, S. and V. Koch (2000). "Charged particle ratio fluctuation as a signal for QGP". In: *Phys. Rev. Lett.* 85, pp. 2076–2079. DOI: 10.1103/PhysRevLett.85.2076. arXiv: hep-ph/0003168 [hep-ph].

Kapusta, Joseph I. and Keith A. Olive (1983). "Thermodynamics of Hadrons: Delimiting the Temperature". In: *Nucl. Phys.* A408, pp. 478–494. DOI: 10.1016/0375-9474(83)90241-5.

Karsch, Frithjof and Krzysztof Redlich (2011a). "Has Tc been measured by heavy ion experiments?" In: *Phys. Rev.* D84, p. 051504. DOI: 10.1103/PhysRevD.84.051504. arXiv: 1107.1412 [hep-ph].

– (2011b). "Probing freeze-out conditions in heavy ion collisions with moments of charge fluctuations". In: *Physics Letters B* 695.1-4, pp. 136–142.

Kashiwa, Kouji, Thomas Hell, and Wolfram Weise (2011). "Nonlocal Polyakov-Nambu-Jona-Lasinio model and imaginary chemical potential". In: *Phys. Rev.* D84, p. 056010. DOI: 10.1103/PhysRevD.84.056010. arXiv: 1106.5025 [hep-ph].

Kitazawa, Masakiyo (2016). "Efficient formulas for efficiency correction of cumulants". In: *Physical Review C* 93.4, p. 044911.

Kitazawa, Masakiyo and Masayuki Asakawa (2012). "Relation between baryon number fluctuations and experimentally observed proton number fluctuations in relativistic heavy ion collisions". In: *Phys. Rev.* C86. [Erratum: Phys. Rev.C86,069902(2012)], p. 024904.

DOI: 10.1103/PhysRevC.86.024904, 10.1103/PhysRevC.86.069902. arXiv: 1205.3292 [nucl-th].

Klein, B., D. Toublan, and J. J. M. Verbaarschot (2003). "The QCD phase diagram at nonzero temperature, baryon and isospin chemical potentials in random matrix theory". In: *Phys. Rev.* D68, p. 014009. DOI: 10.1103/PhysRevD.68.014009. arXiv: hep-ph/0301143 [hep-ph].

Koch, Volker (2010). "Hadronic Fluctuations and Correlations". In: *Chapter of the book , R. Stock (Ed.), Springer, Heidelberg, 2010, p. 626-652. (Landolt-Boernstein New Series I, v. 23). (ISBN: 978-3-642-01538-0, 978-3-642-01539-7 (eBook))*, pp. 626–652. DOI: 10.1007/978-3-642-01539-7_20. arXiv: 0810.2520 [nucl-th]. URL: http://materials.springer.com/lb/docs/sm_lbs_978-3-642-01539-7_20.

Kovács, P. and Zs. Szép (2008). "Influence of the isospin and hypercharge chemical potentials on the location of the critical end point in the μ_B-T phase diagram of the $SU(3)_L \times SU(3)_R$ chiral quark model". In: *Phys. Rev. D* 77 (6), p. 065016. DOI: 10.1103/PhysRevD.77.065016. URL: https://link.aps.org/doi/10.1103/PhysRevD.77.065016.

Kunihiro, Teiji (1991). "Quark-number susceptibility and fluctuations in the vector channel at high temperatures". In: *Physics Letters B* 271.3-4, pp. 395–402.

Kurkela, Aleksi et al. (2014). "Constraining neutron star matter with Quantum Chromodynamics". In: *Astrophys. J.* 789, p. 127. DOI: 10.1088/0004-637X/789/2/127. arXiv: 1402.6618 [astro-ph.HE].

Lattimer, James M. (2012). "The nuclear equation of state and neutron star masses". In: *Ann. Rev. Nucl. Part. Sci.* 62, pp. 485–515. DOI: 10.1146/annurev-nucl-102711-095018. arXiv: 1305.3510 [nucl-th].

Lattimer, James M. and Yeunhwan Lim (2013). "Constraining the Symmetry Parameters of the Nuclear Interaction". In: *Astrophys. J.* 771, p. 51. DOI: 10.1088/0004-637X/771/1/51. arXiv: 1203.4286 [nucl-th].

Li, Qing-feng et al. (2006). "Probing the equation of state with pions". In: *J. Phys.* G32.2, pp. 151–164. DOI: 10.1088/0954-3899/32/2/007. arXiv: nucl-th/0509070 [nucl-th].

Li, QingFeng et al. (2016a). "Influence of coalescence parameters on the production of protons and Helium-3 fragments". In: *Sci. China Phys. Mech. Astron.* 59.7, p. 672013. DOI: 10.1007/s11433-016-0120-3. arXiv: 1604.01098 [nucl-th].

– (2016b). "Rapidity distribution of protons from the potential version of UrQMD model and the traditional coalescence afterburner". In: *Sci. China Phys. Mech. Astron.* 59.2, p. 622001. DOI: 10.1007/s11433-015-5768-2. arXiv: 1603.09081 [nucl-th].

Luo, Xiaofeng (2012). "Error Estimation for Moments Analysis in Heavy Ion Collision Experiment". In: *J. Phys.* G39, p. 025008. DOI: 10.1088/0954-3899/39/2/025008. arXiv: 1109.0593 [physics.data-an].

Luo, Xiaofeng and Nu Xu (2017). "Search for the QCD Critical Point with Fluctuations of Conserved Quantities in Relativistic Heavy-Ion Collisions at RHIC : An Overview". In: *Nucl. Sci. Tech.* 28.8, p. 112. DOI: 10.1007/s41365-017-0257-0. arXiv: 1701.02105 [nucl-ex].

Mao, Hong, Jinshuang Jin, and Mei Huang (2010). "Phase diagram and thermodynamics of the Polyakov linear sigma model with three quark flavors". In: *J. Phys.* G37, p. 035001. DOI: 10.1088/0954-3899/37/3/035001. arXiv: 0906.1324 [hep-ph].

Matsui, T. and H. Satz (1986). "J/ψ Suppression by Quark-Gluon Plasma Formation". In: *Phys. Lett.* B178, pp. 416–422. DOI: 10.1016/0370-2693(86)91404-8.

McLerran, Larry D. and T. Toimela (1985). "Photon and Dilepton Emission from the Quark - Gluon Plasma: Some General Considerations". In: *Phys. Rev.* D31, p. 545. DOI: 10.1103/PhysRevD.31.545.

Mishustin, I., J. Bondorf, and Mannque Rho (1993). "Chiral symmetry, scale invariance and properties of nuclear matter". In: *Nucl. Phys.* A555, pp. 215–224. DOI: 10.1016/0375-9474(93)90319-S.

Molnar, Denes and Pasi Huovinen (2004). "Dissipation and elliptic flow at RHIC". In: *Phys.Rev.Lett. 94 (2005) 012302*. DOI: 10.1103/PhysRevLett.94.012302. arXiv: nucl-th/0404065v1 [nucl-th].

Motohiro, Yuichi, Youngman Kim, and Masayasu Harada (2015). "Asymmetric nuclear matter in a parity doublet model with hidden local symmetry". In: *Phys. Rev.* C92.2. [Erratum: Phys. Rev.C95,no.5,059903(2017)], p. 025201. DOI: 10.1103/PhysRevC.92.025201,10.1103/PhysRevC.95.059903. arXiv: 1505.00988 [nucl-th].

Motornenko, Anton et al. (2018). "QCD at high density: Equation of state for nuclear collisions and neutron stars". In: *27th International Conference on Ultrarelativistic Nucleus-Nucleus Collisions (Quark Matter 2018) Venice, Italy, May 14-19, 2018*. arXiv: 1809.02000 [hep-ph].

Moustakidis, Ch. C. et al. (2017). "Bounds on the speed of sound in dense matter, and neutron star structure". In: *Phys. Rev. C* 95 (4), p. 045801. DOI: 10.1103/PhysRevC.95.045801. URL: https://link.aps.org/doi/10.1103/PhysRevC.95.045801.

Mukherjee, A., J. Steinheimer, and S. Schramm (2017). "Higher-order baryon number susceptibilities: interplay between the chiral and the nuclear liquid-gas transitions". In: *Phys. Rev.* C96.2, p. 025205. DOI: 10.1103/PhysRevC.96.025205. arXiv: 1611.10144 [nucl-th].

Mukherjee, A. et al. (2017). "The application of the Quark-Hadron Chiral Parity-Doublet Model to neutron star matter". In: *Astron. Astrophys.* 608, A110. DOI: 10.1051/0004-6361/201731505. arXiv: 1706.09191 [nucl-th].

Mukherjee, Ayon, Abhijit Bhattacharyya, and Stefan Schramm (2018). "Effects of a non-zero strangeness-chemical potential in strong interaction models". In: arXiv: 1807.11319 [hep-ph].

Mukherjee, Swagato, Munshi G. Mustafa, and Rajarshi Ray (2007). "Thermodynamics of the PNJL model with nonzero baryon and isospin chemical potentials". In: *Phys. Rev.* D75, p. 094015. DOI: 10.1103/PhysRevD.75.094015. arXiv: hep-ph/0609249 [hep-ph].

Nakamura, Kenzo, Particle Data Group, et al. (2010). "Review of particle physics". In: *Journal of Physics G: Nuclear and Particle Physics* 37.7A, p. 075021.

Negreiros, Rodrigo, V. A. Dexheimer, and S. Schramm (2012). "Quark core impact on hybrid star cooling". In: *Phys. Rev.* C85, p. 035805. DOI: 10.1103/PhysRevC.85.035805. arXiv: 1011.2233 [astro-ph.HE].

Negreiros, Rodrigo, Stefan Schramm, and Fridolin Weber (2013). "Impact of rotation-driven particle repopulation on the thermal evolution of pulsars". In: *Physics Letters B* 718.4, pp. 1176–1180.

Nemoto, Y. et al. (1998). "Decays of 1/2- baryons in chiral effective theory". In: *Phys. Rev.* D57, pp. 4124–4135. DOI: 10.1103/PhysRevD.57.4124. arXiv: hep-ph/9710445 [hep-ph].

Nishida, Y (2004). "Phase structures of strong coupling lattice QCD with finite baryon and isospin density". In: *Phys. Rev. D* 69, p. 094501.

Oppenheimer, J. R. and G. M. Volkoff (1939). "On Massive Neutron Cores". In: *Phys. Rev.* 55 (4), pp. 374–381. DOI: 10.1103/PhysRev.55.374. URL: https://link.aps.org/doi/10.1103/PhysRev.55.374.

Ozel, Feryal and Paulo Freire (2016). "Masses, Radii, and Equation of State of Neutron Stars". In: *Ann. Rev. Astron. Astrophys.* 54, p. 401. DOI: 10.1146/annurev-astro-081915-023322. arXiv: 1603.02698 [astro-ph.HE].

Ozel, Feryal and Dimitrios Psaltis (2015). "Statistics of Measuring Neutron Star Radii: Assessing A Frequentist and A Bayesian Approach". In: *Astrophys. J.* 810.2, p. 135. DOI: 10.1088/0004-637X/810/2/135. arXiv: 1505.05156 [astro-ph.HE].

Page, Dany, Ulrich Geppert, and Fridolin Weber (2006). "The Cooling of compact stars". In: *Nucl. Phys.* A777, pp. 497–530. DOI: 10.1016/j.nuclphysa.2005.09.019. arXiv: astro-ph/0508056 [astro-ph].

Page, Dany et al. (2004). "Minimal cooling of neutron stars: A New paradigm". In: *Astrophys. J. Suppl.* 155, pp. 623–650. DOI: 10.1086/424844. arXiv: astro-ph/0403657 [astro-ph].

Pagura, V., D. Gomez Dumm, and N. N. Scoccola (2012). "Deconfinement and chiral restoration in nonlocal PNJL models at zero and imaginary chemical potential". In: *Phys. Lett.* B707, pp. 76–82. DOI: 10.1016/j.physletb.2011.11.064. arXiv: 1105.1739 [hep-ph].

Papazoglou, P. et al. (1998). "Chiral Lagrangian for strange hadronic matter". In: *Phys. Rev.* C57, pp. 2576–2588. DOI: 10.1103/PhysRevC.57.2576. arXiv: nucl-th/9706024 [nucl-th].

Papazoglou, P. et al. (1999). "Nuclei in a chiral SU(3) model". In: *Phys. Rev.* C59, pp. 411–427. DOI: 10.1103/PhysRevC.59.411. arXiv: nucl-th/9806087 [nucl-th].

Petersen, Hannah et al. (2008). "Fully integrated transport approach to heavy ion reactions with an intermediate hydrodynamic stage". In: *Physical Review C* 78.4, p. 044901.

Pisarski, Robert D. (1982). "Phenomenology of the Chiral Phase Transition". In: *Phys. Lett.* 110B, pp. 155–158. DOI: 10.1016/0370-2693(82)91025-5.

Radzhabov, A. E. et al. (2011). "Nonlocal PNJL model beyond mean field and the QCD phase transition". In: *Phys. Rev.* D83, p. 116004. DOI: 10.1103/PhysRevD.83.116004. arXiv: 1012.0664 [hep-ph].

Rafelski, Johann and Berndt Muller (1982). "Strangeness Production in the Quark - Gluon Plasma". In: *Phys. Rev. Lett.* 48. [Erratum: Phys. Rev. Lett.56,2334(1986)], p. 1066. DOI: 10.1103/PhysRevLett.48.1066,10.1103/PhysRevLett.56.2334.

Randrup, Jorgen (2004). "Spinodal decomposition during the hadronization stage at RHIC?" In: *Phys. Rev. Lett.* 92, p. 122301. DOI: 10.1103/PhysRevLett.92.122301. arXiv: hep-ph/0308271 [hep-ph].

Rapp, R. and H. van Hees (2016a). "Thermal Electromagnetic Radiation in Heavy-Ion Collisions". In: *Eur. Phys. J.* A52.8, p. 257. DOI: 10.1140/epja/i2016-16257-0. arXiv: 1608.05279 [hep-ph].

Rapp, Ralf and Hendrik van Hees (2016b). "Thermal Dileptons as Fireball Thermometer and Chronometer". In: *Phys. Lett.* B753, pp. 586–590. DOI: 10.1016/j.physletb.2015.12.065. arXiv: 1411.4612 [hep-ph].

Ratti, C. et al. (2007). "Thermodynamics of the PNJL model". In: *Eur. Phys. J.* C49, pp. 213–217. DOI: 10.1140/epjc/s10052-006-0065-x. arXiv: hep-ph/0609218 [hep-ph].

Ratti, Claudia, Simon Roessner, and Wolfram Weise (2007). "Quark number susceptibilities: Lattice QCD versus PNJL model". In: *Phys. Lett.* B649, pp. 57–60. DOI: 10.1016/j.physletb.2007.03.038. arXiv: hep-ph/0701091 [hep-ph].

Ratti, Claudia, Michael A. Thaler, and Wolfram Weise (2006). "Phases of QCD: Lattice thermodynamics and a field theoretical model". In: *Phys. Rev.* D73, p. 014019. DOI: 10.1103/PhysRevD.73.014019. arXiv: hep-ph/0506234 [hep-ph].

Ratti, Claudia and Wolfram Weise (2004). "Thermodynamics of two-color QCD and the Nambu Jona-Lasinio model". In: *Phys. Rev. D* 70 (5), p. 054013. DOI: 10.1103/PhysRevD.70.054013. URL: https://link.aps.org/doi/10.1103/PhysRevD.70.054013.

Rau, Philip (2013). "Chiral effective model for the QCD equation of state and medium properties from heavy ion collisions". Frankfurt (Main), Univ., Diss., 2013. PhD thesis. URL: http://d-nb.info/1043611908/04.

Reisdorf, W. et al. (2010). "Systematics of central heavy ion collisions in the 1A GeV regime". In: *Nucl. Phys.* A848, pp. 366–427. DOI: 10.1016/j.nuclphysa.2010.09.008. arXiv: 1005.3418 [nucl-ex].

Rezzolla, Luciano and Kentaro Takami (2016). "Gravitational-wave signal from binary neutron stars: A systematic analysis of the spectral properties". In: *Phys. Rev. D* 93 (12), p. 124051. DOI: 10.1103/PhysRevD.93.124051. URL: https://link.aps.org/doi/10.1103/PhysRevD.93.124051.

Rischke, Dirk H. (1998). "Fluid dynamics for relativistic nuclear collisions". In: [Lect. Notes Phys.516,21(1999)]. DOI: 10.1007/BFb0107310. arXiv: nucl-th/9809044 [nucl-th].

Rischke, Dirk H., Stefan Bernard, and Joachim A. Maruhn (1995). "Relativistic hydrodynamics for heavy ion collisions. 1. General aspects and expansion into vacuum". In: *Nucl. Phys.* A595, pp. 346–382. DOI: 10.1016/0375-9474(95)00355-1. arXiv: nucl-th/9504018 [nucl-th].

Rischke, Dirk H., Yaris Pursun, and Joachim A. Maruhn (1995). "Relativistic hydrodynamics for heavy ion collisions. 2. Compression of nuclear matter and the phase transition to the quark - gluon plasma". In: *Nucl. Phys.* A595. [Erratum: Nucl. Phys.A596,717(1996)], pp. 383–408. DOI: 10.1016/0375-9474(95)00356-3,10.1016/0375-9474(96)89543-1. arXiv: nucl-th/9504021 [nucl-th].

Rischke, Dirk H. et al. (1991). "Excluded volume effect for the nuclear matter equation of state". In: *Z. Phys.* C51, pp. 485–490. DOI: 10.1007/BF01548574.

Roessner, Simon, Claudia Ratti, and W. Weise (2007). "Polyakov loop, diquarks and the two-flavour phase diagram". In: *Phys. Rev.* D75, p. 034007. DOI: 10.1103/PhysRevD.75.034007. arXiv: hep-ph/0609281 [hep-ph].

Roessner, Simon et al. (2008). "The chiral and deconfinement crossover transitions: PNJL model beyond mean field". In: *Nucl. Phys.* A814, pp. 118–143. DOI: 10.1016/j.nuclphysa.2008.10.006. arXiv: 0712.3152 [hep-ph].

Romatschke, Paul and Ulrike Romatschke (2017). "Relativistic Fluid Dynamics In and Out of Equilibrium – Ten Years of Progress in Theory and Numerical Simulations of Nuclear Collisions". In: arXiv: 1712.05815 [nucl-th].

Rößner, S., C. Ratti, and W. Weise (2007). "Polyakov loop, diquarks, and the two-flavor phase diagram". In: *Phys. Rev. D* 75 (3), p. 034007. DOI: 10.1103/PhysRevD.75.034007. URL: https://link.aps.org/doi/10.1103/PhysRevD.75.034007.

Sakai, Yuji et al. (2012). "Equation of state in the PNJL model with the entanglement interaction". In: *J. Phys.* G39, p. 035004. DOI: 10.1088/0954-3899/39/3/035004. arXiv: 1104.2394 [hep-ph].

Sangaline, Evan (2015). "Strongly Intensive Cumulants: Fluctuation Measures for Systems With Incompletely Constrained Volumes". In: arXiv: 1505.00261 [nucl-th].

Sasaki, C., B. Friman, and K. Redlich (2007a). "Density fluctuations in the presence of spinodal instabilities". In: *Phys. Rev. Lett.* 99, p. 232301. DOI: 10.1103/PhysRevLett.99.232301. arXiv: hep-ph/0702254 [HEP-PH].

– (2007b). "Susceptibilities and the Phase Structure of a Chiral Model with Polyakov Loops". In: *Phys. Rev.* D75, p. 074013. DOI: 10.1103/PhysRevD.75.074013. arXiv: hep-ph/0611147 [hep-ph].

Sasaki, Chihiro and Igor Mishustin (2010). "Thermodynamics of dense hadronic matter in a parity doublet model". In: *Phys. Rev.* C82, p. 035204. DOI: 10.1103/PhysRevC.82.035204. arXiv: 1005.4811 [hep-ph].

Satarov, L. M., M. N. Dmitriev, and I. N. Mishustin (2009). "Equation of state of hadron resonance gas and the phase diagram of strongly interacting matter". In: *Phys. Atom. Nucl.* 72, pp. 1390–1415. DOI: 10.1134/S1063778809080146. arXiv: 0901.1430 [hep-ph].

Schaefer, B. J. and M. Wagner (2012). "QCD critical region and higher moments for three flavor models". In: *Phys. Rev.* D85, p. 034027. DOI: 10.1103/PhysRevD.85.034027. arXiv: 1111.6871 [hep-ph].

Schaefer, Bernd-Jochen, Jan M. Pawlowski, and Jochen Wambach (2007). "The Phase Structure of the Polyakov–Quark-Meson Model". In: *Phys. Rev.* D76, p. 074023. DOI: 10.1103/PhysRevD.76.074023. arXiv: 0704.3234 [hep-ph].

Schaefer, Bernd-Jochen, Mathias Wagner, and Jochen Wambach (2010). "Thermodynamics of (2+1)-flavor QCD: Confronting Models with Lattice Studies". In: *Phys. Rev.* D81, p. 074013. DOI: 10.1103/PhysRevD.81.074013. arXiv: 0910.5628 [hep-ph].

Schaffner, Jürgen et al. (1993). "Strange hadronic matter". In: *Physical review letters* 71.9, p. 1328.

Schaffner-Bielich, Jürgen et al. (1997a). "Detectability of strange matter in heavy ion experiments". In: *Physical Review C* 55.6, p. 3038.

Schaffner-Bielich, Jürgen et al. (1997b). "Properties of exotic matter for heavy-ion searches". In: *Journal of Physics G: Nuclear and Particle Physics* 23.12, p. 2107.

Schramm, S. (2003). "Nuclear and neutron star radii". In: *Phys. Lett.* B560, pp. 164–170. DOI: 10.1016/S0370-2693(03)00408-8. arXiv: nucl-th/0210053 [nucl-th].

Schramm, S. et al. (2018a). "Neutron stars and the equation of state". In: *Journal of Astrophysics and Astronomy* 39.4, p. 42. ISSN: 0973-7758. DOI: 10.1007/s12036-018-9534-5. URL: https://doi.org/10.1007/s12036-018-9534-5.

Schramm, Stefan et al. (2018b). "Dense and hot matter in compact stars and heavy-ion collisions". In: *EPJ Web of Conferences*. Vol. 171. EDP Sciences, p. 08002.

Schulze, H-J et al. (1998). "Hyperonic nuclear matter in Brueckner theory". In: *Physical Review C* 57.2, p. 704.

Schwinger, Julian S. (1957). "A Theory of the Fundamental Interactions". In: *Annals Phys.* 2, pp. 407–434. DOI: 10.1016/0003-4916(57)90015-5.

Spieles, C. et al. (1996). "Creation of strange matter at low initial mu / T". In: *Phys. Rev. Lett.* 76, pp. 1776–1779. DOI: 10.1103/PhysRevLett.76.1776.

Steinheimer, J. and S. Schramm (2011). "The problem of repulsive quark interactions - Lattice versus mean field models". In: *Phys. Lett.* B696, pp. 257–261. DOI: 10.1016/j.physletb.2010.12.046. arXiv: 1005.1176 [hep-ph].

Steinheimer, J., S. Schramm, and H. Stocker (2011a). "An Effective chiral Hadron-Quark Equation of State". In: *J. Phys.* G38, p. 035001. DOI: 10.1088/0954-3899/38/3/035001. arXiv: 1009.5239 [hep-ph].

– (2011b). "The hadronic SU(3) Parity Doublet Model for Dense Matter, its extension to quarks and the strange equation of state". In: *Phys. Rev.* C84, p. 045208. DOI: 10.1103/PhysRevC.84.045208. arXiv: 1108.2596 [hep-ph].

Steinheimer, J. et al. (2016). "Conserved charge fluctuations are not conserved during the hadronic phase". In: arXiv: 1608.03737 [nucl-th].

Steinheimer, J. et al. (2018a). "The Hot and Dense QCD Equation of State in Heavy Ion Collisions and Neutron Star Mergers". In: *2nd Karl Schwarzschild Meeting on Gravitational Physics*. Ed. by Piero Nicolini et al. Cham: Springer International Publishing, pp. 191–198. ISBN: 978-3-319-94256-8.

Steinheimer, Jan and Volker Koch (2017). "Effect of finite particle number sampling on baryon number fluctuations". In: *Phys. Rev.* C96.3, p. 034907. DOI: 10.1103/PhysRevC.96.034907. arXiv: 1705.08538 [nucl-th].

Steinheimer, Jan and Jørgen Randrup (2012). "Spinodal Amplification of Density Fluctuations in Fluid-Dynamical Simulations of Relativistic Nuclear Collisions". In: *Phys. Rev. Lett.* 109 (21), p. 212301. DOI: 10.1103/PhysRevLett.109.212301. URL: https://link.aps.org/doi/10.1103/PhysRevLett.109.212301.

Steinheimer, Jan et al. (2009). "Strangeness fluctuations and MEMO production at FAIR". In: *Phys. Lett.* B676, pp. 126–131. DOI: 10.1016/j.physletb.2009.04.062. arXiv: 0811.4077 [hep-ph].

Steinheimer, Jan et al. (2018b). "Nuclear interactions and net-proton number fluctuations in heavy ion collisions at the SIS18 accelerator". In: *Physics Letters B* 785, pp. 40 –

45. ISSN: 0370-2693. DOI: https://doi.org/10.1016/j.physletb.2018.07.068. URL: http://www.sciencedirect.com/science/article/pii/S0370269318306439.

Steinheimer-Froschauer, Jan (2011). "A model for heavy ion collisions with quark and hadronic degrees of freedom". Frankfurt (Main), Univ., Diss., 2011. PhD thesis.

Stephanov, M. A. (2009). "Non-Gaussian fluctuations near the QCD critical point". In: *Phys. Rev. Lett.* 102, p. 032301. DOI: 10.1103/PhysRevLett.102.032301. arXiv: 0809.3450 [hep-ph].

Stephanov, Misha A., K. Rajagopal, and Edward V. Shuryak (1998). "Signatures of the tricritical point in QCD". In: *Phys. Rev. Lett.* 81, pp. 4816–4819. DOI: 10.1103/PhysRevLett.81.4816. arXiv: hep-ph/9806219 [hep-ph].

Stergioulas, Nikolaos and John.L. Friedman (1995). "Comparing models of rapidly rotating relativistic stars constructed by two numerical methods". In: *Astrophys. J.* 444, p. 306. DOI: 10.1086/175605. arXiv: astro-ph/9411032 [astro-ph].

Stoecker, Horst and W. Greiner (1986). "High-Energy Heavy Ion Collisions: Probing the Equation of State of Highly Excited Hadronic Matter". In: *Phys. Rept.* 137, pp. 277–392. DOI: 10.1016/0370-1573(86)90131-6.

Takami, Kentaro, Luciano Rezzolla, and Luca Baiotti (2014). "Constraining the Equation of State of Neutron Stars from Binary Mergers". In: *Phys. Rev. Lett.* 113 (9), p. 091104. DOI: 10.1103/PhysRevLett.113.091104. URL: https://link.aps.org/doi/10.1103/PhysRevLett.113.091104.

– (2015). "Spectral properties of the post-merger gravitational-wave signal from binary neutron stars". In: *Phys. Rev. D* 91 (6), p. 064001. DOI: 10.1103/PhysRevD.91.064001. URL: https://link.aps.org/doi/10.1103/PhysRevD.91.064001.

Tanabashi, M. et al. (2018). "Review of Particle Physics". In: *Phys. Rev. D* 98 (3), p. 030001. DOI: 10.1103/PhysRevD.98.030001. URL: https://link.aps.org/doi/10.1103/PhysRevD.98.030001.

Tarnowsky, Terence J. and Gary D. Westfall (2013). "First Study of the Negative Binomial Distribution Applied to Higher Moments of Net-charge and Net-proton Multiplicity Distributions". In: *Phys. Lett.* B724, pp. 51–55. DOI: 10.1016/j.physletb.2013.05.064. arXiv: 1210.8102 [nucl-ex].

Taub, A. H. (1948). "Relativistic Rankine-Hugoniot Equations". In: *Phys. Rev.* 74 (3), pp. 328–334. DOI: 10.1103/PhysRev.74.328. URL: https://link.aps.org/doi/10.1103/PhysRev.74.328.

Tolman, Richard C. (1939). "Static Solutions of Einstein's Field Equations for Spheres of Fluid". In: *Phys. Rev.* 55 (4), pp. 364–373. DOI: 10.1103/PhysRev.55.364. URL: https://link.aps.org/doi/10.1103/PhysRev.55.364.

Torrieri, Giorgio (2006). "Resonances and fluctuations of strange particle in 200-GeV Au-Au collisions". In: *J. Phys.* G32, S195–S204. DOI: 10.1088/0954-3899/32/12/S25. arXiv: nucl-th/0606009 [nucl-th].

Toublan, D., B. Klein, and J. J. M. Verbaarschot (2005). "The QCD phase diagram at non-zero baryon and isospin chemical potentials". In: *Nucl. Phys. Proc. Suppl.* 140. [,562(2004)], pp. 562–564. DOI: 10.1016/j.nuclphysbps.2004.11.128. arXiv: hep-lat/0409035 [hep-lat].

Toublan, D. and J. B. Kogut (2003). "Isospin chemical potential and the QCD phase diagram at nonzero temperature and baryon chemical potential". In: *Phys. Lett.* B564, pp. 212–216. DOI: 10.1016/S0370-2693(03)00701-9. arXiv: hep-ph/0301183 [hep-ph].

Toublan, D and John B Kogut (2005). "The QCD phase diagram at nonzero baryon, isospin and strangeness chemical potentials: Results from a hadron resonance gas model". In: *Physics Letters B* 605.1-2, pp. 129–136.

Tsubakihara, K. et al. (2010). "Lambda hypernuclei and neutron star matter in a chiral SU(3) relativistic mean field model with a logarithmic potential". In: *Phys. Rev.* C81, p. 065206. DOI: 10.1103/PhysRevC.81.065206. arXiv: 0909.5058 [nucl-th].

Vovchenko, V. et al. (2015). "Scaled variance, skewness, and kurtosis near the critical point of nuclear matter". In: *Phys. Rev.* C92.5, p. 054901. DOI: 10.1103/PhysRevC.92.054901. arXiv: 1506.05763 [nucl-th].

Vovchenko, Volodymyr, Mark I. Gorenstein, and Horst Stoecker (2017). "van der Waals Interactions in Hadron Resonance Gas: From Nuclear Matter to Lattice QCD". In: *Phys. Rev. Lett.* 118.18, p. 182301. DOI: 10.1103/PhysRevLett.118.182301. arXiv: 1609.03975 [hep-ph].

Walecka, J. D. (1974). "A Theory of highly condensed matter". In: *Annals Phys.* 83, pp. 491–529. DOI: 10.1016/0003-4916(74)90208-5.

Wang, X. and C. B. Yang (2012). "On the Energy and Centrality Dependence of Higher Order Moments of Net-Proton Distributions in Relativistic Heavy Ion Collisions". In: *Phys. Rev.* C85, p. 044905. DOI: 10.1103/PhysRevC.85.044905. arXiv: 1202.4857 [nucl-th].

Wang, Yongjia et al. (2014a). "Collective flows of light particles in the Au+Au collisions at intermediate energies". In: *Phys. Rev.* C89.3, p. 034606. DOI: 10.1103/PhysRevC.89.034606. arXiv: 1305.4730 [nucl-th].

Wang, Yongjia et al. (2014b). "Constraining the high-density nuclear symmetry energy with the transverse-momentum dependent elliptic flow". In: *Phys. Rev.* C89.4, p. 044603. DOI: 10.1103/PhysRevC.89.044603. arXiv: 1403.7041 [nucl-th].

Wang, Yongjia et al. (2015). "^{3}H/^{3}He ratio as a probe of the nuclear symmetry energy at sub-saturation densities". In: *Eur. Phys. J.* A51.3, p. 37. DOI: 10.1140/epja/i2015-15037-8. arXiv: 1407.7625 [nucl-th].

Wei, J. B et al. (2017). "Rotating hybrid stars with the Dyson-Schwinger quark model". In: arXiv: 1703.08952 [nucl-th].

Weinberg, Steven (1967). "Dynamical Approach to Current Algebra". In: *Phys. Rev. Lett.* 18 (5), pp. 188–191. DOI: 10.1103/PhysRevLett.18.188. URL: https://link.aps.org/doi/10.1103/PhysRevLett.18.188.

– (1968). "Nonlinear Realizations of Chiral Symmetry". In: *Phys. Rev.* 166 (5), pp. 1568–1577. DOI: 10.1103/PhysRev.166.1568. URL: https://link.aps.org/doi/10.1103/PhysRev.166.1568.

Weise, Wolfram (2010). "Chiral symmetry in strongly interacting matter: From Nuclear Matter to Phases of QCD". In: *Prog. Theor. Phys. Suppl.* 186, pp. 390–403. DOI: 10.1143/PTPS.186.390. arXiv: 1009.6201 [nucl-th].

Wilson, Kenneth G. (1974). "Confinement of Quarks". In: *Phys. Rev.* D10. [,45(1974)], pp. 2445–2459. DOI: 10.1103/PhysRevD.10.2445.

Xu, Nu (2014). "An Overview of STAR Experimental Results". In: *Nucl. Phys.* A931, pp. 1–12. DOI: 10.1016/j.nuclphysa.2014.10.022. arXiv: 1408.3555 `[nucl-ex]`.

Xu, Zhe and Carsten Greiner (2004). "Thermalization of gluons in ultrarelativistic heavy ion collisions by including three-body interactions in a parton cascade". In: *Phys.Rev. C71 (2005) 064901*. DOI: 10.1103/PhysRevC.71.064901. arXiv: hep-ph/0406278v2 `[hep-ph]`.

Yao, W.-M., P. D. Group, et al. (2006). "Review of particle physics". In: *Journal of Physics G: Nuclear and Particle Physics* 33.1, p. 1.

Zschiesche, D. et al. (2007). "Cold, dense nuclear matter in a SU(2) parity doublet model". In: *Phys. Rev. C* 75 (5), p. 055202. DOI: 10.1103/PhysRevC.75.055202. URL: https://link.aps.org/doi/10.1103/PhysRevC.75.055202.

Danksagung

There are people who, by simply being what they are, greatly inspire others around them. In the course of my doctoral studies at the Frankfurt Institute for Advanced Studies (FIAS), as a student of the Johann Wolfgang Goethe-Universität in Frankfurt am Main, Germany, I've been fortunate enough to have come across a few such people. Here, at the end of my thesis, the swansong of my time at FIAS, I would like to take the opportunity to express my gratitude towards them.

I would like to start by thanking my supervisor, Prof. Dr. Stefan Wolfgang Schramm, for his constant support, encouragement and diligent involvement in my work. Without his omnipresent oversight, this thesis would never have been possible. He is, quite simply, the best boss a person could ever hope for.

I would also like to profusely thank my senior collaborator on this project, Dr. Jan Mattes Steinheimer-Froschauer of FIAS; not only for helping me with even the simplest; and at times, the silliest; of work-related problems, but also for making me feel welcome and helping me find my feet in a new city on foreign shores. Jan-da is, probably, the best possible senior colleague to have in any work environment.

I am grateful to Dr. Rana Nandi, formerly of FIAS, currently a post-doctoral fellow at the Tata Institute of Fundamental Research (TIFR) in Mumbai, Maharashtra, India; for being a friend, philosopher and guide during my early days in Germany. Although his contributions to my FORTRAN coding skills alone could fill a book, I'd like to thank him instead for the warmth and generosity he showed towards me, while he was in Frankfurt. His, and his wife's, presence made this city a "home-away-from-home" for me. Without Rana-da, Germany in general, and Frankfurt in particular, would not have been as great an experience for me as it has been.

I would like to thank the research group of Prof. Dr. Qingfeng Li; of the Huzhou University in Huzhou, Zhejiang, China, for their invaluable contributions to parts of this project; and Dr. Verônica Antocheviz Dexheimer-Strickland, of the Kent State University in Kent, Ohio, the United States of America, for collaborating on the neutron star calculations and for piquing my interest in the field of nuclear astrophysics.

I would also like to take this opportunity to convey my utmost respect and to express my sincerest gratitude towards Prof. Dr. Abhijit Bhattacharyya; of the University of Calcutta in Kolkata, West Bengal (WB), India, for recommending me as a doctoral fellow to Prof. Dr. Schramm, for bringing me up-to-date with the events in the world of high-energy physics research and for collaborating with me on parts of this project; and towards Prof. Dr. Debades Bandyopadhyay; of the Saha Institute of Nuclear Physics (SINP) in Kolkata, WB, India, for deeming me worthy of this position and for forwarding my CV to Prof.

Dr. Schramm, thereby establishing the first line of communication between me and my supervisor.

The HGS-HIRe Graduate School; and Henner Büsching, the man behind it; deserve special thanks for the support provided towards my attendances at seminars and conferences, both in Germany and abroad.

A majority of the calculations for this thesis was carried out using the CSC computer clusters (LOEWE & FUCHS) at the Goethe-Universität Frankfurt, thanks to the administration and the team at CSC.

I will remain perpetually grateful to my close friends Dr. Rome Samanta and Mr. Biswajit Banerjee, and my senior, Dr. Prasanta Char; all formerly of the SINP; for their enthusiasm and encouragement, and for the fact that, without their thoughtfulness and kindness, I would never have had a chance of doing exciting research at this incredible facility.

It takes a special kind of person to become friends with from work, and Dr. Rosana de Oliveira Gomes, of FIAS, is nothing but. I would like to thank her for the constancy of her compassion and friendship, and for her selfless assistance with the writing of my thesis, offering voluntarily to proof-read the manuscript, provide valuable insights into its content and comment on its overall cohesiveness.

It is impossible to overstate the value of my parents' love, blessings, encouragement and support in my quest of establishing myself as an academician. So, the only worthwhile thing to do is to humbly acknowledge their influence in my life and their acute sense of understanding towards the realisation of my dream of becoming a physicist. Thank you Ma and Baba.

Lebenslauf

Name:	Ayon Mukherjee
Geburtsdatum:	14.01.1991
Geburtsort:	Kolkata, West Bengal (WB), India
Nationalität:	Indien
Familienstand:	Ledig

Schulische Ausbildung:

1994-1998:	Nava Nalanda Primary School, Gobindapur, Kolkata, WB, Indien.
1998-2006:	St. Xavier's Institution, Panihati, Kolkata, WB, Indien.
2006-2008:	Ramakrishna Mission Vidyalaya, Narendrapur, Kolkata, WB, Indien.

Sonstige Dienstleistungen:

2008-2016:	Privatunterricht für Schüler der Mittel- und Oberstufe in Physik und Mathematik.

Studium:

06/2008 - 06/2011:	Studium der Physik (Honours), als Bachelor of Science (B. Sc.), Am Scottish Church College, University of Calcutta, Kolkata, WB, Indien.
Abschluss:	Erste Klasse ($64, 3\%$ Punkte).
08/2011 - 06/2013:	Studium der Physik, als Master of Science (M. Sc.), An der University of Calcutta (The Rashbehari Siksha Prangan), Kolkata, WB, Indien.
Abschluss:	Erste Klasse ($60, 0\%$ Punkte).
Seit 04/2016:	Promotion an der Johann Wolfgang Goethe-Universität, Frankfurt am Main, Hessen, Deutschland.
Seit 11/2016:	Mitglied der Graduiertenschule HGS-HIRe (Helmholtz Graduate School for Hadron and Ion Research).

Liste der Veröffentlichungen:

- Higher-order baryon number susceptibilities: interplay between the chiral and the nuclear liquid-gas transitions (Mukherjee, Steinheimer, and Schramm, 2017)

- The application of the Quark-Hadron Chiral Parity-Doublet Model to neutron star matter (Mukherjee et al., 2017)

- Nuclear interactions and net-proton number fluctuations in heavy ion collisions at the SIS18 accelerator (Steinheimer et al., 2018b)

- Effects of a non-zero strangeness-chemical potential in strong interaction models (Mukherjee, Bhattacharyya, and Schramm, 2018)

- Concluding Remarks: Connecting Relativistic Heavy Ion Collisions and Neutron Star Mergers by the Equation of State of Dense Hadron- and Quark Matter as signalled by Gravitational Waves (Hanauske et al., 2017)

- Dense and hot matter in compact stars and heavy-ion collisions (Schramm et al., 2018b)

- Neutron stars and the equation of state (Schramm et al., 2018a)

- The Hot and Dense QCD Equation of State in Heavy Ion Collisions and Neutron Star Mergers (Steinheimer et al., 2018a)

Akademische Lehrer

Dr. S. Bhattacharyya
Dr. Chakraborty
Dr. Chowdhury
Mr. Mandal
Dr. J. Mitra
Dr. Nandi
Dr. A. Roy
Mr. Sasmal
Dr. Bandyopadhyay
Dr. A. Banerjee
Dr. S. Banerjee
Prof. Dr. A. Bhattacharyya
Prof. Dr. Biswas
Prof. Dr. Dasgupta
Dr. Datta
Prof. Dr. Gangopadhyay
Prof. Dr. Jana
Prof. Dr. Kundu
Dr. I. Mitra
Dr. B. Ray
Prof. Emeritus Dr. Raychaudhuri
Dr. Saha
Prof. Dr. Sen
Dr. Shamanna
Prof. Dr. Bratkovskaya
Prof. Dr. Mishustin
Prof. Dr. Schramm
Dr. Steinheimer